PNNL-35956, Rev. 0
DFTP-RPT-041, Rev. 0

Filtration of Hanford Tank 241-AN-107 Supernatant at 16 °C

June 2024

JR Allred
C Alvarez
EC Buck
CA Burns
RC Daniel
JE Turner
AM Westesen
RA Peterson

U.S. DEPARTMENT OF ENERGY

Prepared for the U.S. Department of Energy
under Contract DE-AC05-76RL01830

DISCLAIMER

PACIFIC NORTHWEST NATIONAL LABORATORY
operated by
BATTELLE
for the
UNITED STATES DEPARTMENT OF ENERGY
under Contract DE-AC05-76RL01830

Printed in the United States of America

Available to DOE and DOE contractors from the
Office of Scientific and Technical Information,
P.O. Box 62, Oak Ridge, TN 37831-0062;
ph: (865) 576-8401
fax: (865) 576-5728
email: reports@adonis.osti.gov

Available to the public from the National Technical Information Service
5301 Shawnee Rd., Alexandria, VA 22312
ph: (800) 553-NTIS (6847)
email: orders@ntis.gov <https://www.ntis.gov/about>
Online ordering: http://www.ntis.gov

PNNL-35956, Rev. 0
DFTP-RPT-041, Rev. 0

Filtration of Hanford Tank 241-AN-107 Supernatant at 16 °C

June 2024

JR Allred
C Alvarez
EC Buck
CA Burns
RC Daniel
JE Turner
AM Westesen
RA Peterson

Prepared for
the U.S. Department of Energy
under Contract DE-AC05-76RL01830

Pacific Northwest National Laboratory
Richland, Washington 99354

Summary

Approximately 9 L of supernatant from Hanford waste tank 241-AN-107 was delivered by Washington River Protection Solutions (WRPS) to the Radiochemical Processing Laboratory (RPL) at Pacific Northwest National Laboratory (PNNL). The thirty-six 241-AN-107 sample bottles consisted of six sets of six samples, with each set pulled from a unique tank sampling level. Prior to testing, samples from each level were composited and diluted to 5.5 M Na to provide nominally level-independent feed for dead-end filtration and ion exchange testing.

The composited 241-AN-107 supernatant was chilled to 16 °C for 1 week prior to testing. Filtration testing was then conducted using a backpulse dead-end filter (BDEF) system equipped with a feed vessel and a Mott inline filter Model 6610 (Media Grade 5) in the hot cells of the RPL. The purpose of this testing was to a) demonstrate dead-end filtration (DEF) of 241-AN-107 feed at reduced temperature to obtain prototypic tank side cesium removal (TSCR) flux rates and identify issues that may impact filtration after dilution to 5.5 M Na, and b) provide feed for a follow-on ion exchange unit operation.

The feed was filtered through the BDEF system at a targeted flux of 0.065 gpm/ft^2. During filtration the differential pressure required to effect filtration at 0.065 gpm/ft^2 was slow to increase for most of the filtration campaign. After all the feed bottles had been pumped into the slurry reservoir, the bottoms of the bottles were added to the reservoir and transmembrane pressure reached 2.0 psid (the TSCR action limit). The filter was cleaned after completing filtration of the 241-AN-107 feed. The prototypic filter cleaning process was unable to effectively restore filter performance, and cleaning with oxalic acid was required before flow through the filter could be restored. This indicates that the Media Grade 5 filter may require an alternative cleaning protocol when processing 241-AN-107 supernatant.

Solids concentrated from the backpulse solutions were composed of natrophosphate, Mn-Fe phases, and fluoro-natrophosphate that occurred as particle agglomerates. The individual particles were in some cases hundreds of micrometers across, which is consistent with prior observations from 241-AN-107 supernatant waste characterizations.

Acknowledgments

The authors gratefully acknowledge the help of hot cell technicians Victor Aguilar, Robert Cox, Erick Larios, and Jose Diaz in conducting this work. We thank Renee Russell for conducting the technical review of this report. We also thank Matt Wilburn for technical editing of this report and David MacPherson for the quality reviews of the calculation packages and this report.

Microscopy work was performed at the Radiochemical Processing Laboratory Quiet-Suite at Pacific Northwest National Laboratory.

Acronyms and Abbreviations

AEA	alpha energy analysis
BDEF	backpulse dead-end filter (system)
CWF	clean water flux
DEF	dead-end filtration
EDS	X-ray energy dispersive spectroscopy
HAADF	high-angle annular dark-field
HDPE	high-density polyethylene
ICP-OES	inductively coupled plasma optical emission spectroscopy
IX	ion exchange
LAW	low-activity waste
MFC	mass flow controller
NQAP	Nuclear Quality Assurance Program
PNNL	Pacific Northwest National Laboratory
RPL	Radiochemical Processing Laboratory
SAED	selected area electron diffraction
SEM	scanning electron microscopy
STEM	scanning transmission electron microscopy
TEM	transmission electron microscopy
TMP	transmembrane pressure
TRU	transuranic
TSCR	Tank Side Cesium Removal
WRPS	Washington River Protection Solutions
WTP	Waste Treatment and Immobilization Plant

Contents

Summary ii
Acknowledgments iii
Acronyms and Abbreviations iv
Contents v
1.0 Introduction 1.1
2.0 Quality Assurance 2.1
3.0 Test Conditions 3.1
3.1 BDEF Filtration 3.1
3.1.1 Backpulse Dead-End Filter System Description 3.1
3.1.2 System Operation during Testing 3.3
3.2 Feed Composite and Dilution 3.5
3.3 Feed Temperature Control 3.6
3.4 Sample Analysis 3.7
4.0 Results 4.1
4.1 Dilution Process Results 4.1
4.1.1 Clean Water Flux 4.1
4.2 Waste Filtering 4.2
4.3 Final CWF 4.10
4.4 Analytical Results 4.11
4.4.1 Diluted and Composited AN-107 Supernatant Tank Waste Analysis 4.11
4.4.2 Total Alpha Energy Analysis 4.12
4.4.3 Rheology Analysis of Filtered and Cesium Decontaminated AN-107 Supernatant Tank Waste 4.12
4.5 Microscopy Solids Analysis 4.13
4.5.1 SEM Analysis of AN-107 Solids 4.14
4.5.2 Solution 1 ..... 4.15
4.5.3 Solution 3 ..... 4.16
4.5.4 Solution-4 ..... 4.17
5.0 Conclusions 5.1
6.0 References 6.1
Appendix A – BDEF Piping and Instrumentation Diagram A.1
Appendix B – Feed Bottle Composite and Dilution B.1
Appendix C – Total Alpha Analysis for Filtration Permeate Samples C.1
Appendix D – ICP-OES Analysis for Diluted and Composited 241-AN-107 Supernatant D.1
Appendix E – Backpulsed Solids from AN-107 Characterization with Scanning Transmission Electron Microscopy E.1

Figures

Figure 3.1. BDEF system installed in hot cell. HTX = heat exchanger. 3.2
Figure 3.2. (a) Filter housing schematic (note that the 6610 series filter was welded to a 3/8-in. pipe fitting, making the configuration similar to the 6480 series illustrated here); (b) photo of modified filters with filter housings removed. (Mott 6480 line filter schematic from https://mottcorp.com.) 3.3
Figure 3.3. AN-107 temperature in the trough heat exchanger. 3.6
Figure 3.4. AN-107 temperatures in the BDEF recirculation loop (TE-101) and clamshell (TE-102, TE-103). 3.7
Figure 3.5. Concentrated solids after centrifuging in hot cell. 3.8
Figure 3.6. Concentrated solids in fume hood after centrifuging. 3.9
Figure 3.7. Solids being collected from DEF membrane in the Shielded Analytical Laboratory. 3.10
Figure 4.1. CWF measurements for Media Grade 5 BDEF at 2.57 mL/min (0.065 gpm/ft^2) permeate rate (nominal) before testing. (Dashed line is average pressure over the 10-minute period.) 4.2
Figure 4.2. Filter differential pressure and MFC flow rate during filtering operations. 4.4
Figure 4.3. Material plating out on BDEF system surfaces; (Top) HDPE feed bottles; (Left) Glass flow meter; (Right) Permeate line to product bottle (Tygon 2375) 4.5
Figure 4.4. AN-107 filter resistance and permeate density during filtration process. 4.6
Figure 4.6. Fit to initial fouling experimental data using classical fouling mechanisms. 4.9
Figure 4.7. Fit to "5th" fouling section prior to Backflush 1 experimental data using classical fouling mechanisms. 4.10
Figure 4.11. Initial, post 0.1 M NaOH filter clean, and post 0.5 M oxalic acid clean CWF. 4.11
Figure 4.7 SEM image and EDS maps of Mn-Fe phases found in the AN-107 Solids sample. 4.14
Figure 4.8 Further SEM images of Mn-Fe particles in the AN-107 Solids sample. 4.15
Figure 4.9 SEM image of large particles observed in AN-107 Solution-1 ..... 4.15
Figure 4.10 SEM and EDS analysis of a possible mixed salt sodium nitrate/fluoro-phosphate phase with particles of the Mn-Fe phase attached to the crystal surfaces in AN-107 Solution-1. ..... 4.16
Figure 4.11 Different morphologies of a Fe-rich phase found in Solution-3. ..... 4.16
Figure 4.12 SEM image and EDS maps of Mn-Fe phase in Solution-3 ..... 4.17
Figure 4.13 SEM image of particles observed in Solution-4. ..... 4.18
Figure 4.14 Low magnification TEM image of Solution 4 showing the same type of morphology as shown in Figure 4.13. ..... 4.18
Figure E.1 XRD Results from Reynolds and co-workers on AN-107 (Reynolds et al., 2012) reporting the occurrence of nitratine ($NaNO_3$), sodium nitrite ($NaNO_2$), dawsonite, sodium oxalate ($C_2Na_2O_4$), and thermonatrite; however, no indication of phosphfluorite minerals or trona was in these XRD results. E.2
Figure E.2 Results from the solids characterization of AN-107 reported by Martin and co-workers (Martin, 2004). E.2
Figure E.1 SEM Image and EDS maps of Mn-Fe phases found in the AN-107 Solids sample. E.4

Figure E.2 Further SEM images of Mn-Fe particles in the AN-107 Solids sample.....E.5
Figure E.3 SEM image of large particles observed in AN-107 Solution-1.....E.5
Figure E.4 SEM and EDS analysis of a possible mixed salt sodium nitrate/fluoro-phosphate phase with particles of the Mn-Fe phase attached to the crystal surfaces in AN-107 Solution-1.....E.6
Figure E.5 Different morphologies of a Fe-rich phase found in Solution-3. .....E.7
Figure E.6 SEM image and EDS maps of Mn-Fe phase in Solution-3.....E.7
Figure E.7 SEM image of particles observed in Solution-4.....E.8
Figure E.8 Low-magnification TEM image of Solution-4 showing the same type of morphology as shown in Figure E.7. .....E.8
Figure E.9 HAADF image and STEM-EDS maps of sodium-rich particles, possibly sodium oxalate in Solution-3. .....E.9
Figure E.10 HAADF image and STEM-EDS analysis of a particle agglomerate consisting of possibly silicon but had a noticeable quantity of uranium. E.10
Figure E.11 TEM images and electron diffraction patterns of a particle agglomerate in Solution-3. .....E.11
Figure E.12 TEM images of particles observed in the AN-107 Solution-3 sample.....E.11
Figure E.13 TEM analysis and insert SAED of a particle observed in the Solution-3 sample. E.12
Figure E.14 TEM image and electron diffraction patterns obtained from a particle in Solution-3. .....E.12
Figure E.15 TEM image and STEM-HAADF image together with an electron diffraction pattern and a series of STEM-EDS elemental maps of a particle consisting of an aluminosilicate and a titanium oxide phase.....E.13
Figure E.16 STEM-EDS of particles from AN-107 Solution-3 and shown in Figure E.11.....E.14
Figure E.17 STEM EDS analysis of possible oxalate phase. The Mg, Al, Si, and Ca were minor components. The Ca appeared to be on the surface of the particle. E.14
Figure E.18 STEM HAADF image and STEM-EDS maps of an aluminosilicate particle observed in Solution-3.....E.15
Figure E.19 STEM image and STEM-EDS maps of possible sodium carbonate (Na_2CO_3) particle.....E.16
Figure E.20 STEM-HAADF image and STEM-EDS maps of a carbon-based particle that was carrying other minor phases. E.16
Figure E.21 STEM-HAADF image and STEM EDS analysis of possible Mg-phosphate phase. E.17
Figure E.22 STEM-HAADF and STEM-BF image together with STEM-EDS maps of a Na-C-N phase. Minor particles containing P, Al, and Mg were also present and attached to this larger particle.....E.18
Figure E.23 TEM image and a diffraction pattern of particles from the Solution-4 sample that has been matched to reflections from trona and dawsonite. E.18
Figure E.24 STEM-EDS elemental maps of the large particle agglomerates containing C, Na, and O as major elements, as well as minor Al and Fe. E.19
Figure E.25 TEM images and ring diffraction pattern from particles found in the Solution-4 sample. E.20
Figure E.26 STEM-EDS elemental maps of particles found in the Solution-4 sample dominated by C, O, and Na with Al and Fe also. E.21
Figure E.27 TEM image, insert SAED pattern, and STEM-HAADF image of particle agglomerates found in Solution-4. .....E.21

Figure E.28 STEM-EDS elemental maps of particle agglomerate found in Solution-4. .....E.22

Tables

Table 3.1. Mass balance – BDEF. 3.5
Table 3.2. As-received samples. 3.5
Table 4.1. System timeline. 4.3
Table 4.2. Test parameters prior to backpulsing. 4.4
Table 4.4. Post filtration density measurements of product bottles. 4.7
Table 4.3. Filtration regime exponent n and blocking parameter σ. 4.8
Table 4.5. ICP-OES results of diluted and composited AN-107 supernatant tank waste. 4.11
Table 4.6. AEA for permeate samples. 4.12
Table 4.7. Viscosity results of filtered and Cs decontaminated sample. 4.13
Table 4.8. Microscopy Sample IDs 4.13
Table 4.9. Sample Analysis Summary 4.13
Table E.1 Electron diffraction from Figure E.15 E.13
Table E.2 Electron diffraction from Figure E.9D with possible matches to trona ($Na_3C_2O_8H_5$) and dawsonite ($NaAlCO_5H_2$) E.19
Table E.3 Electron diffraction from E.9D with possible match to trona and dawsonite E.20

1.0 Introduction

The U.S. Department of Energy's Hanford Site houses 56 million gallons of highly radioactive tank waste generated from plutonium production from 1944 to 1988 (Gerber 1992). The supernatant waste, currently stored in underground tanks, is intended to be vitrified following filtration and ^{137}Cs removal at the Waste Treatment and Immobilization Plant (WTP) Pretreatment Facility. Because the WTP Pretreatment Facility is not currently operational, ^{137}Cs will be removed from low-activity waste (LAW) vitrification feeds using the tank side cesium removal (TSCR) system that will filter and then remove cesium using ion exchange (IX) from tank waste supernatant to support transferring the TSCR-processed waste directly to the WTP LAW Facility. The TSCR system is skid-mounted and employs two key technologies: (1) dead-end filtration (DEF) for solids removal, which is necessary to protect the functionality of the IX columns, and (2) IX processing for cesium removal.

A small-scale test platform was established in 2017 to demonstrate these processes in the Radiological Processing Laboratory (RPL) at Pacific Northwest National Laboratory (PNNL).

Hanford waste tank 241-AN-107 (herein AN-107) is anticipated to be a future feed to TSCR. The purpose of this filtration testing was to (a) demonstrate DEF of an actual waste feed at reduced temperature (16 °C) to obtain prototypic TSCR flux rates and identify issues that may impact filtration and (b) provide feed for the IX-unit operation (also part of the test platform). Approximately 9 L of AN-107 tank waste supernatant was delivered to PNNL in thirty-six 250-mL bottles. The thirty-six AN-107 sample bottles consisted of six sets of six samples with each set pulled from a unique tank sampling level. Prior to testing, samples from each level were composited and diluted to 5.5 M Na with process water sourced from the Columbia River to provide nominally level-independent feed for DEF and IX testing.

The AN-107 tank waste was filtered at reduced temperature (16 °C) to mimic the low end of temperatures that tank AN-107 can experience during the winter and spring months. Note that the AN-107 sample feed temperature was not controlled after the feed samples were collected from the tank by WRPS and stored at the PNNL hot cell ambient temperature (~25 °C) from delivery until approximately 1 week prior to filtration at PNNL. The sodium content of the as-received AN-107 samples was expected to range from 8.9 to 9.1 M Na (Urie et al. 1999), and as such, AN-107 level-composites were diluted with Columbia River water to reduce their sodium molarity as has been done in previous DEF and IX test campaigns (e.g., see Allred et al. 2023a,b).

The current filtration testing was conducted using a purpose-built backpulse dead-end filter (BDEF) system, which was designed to mimic planned filtration to be used in the full-scale TSCR system. This equipment was used in fiscal years (FYs) 20, 21, 22, and 23, and is described in Allred et al. (2020).

2.0 Quality Assurance

This work was performed in accordance with the PNNL Nuclear Quality Assurance Program (NQAP). The NQAP complies with DOE Order 414.1D, *Quality Assurance*, and 10 CFR 830, Subpart A, *Quality Assurance Requirements*. The NQAP uses NQA-1-2012, *Quality Assurance Requirements for Nuclear Facility Applications*, as its consensus standard and NQA-1-2012, Subpart 4.2.1, as the basis for its graded approach to quality (ASME 2012).

The NQAP works in conjunction with PNNL's laboratory-level Quality Management Program, which is based upon the requirements as defined in the DOE Order 414.1D, *Quality Assurance*, and 10 CFR 830, Subpart A, *Quality Assurance Requirements*.

The work described in this report was assigned the technology readiness level 5. All staff members contributing to the work received proper technical and quality assurance training prior to performing quality-affecting work.

3.0 Test Conditions

In October 2023, WRPS provided 36 supernatant samples (~250 mL each) from tank AN-107 in two batches. These samples were taken at six depths (25, 74, 123, 172, 221, and 270 in. below the liquid surface level[1]) in groups of six and provided to PNNL for filtration testing. At the RPL, the as-received AN-107 samples from each level were composited to provide nominally level-independent feed for filtration and IX testing. The bottles of composited AN-107 tank waste were chilled (16 °C setpoint) for approximately 1 week prior to testing. Filtration testing of the tank waste used a Mott Model 6610 (Media Grade 5) sintered 316L stainless steel line filter with a 0.317-in. porous diameter, 1.463-in. porous length, and 1.51-in.^{2} filter area with porous end cap. Filtration testing of the AN-107 tank waste began on November 26, 2023.

3.1 BDEF Filtration

3.1.1 Backpulse Dead-End Filter System Description

The filtration system is the same system that was used in FY23 (Allred et al. 2023a,b), again using the trough heat exchanger to keep all the feed at the setpoint temperature until it was added to the BDEF system. The feed bottles were stored in the trough heat exchanger with a cover until the feed was transferred to the BDEF system.

Once the feed was added to the BDEF, the existing heat exchanger kept the feed at the setpoint temperature in the reservoir and in the BDEF recirculation loop. The filter housing clamshell heat exchanger kept the feed at the setpoint temperature as it exited the recirculation loop until it was filtered. After filtration, the temperature was no longer controlled. A piping and instrumentation diagram is provided in Appendix A. Figure 3.1 shows a photograph of the BDEF system installed in the RPL Shielded Analytical Laboratory hot cell.

[1] Per RPP-PLAN-65668, *Tank 241-AN-107 Large Volume Sample Collection to Support Platform Testing, Phase 1, FY23*, and RPP-PLAN-65669, *Tank 241-AN-107 Large Volume Sample Collection to Support Platform Testing, Phase 2, FY23*.

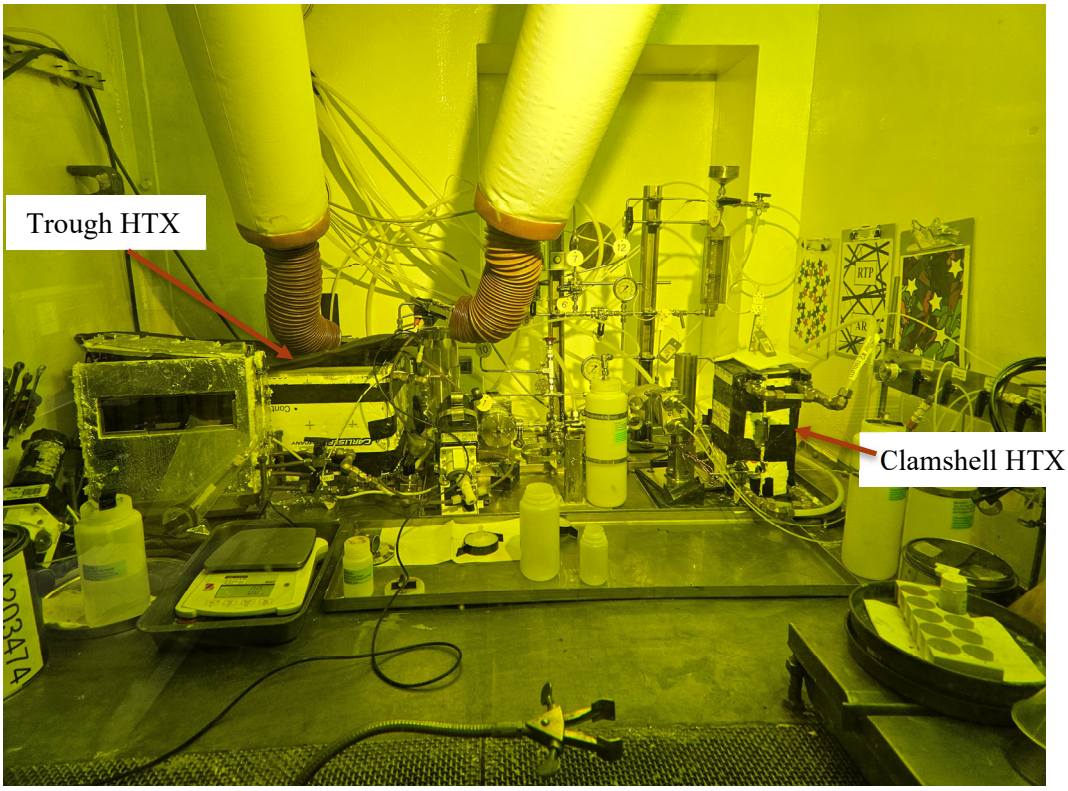

Figure 3.1. BDEF system installed in hot cell. HTX = heat exchanger.

The BDEF system is composed of a slurry recirculation loop, a filter assembly, and a permeate system. The main recirculation loop consists of a 1-L stainless steel container (Eagle, EPV1A), a low-shear quaternary diaphragm pump (Quattro Flow QF150), a heat exchanger, and a throttle valve. The pump speed is controlled by a variable frequency drive that is located outside the hot cell. The slurry flow rate and pressure are controlled by adjusting the pump variable frequency drive (pump speed control) and throttle valve. The recirculation loop provides mixed, pressurized feed to the filter assembly. During the testing described in this report, the slurry temperature was controlled at a 16 °C setpoint.

The filter assembly receives pressurized slurry from the slurry recirculation loop. The filter assembly is composed of a filter, a Rosemount differential pressure transducer, and a flush valve (V3 in Appendix A). The flush valve is actuated during backpulse operations to clear solids off the filter and out of the system.

The permeate system receives permeate produced by the filter assembly. The permeate flow rate is controlled with a mass flow controller (MFC), which can control feed in the range of 0.15 to 0.33 L/hour. (These rates equate to allowable filter areas of 1.5 to 3.3 $in.^2$ assuming flux of 0.065 gpm/ft^2.) The MFC measures flow rate and density of the permeate, and a glass flowmeter is provided as a secondary flow rate measurement device. The permeate system can also perform a backpulse function. Pressurized air can be introduced into the backpulse chamber and used to force permeate (or other fluids) backward through the filter and out of the system.

The Mott 6610 filter used in testing is cylindrical, with dimensions of 0.317-in. diameter × 1.5-in. length and a filtration area of 1.51 $in.^2$. The filter element is fabricated from a seamless sintered stainless-steel tube that is a closed/dead-end porous tube (with a porous end cap); the open end is welded to a pipe-reducing bushing. At 0.065 gpm/ft^2, the rate of filter processing is 3.7 L of feed per 24-hour day. Figure 3.2 shows a schematic of the filter assembly and a photo of the filter.

(a)

(b)

Figure 3.2. (a) Filter housing schematic (note that the 6610 series filter was welded to a 3/8-in. pipe fitting, making the configuration similar to the 6480 series illustrated here); (b) photo of modified filters with filter housings removed. (Mott 6480 line filter schematic from https://mottcorp.com.)

3.1.2 System Operation during Testing

The steps used to test the AN-107 waste samples are outlined below.

1. Compositing and dilution of AN-107 feed: Six sets of ~1.5 L of waste were collected from six unique sampling depths in tank AN-107. To provide level-independent feed for BDEF and IX testing, samples from each set were composited with each other to minimize set-to-set variation in physical/chemical properties. Twelve separate, nominally 1.2 L, composites were created by combining subsets of the as-received waste into 1.5 L feed-bottles and diluting with sufficient process water sourced from the Columbia River to lower the sodium molarity from 9.1 to 5.5 M Na (Urie et al, 1999). Make-up of each individual composite used the entire volume of three as-received AN-107 waste jars. To minimize differences in the composites resulting from sampling locations, jars were selected from sampling depths of 25, 123, and 270 inches for six of the twelve feeds. The remaining feeds used jars derived from sampling depths 74, 172, and 221 inches. Appendix B provides a detailed tabulation of how the 36 as-received sample jars were partitioned into the twelve feed composites bottles.

The AN-107 compositing strategy yielded two sets of composites with distinct sampling locations, namely six Set "A" composites derived from jars taken at 25-, 123-, and 270-inch depths and six Set "B" composites derived from jars taken at 74-, 172-, and 221-inch depths. While it would have been possible to create twelve nominally identical composites by sub-sampling (or more precisely, halving) the contents of as-received jars, jar sub-sampling would have increased the complexity of hot cell waste handling operations, which in turn, could have increased the potential for sample handling errors. Given the high-value nature of the AN-107 waste samples and the general inability to recover from compositing errors, jar subsampling was forgone, and the simpler (Set "A" and "B") strategy described above employed. AN-107 waste compositing and dilution activities yielded ~14 L of diluted (5.5 M Na) waste for BDEF performance evaluations. The diluted AN-107 was stored at the ambient RPL hot cell temperature, ~25 °C, until 1 week before the filtration campaign began.

2. Approximately 1 week prior to filtration, the composited and diluted AN-107 feeds were chilled to 16 °C and held for approximately 1 week at the reduced temperature until testing.

3. The clean water flux (CWF) measurement served as a system leak test and provided a baseline measurement of the filter resistance and was conducted at nominal test conditions of 0.065 gpm/ft^2 with 0.01 M NaOH inhibited water for approximately 10 minutes.

4. Filtration of the 5.5 M Na AN-107 feed was performed using a Mott Grade 5 sintered metal filter at a targeted flux of 0.065 gpm/ft^2. The targeted flux is based on the scaled flux detailed in RPP-CALC-62496 Rev. 03 "TSCR Filter Sizing" (5.0 gpm through 77 ft^2 of Mott sintered metal filter [0.065 gpm/ft^2]). Filtration was performed at a targeted temperature of 16 °C. Filter resistance as a function of time was measured; filter backflushing ("backpulsing") was implemented when the filter differential pressure increased to 2 psi as specified in RPP-CALC-62496 Rev. 03. Backflush solutions were collected and analyzed.

5. The filter was cleaned using a prototypic TSCR protocol by soaking it in 0.1 M NaOH for a minimum of 2 hours. For the present AN-107 testing, filter cleaning was unable to restore the filter flux performance, so the filter cleaning process was repeated with 0.5 M oxalic acid.

6. Filtered permeate from testing was collected and retained for use as feed for subsequent IX testing. Temperature control (to 16 °C) of the filtered samples was maintained to the best extent practical, such that filtered permeates were returned to the trough after collection in any given bottle was complete.

7. After cleaning, the BDEF was rinsed and another CWF test was executed on the filter.

8. The BDEF system was laid-up for storage.

Table 3.1 provides a mass balance for BDEF testing. A total of 17,629 g of AN-107 supernatant was added to the BDEF system during testing, and a total of 17,598.4 g was removed. The missing mass (~30.6 g) is due to evaporation and material that wets the inside of the BDEF system. It is not recoverable and represents less than 0.2% of the initial feed.

Table 3.1. Mass balance – BDEF.

Description	In (g)	Out (g)
Decanted supernatant filtration	17,629	
Product to IX		17,115.5
Permeate samples		19.3
Backpulse samples		59.3
Drained from BDEF		404.3
Total	17,629	17,598.4

3.2 Feed Composite and Dilution

Tank waste supernatant was sampled from six unique liquid levels of tank AN-107, with six 250-mL bottles received from each sample level for a total of 36 bottles. The samples were taken from tank liquid depths of 25, 74, 123, 172, 221, and 270 in. as shown in Table 3.2. Liquid properties such as viscosity, sodium molarity, and density can vary based on depth beneath the liquid surface due to stratification. A density measurement was taken from one bottle of 25 in., 123 in., and 270 in. depth prior to the compositing process. Three receipt bottles from three different sampling locations were combined into single 1.5-L filtration feed bottles for ~700 mL of composited waste in each feed bottle. Process water sourced from the Columbia River – a practice used in TSCR – was then added to each filtration feed bottle to dilute the wastes from ~9.1 to 5.5 M Na. Diluted bottle composition details can be found in Appendix B.

Table 3.2. As-received samples.

Sample Location (depth below liquid surface, in.)	Receipt Sample Jar ID		Density (g/mL)
25	7AN-23-01	7AN-23-02	1.426
	7AN-23-03	7AN-23-04	
	7AN-23-05	7AN-23-06	
74	7AN-23-07	7AN-23-08	n/m
	7AN-23-09	7AN-23-10	
	7AN-23-11	7AN-23-12	
123	7AN-23-13	7AN-23-14	1.426
	7AN-23-15	7AN-23-16	
	7AN-23-17	7AN-23-18	
172	7AN-23-19	7AN-23-20	n/m
	7AN-23-21	7AN-23-22	
	7AN-23-23	7AN-23-24	
221	7AN-23-25	7AN-23-26	n/m
	7AN-23-27	7AN-23-28	
	7AN-23-29	7AN-23-30	
270	7AN-23-31	7AN-23-32	1.424
	7AN-23-33	7AN-23-34	
	7AN-23-35	7AN-23-36	

n/m – not measured

3.3 Feed Temperature Control

Figure 3.3 shows the temperature profile of the chilled AN-107 filtration feed prior to entering the BDEF system. The feed was held at a 16 °C setpoint temperature beginning on 11/16/2023 – 10 days leading up to the filtration test – and continued to be maintained at that setpoint throughout the filtration process. A 100-ohm platinum resistance temperature detector probe (TE-104) was submerged into a feed bottle in the trough heat exchanger to measure feed temperature throughout the chilling. TE-104 was held in place using a lid with a feedthrough fastened to a feed bottle to allow TE-104 to be submerged while mitigating spill risk.

The feed trough temperature was maintained within the range of 16 °C ± 2.2 °C throughout filtration except for two spikes in temperature occurring on 11/29/23. Each of these recorded deviations in temperature are concurrent with movement of TE-104 from one feed bottle to a different one – a common practice when the temperature-monitored feed bottle needs to be removed from the trough to be fed into the BDEF system.

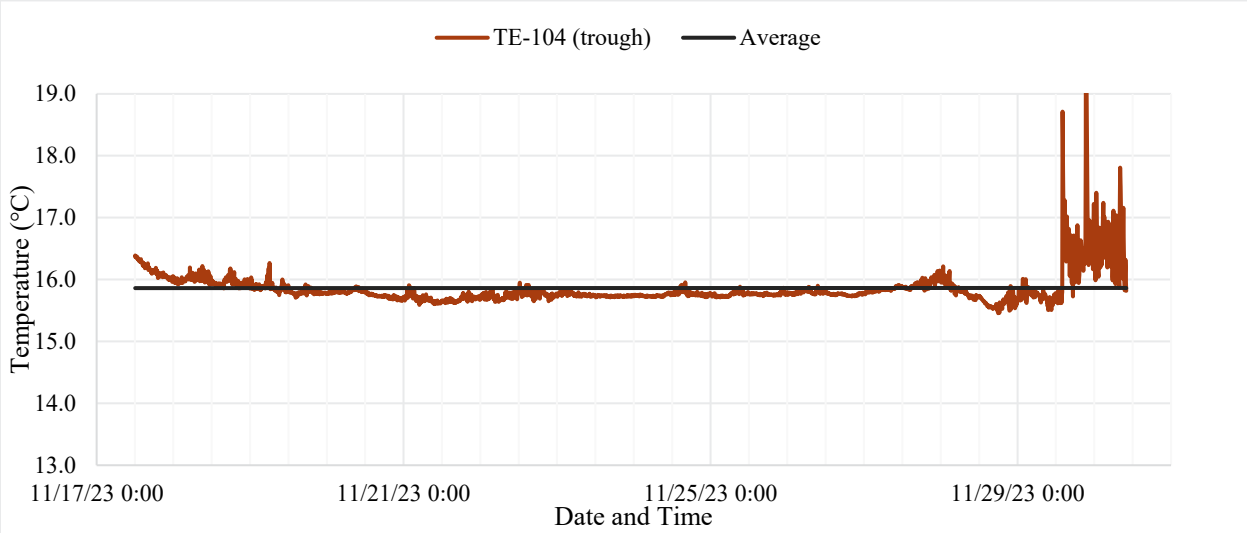

Figure 3.3. AN-107 temperature in the trough heat exchanger.

Figure 3.4 shows the temperature of the AN-107 slurry in the BDEF recirculation loop as reported by TE-101 throughout testing. Overlain in the same figure are the slurry stream temperatures immediately upstream and downstream of the filter measured by thermocouples TE-102 and TE- 103, respectively, contained within the clamshell heat exchanger. The system temperatures remained within 16 °C ± 2.2 °C until immediately following the backpulse completed on 11/30/23 at 0935. During the backpulse process, the slurry in the slurry feed reservoir experienced warming as the recirculation pump was turned off and the return valve to the reservoir was closed. The slurry within the reservoir was unable to recirculate through the in-line chiller during the backpulse process, which typically lasts several minutes. The BDEF recirculation loop and filter experience a sharp increase in temperature when permeate flow continues after the backpulse as the stagnated slurry began to flow through the filtration system again. Filtration ended immediately after the backpulse due to issues reestablishing filter flux.

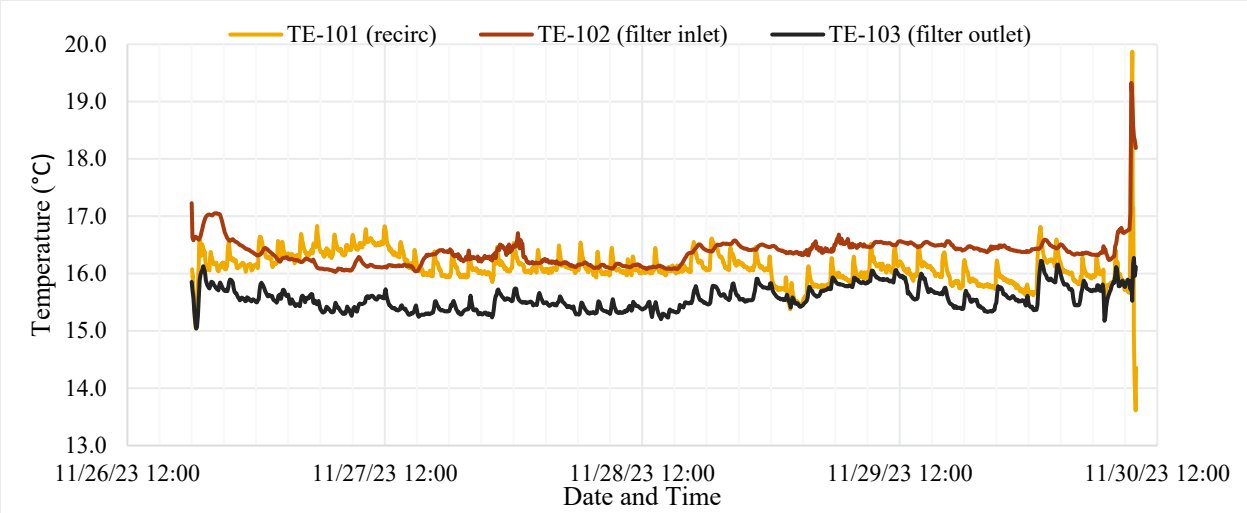

Figure 3.4. AN-107 temperatures in the BDEF recirculation loop (TE-101) and clamshell (TE-102, TE-103).

3.4 Sample Analysis

Three permeate samples were collected (TI-153-P1, TI-153-P2, TI-153-P3) after approximately 1/3, 2/3, and all the AN-107 feed had been filtered. These samples were submitted for total alpha analysis to determine the transuranic (TRU) content of the filtered permeate.

Backpulse concentrates were retained and kept separate (TI-153-S1, TI-152-S3, TI-153-S4). Upon completion of filtration testing, the solids were concentrated as shown in Figure 3.5. To concentrate solids, solution collected was centrifuged at 2,500 rpm for 15 minutes. The bulk amount of the supernatant was decanted and the solids from the centrifuge tubes were suspended and combined. The concentrated solution was again centrifuged at 2,500 rpm for 15 minutes. More supernatant was removed, the solids suspended, and the solution transferred out of the hot cell. Once removed from the hot cell, the concentrated solution was transferred to the smaller 15-mL centrifuge tube and the solids spun down for 2 minutes at 3,000 rpm. Additional supernatant was removed to reduce the dose of the sample prior to sending it to the microscopy staff. Figure 3.6 shows the solids that were collected from the backpulsed solution after centrifuge and decant iterations.

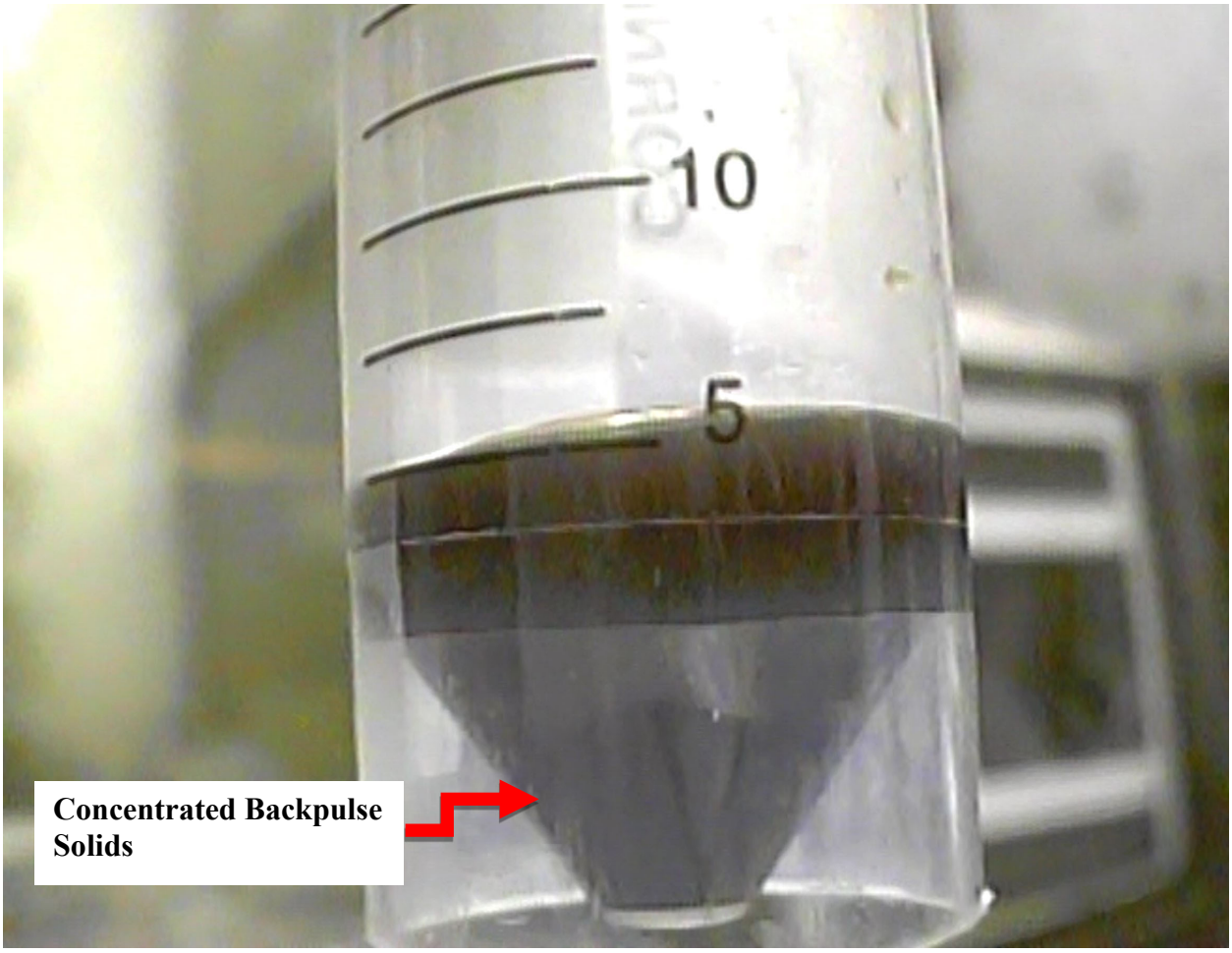

Figure 3.5. Concentrated solids after centrifuging in hot cell.

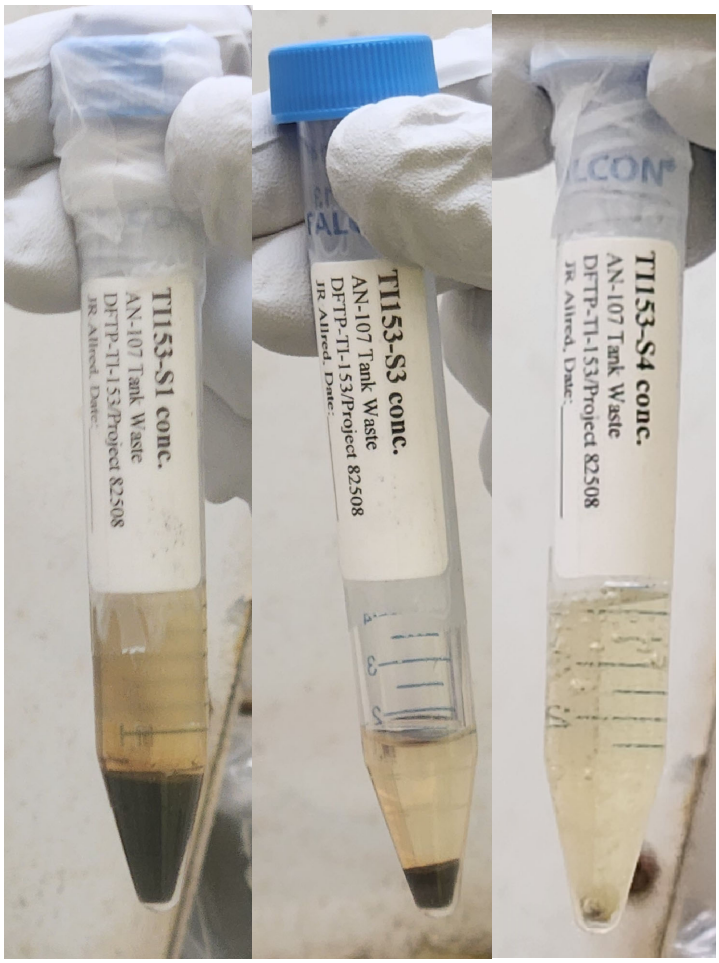

Figure 3.6. Concentrated solids in fume hood after centrifuging.

The AN-107 feed that was unable to be filtered through the BDEF system was transferred to a DEF system detailed in Geeting et al. 2018. A Mott stainless steel 70 mm disc filter Media Grade 5 membrane was installed, and AN-107 feed was pumped into the DEF reservoir (404.3 g). The filter plugged after filtering 118.9 g of the drained BDEF feed at up to 50 psig. The remaining AN-107 feed in the DEF reservoir was pumped back out and split for centrifuge and decant. That clarified feed was sent to the IX system separately for Cs- removal. The solids remaining on the DEF membrane, shown in Figure 3.7, were collected into a vial labeled “TI-153-DEF-Solids-1” and sent for microscopy analysis.

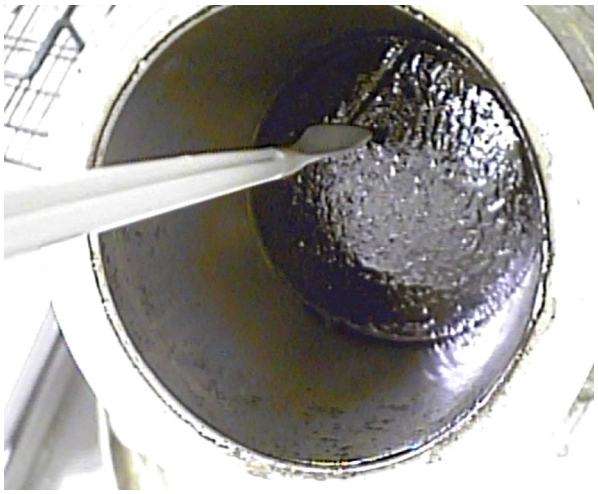

Figure 3.7. Solids being collected from DEF membrane in the Shielded Analytical Laboratory.

4.0 Results

4.1 Dilution Process Results

The density of samples taken from composited and diluted bottles BDEF-AN7-3 and BDEF-AN7-12 was measured and averaged. Density was measured using a 10-mL Class A volumetric flask and an analytical balance. The average density was measured to be 1.254 g/mL at an ambient cell temperature of 24.5 °C. Inductively coupled plasma-optical emission spectroscopy (ICP-OES) results of post-filtration samples showed an average Na concentration of 5.53 M Na[1].

4.1.1 Clean Water Flux

The objective of the CWF was to assess the state of the system at the start of testing to ensure a uniform basis for comparing different filtration trials, and in particular to ensure that the system was "clean" at the start of testing. Figure 4.1 shows the initial CWF at 16.0 °C using 0.01 M NaOH with the Media Grade 5 stainless steel BDEF filter. The CWF tests were conducted at ambient cell temperature at a nominal permeate flow rate of 2.57 mL/min (0.065 gpm/ft^2). The transmembrane pressure (TMP) averaged 0.127 psid in the initial CWF with an average filter resistance of 1.80×10^{10} m^{-1}. Resistance, R [m^{-1}], is calculated via Darcy's law:

$$Q = \frac{PA_t}{\mu R} \tag{4.1}$$

where Q is the volumetric flow rate [m^3/s], P is the TMP [Pa], A_t is the total filter area [m^2] [9.74×10^{-4} m^2], and μ is the filtrate dynamic viscosity [Pa·s] (4.887 mPa s, as measured at 16.0 °C – see Section 4.5.3 for additional details). For the present use, Eq. 4.1 is rearranged to allow calculation of filter resistance by:

$$R(t) = \frac{P(t)A_t}{\mu Q(t)} \tag{4.2}$$

Prior CWF results on the BDEF system with this filter ranged from 0.015 to 0.2 psid TMP (Allred et al. 2022). These values all are likely within the accuracy of the CWF measurement and represent a relatively clean filter. Estimates of the resistance for the Mott 6610 series Grade 5 are on the order of 2×10^{10} m^{-1}. `The average TMP of 0.127 psid (shown in Figure 4.1) during the CWF indicates a lack of fouling on the filter (due to residual solids in the system). As such, these results indicate an overall clean system at the start of testing.

[1]Per DFTP-RPT-042, *Reduced Temperature Cesium Removal from AN-107 Using Crystalline Silicotitanate* (report in preparation)

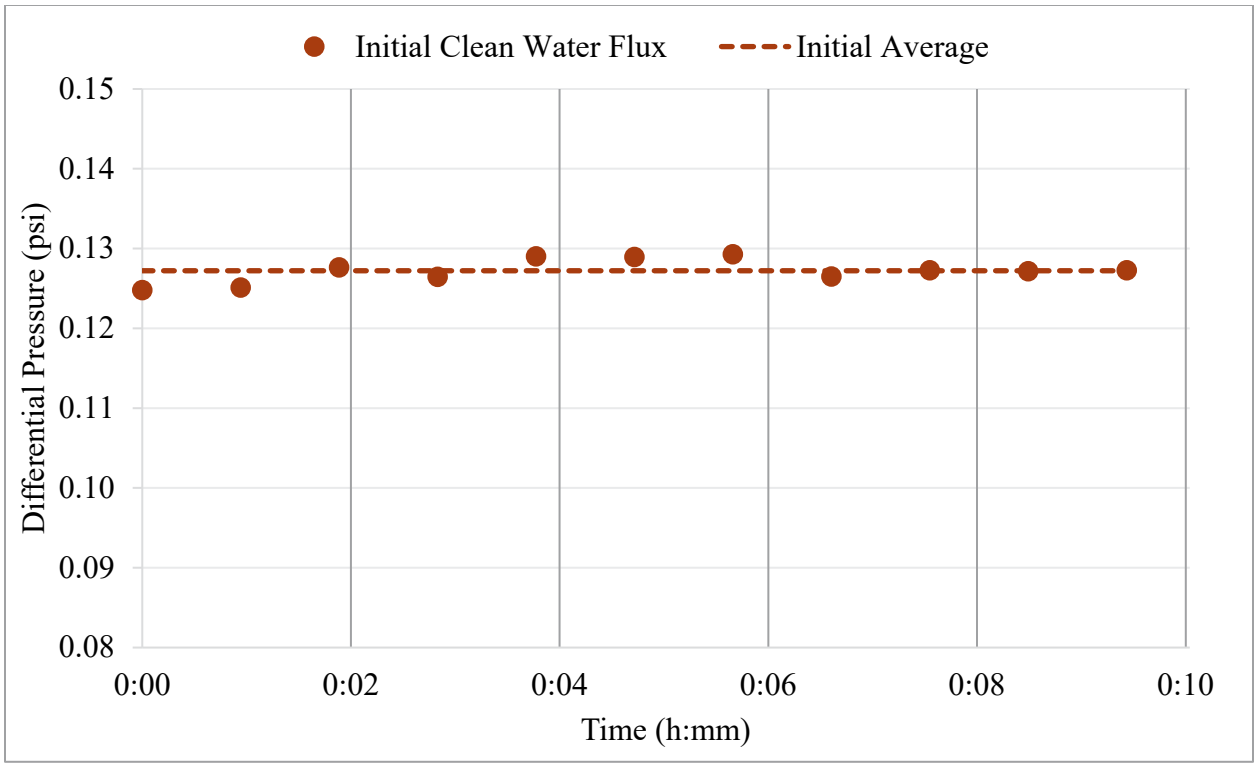

Figure 4.1. CWF measurements for Media Grade 5 BDEF at 2.57 mL/min (0.065 gpm/ft^2) permeate rate (nominal) before testing. (Dashed line is average pressure over the 10-minute period.)

4.2 Waste Filtering

Each BDEF feed bottle was positioned in the trough heat exchanger to maintain feed temperature control (16 ± 2.2 °C). Feed was then transferred into the BDEF reservoir via a metering pump until approximately 2 in. of AN-107 solution remained in the feed bottle. The remaining "bottoms" from each feed bottle were consolidated and fed into the system toward the end of the filtration process. The filtration rate was controlled via an MFC set at 2.57 mL/min (0.065 gpm/ft^2). Slurry recirculation line pressure was kept between 20 and 25 psi, with adjustments to recirculation backpressure made to correct for pressure deviations outside this range. One backpulse was performed during filtration testing while consolidated bottoms were being filtered. The 2-psid TMP limit (the threshold to indicate that a backpulse was needed) was reached during the filtration of the second bottle of consolidated "bottoms".

Table 4.1 provides a timeline for the filtration testing, indicating feed bottle change, permeate bottle change and process liquid flow. Note that the filtration of feed bottle "bottoms" began after 12.43 m^3/m^2 of feed had been filtered.

Testing was started on the afternoon of November 26. After a quick increase in TMP from 0.171 to 0.215 psid, TMP increased steadily from 0.215 psid until it reached 0.335 psid at 7.64 m^3/m^2. A sharp increase in TMP from 0.335 to 0.391 psid was observed between 7.64 and 7.67 m^3/m^2 followed by decreasing TMP until 0.253 psid at 8.815 m^3/m^2. TMP then increased steadily to 0.350 psid at 12.43 m^3/m^2 before TMP began to increase significantly faster, coinciding with the first

introduction of consolidated bottoms into the feed. TMP reached the 2-psid limit at 13.79 m^3/m^2, and a backpulse was performed. See

Table 4.2 for the system parameters prior to backpulse.

Table 4.1. System timeline.

Date	Time	Volume Filtered (m^3/m^2)	Event
26-Nov	18:02	0.00	Filtration started with BDEF-AN7-1, dewatering into product bottle IX-AN7-1
	19:38	0.25	Feed bottle switch to BDEF-AN7-2
27-Nov	2:19	1.31	Feed bottle switch to BDEF-AN7-3
	2:58	1.41	Product bottle switch to IX-AN7-2
	8:51	2.34	Feed bottle switch to BDEF-AN7-4
	11:50	2.81	Product bottle switch to IX-AN7-3
	16:27	3.54	Feed bottle switch to BDEF-AN7-5
	19:55	4.09	Product bottle switch to IX-AN7-4
	22:20	4.47	Feed bottle switch to BDEF-AN7-6
28-Nov	4:07	5.39	Product bottle switch to IX-AN7-5
	6:05	5.70	Feed bottle switch to BDEF-AN7-7
	11:00	6.47	Feed bottle switch to BDEF-AN7-8
	12:20	6.68	Product bottle switch to IX-AN7-6
	18:17	7.62	Feed bottle switch to BDEF-AN7-9
	20:24	7.96	Product bottle switch to IX-AN7-7
29-Nov	1:46	8.80	Feed bottle switch to BDEF-AN7-10
	4:45	9.28	Product bottle switch to IX-AN7-8
	9:07	9.97	Product bottle switch to BDEF-AN7-11
	12:48	10.55	Product bottle switch to IX-AN7-9
	15:54	11.04	Feed bottle switch to BDEF-AN7-12
	21:07	11.86	Product bottle switch to IX-AN7-10
	21:20	11.90	TE-104 moved to empty BDEF-AN7-5
30-Nov	0:44	12.43	Feed bottle switch to BDEF-AN7-2 (consolidated bottoms bottle)
	4:55	13.10	Feed bottle switch to BDEF-AN7-10 (consolidated bottoms bottle)
	5:16	13.15	Product bottle switch to IX-AN7-11
	6:57	13.42	Backpulse chamber filled from slurry reservoir
	8:02	13.57	Heel from BDEF-AN7-2 and BDEF-AN7-10 (consolidated bottoms bottles) poured into slurry reservoir
	9:27	13.79	Differential pressure reached 2.0 psid, prepared for backpulse, backpulsed into TI-153-S1
	9:53	13.80	Dewater mode was unable to refill backpulse chamber
	10:01	n/a	No pressure on permeate pressure gauge (for information only) and differential pressure gauge at max range, no flow through filter, end of filter test

Immediately following the initial backpulse, the TMP was unable to be stabilized below the 2-psid limit, and flowrate could no longer be maintained at 2.57 mL/min. Efforts were made to perform a second backpulse and clean the filter, but subsequent CWF experienced TMP exceeding 6.00 psid while trying to reestablish the target flowrate. The BDEF testing was retroactively declared complete at 13.79 m^3/m^2.

It was noted that as testing progressed a film of material was plating onto the wetted surfaces of the BDEF system. This film is shown in Figure 4.3 this material is dark brown in color and stained the high-density polyethylene (HDPE) feed bottles along with leaving a thicker ring of deposits at the liquid surface level. The 0.5 M oxalic acid cleaning used for filter cleaning also removed is film from the visible BDEF wetted surfaces.

Table 4.2. Test parameters prior to backpulsing.

Test Event	Filtration Resistance (1/m)	Volume Filtered since Last Backpulse (m^3/m^2)	Transmembrane Pressure (psid)
Backpulse 1	6.14×10^{10}	13.79	2.01

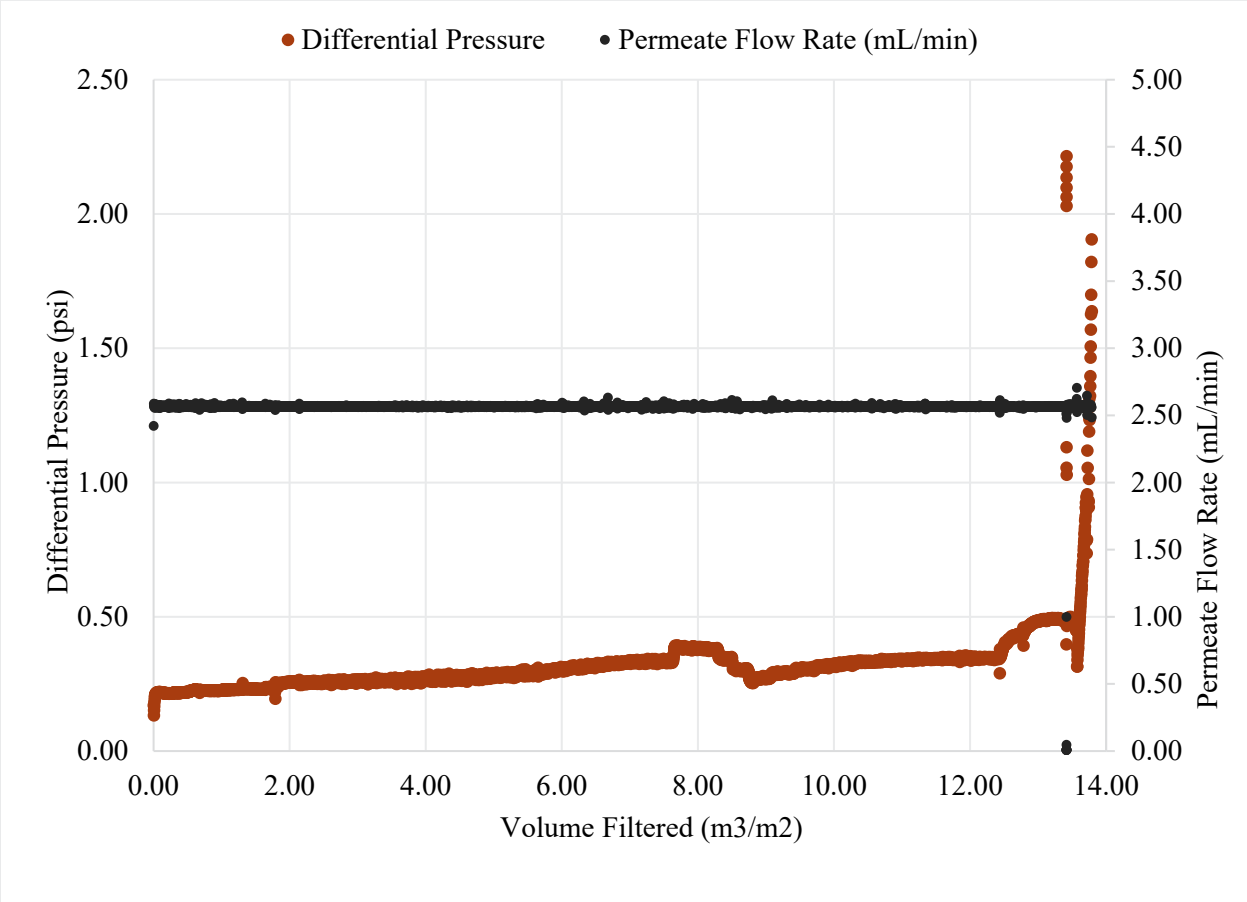

Figure 4.2. Filter differential pressure and MFC flow rate during filtering operations.

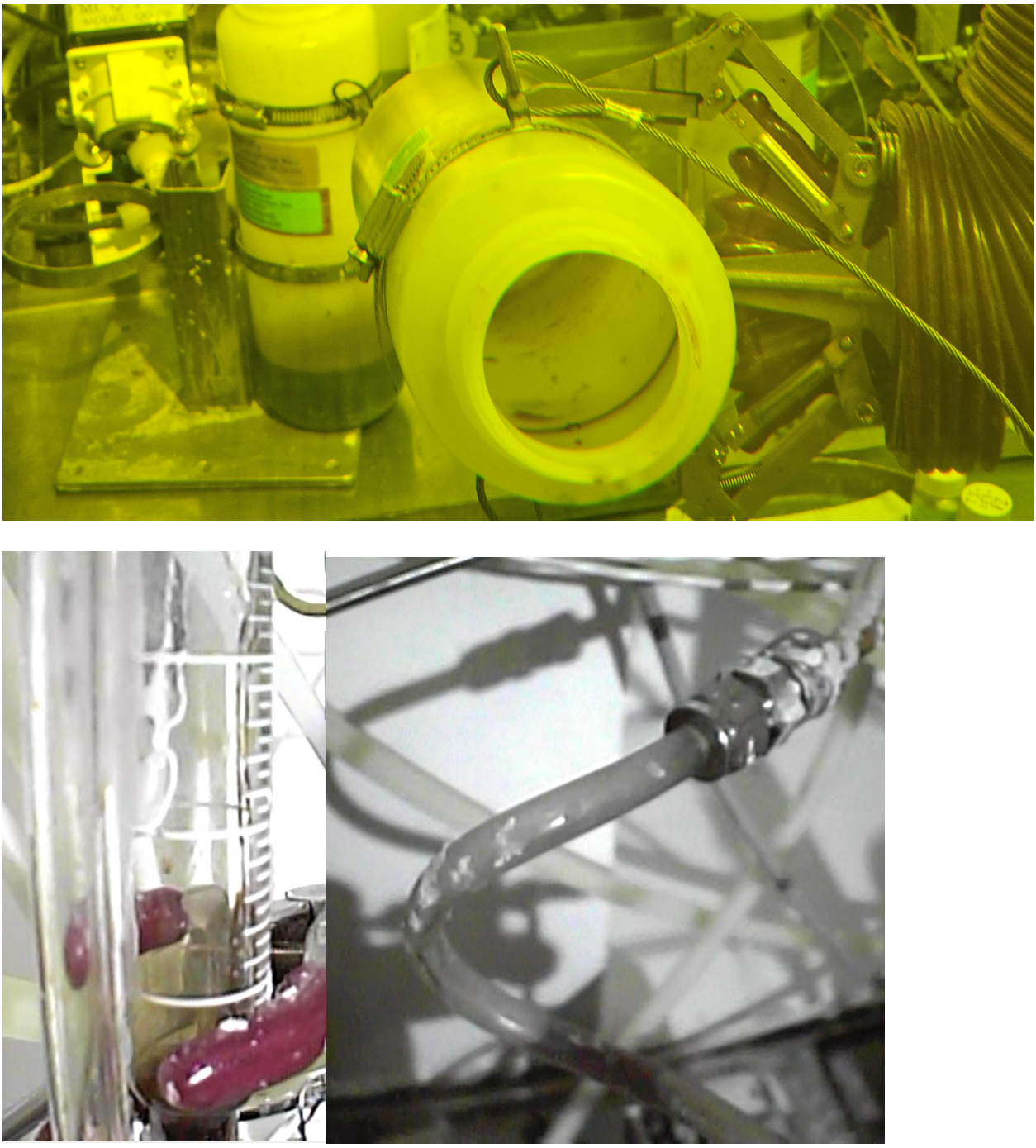

Figure 4.3. Material plating out on BDEF system surfaces; (Top) HDPE feed bottles; (Left) Glass flow meter; (Right) Permeate line to product bottle (Tygon 2375)

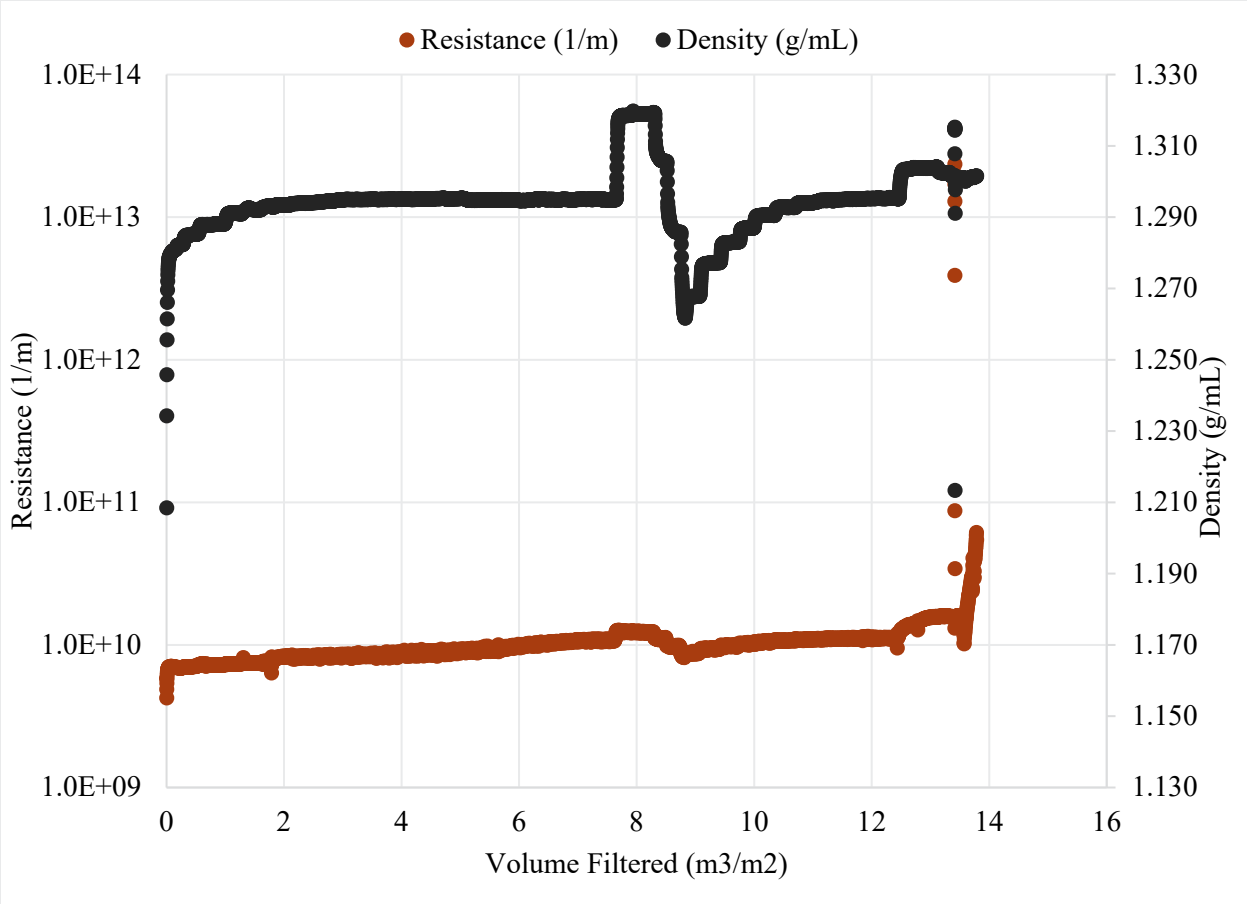

Figure 4.4. AN-107 filter resistance and permeate density during filtration process.

Equations 4.1 and 4.2 relate the flow rate through a porous media to its corresponding filter pressure drop (TMP) and resistance, respectively. When evaluating time rate changes in filter resistance and TMP during constant flow rate filtration, filtration behavior is general evaluated against the specific volume filtered $v(t)$, which is simply the total volume collected over a given filtration period normalized to the filter area, namely

$$v(t) = \frac{1}{A_t}\int_0^t Q(\tau)\,\mathrm{d}\tau \tag{4.3}$$

In the present analysis, Eq. 4.4 references $t = 0$ to the start of filtration.

Figure 4.4 shows both the total filter resistance and permeate density as a function of volume filtered over the 5 days of testing. Filter resistance generally increases throughout the active period of filtration; however, there is a notable step increase and subsequent decrease that spans volumes filtered from approximately 7.5 to 9.0 m^3/m^2. The underlying causes for the observed changes in filter resistance will be discussed in more detail in the pages that follow (after density trends are discussed). The emphasis of this discussion will be on specific volume filtered regions filter resistance increases, as such increases are typically attributable to fouling of the filter by waste particulates, and the time rate change of filter resistance with volume filtered provides information on the underlying fouling mechanism. Before evaluating increases in filter resistance, the density trends observed in Figure 4.4 are considered.

The density of the diluted and composited AN-107 solution ranged between approximately 1.250 and 1.320 g/mL per the MFC as shown in Figure 4.6 and averaged 1.293 g/mL through testing. An appreciable density increase to 1.319 g/mL occurred at 7.66 m^3/m^2; this corresponds closely with a feed bottle change to BDEF-AN7-9. A subsequent density decrease to 1.262 g/mL at 8.83 m^3/m^2 was seen shortly after. Density then recovered to 1.293 g/mL as the BDEF-AN7-10 feed bottle was pumped into the slurry reservoir. This indicates that BDEF-AN7-9 may not have been thoroughly homogenized post composition and dilution. This postulated stratification in BDEF-AN7-9 has implications for interpretation of the filter resistance trends, as a change in feed density may have a corresponding change in feed viscosity (which can lead to apparent changes in resistance when a constant viscosity is assumed).

Post filtration analysis of the product bottles prior to IX included the measurement of product density. Density measurement was performed in a 10-mL volumetric flask at 25.4 °C. These values are reported in Table 4.3. Post filtration density measurements of product bottles. and show little variation in density between bottles. Average bottle density was found to be 1.263 g/mL with a standard deviation of 0.009 g/mL and percent relative standard deviation of 0.74%.

Table 4.3. Post filtration density measurements of product bottles.

Bottle ID	Density (g/mL)
IX-AN7-1	1.258
IX-AN7-2	1.267
IX-AN7-3	1.269
IX-AN7-4	1.265
IX-AN7-5	1.266
IX-AN7-6	1.271
IX-AN7-7	1.244
IX-AN7-8	1.255
IX-AN7-9	1.264
IX-AN7-10	1.272
IX-AN7-11	1.266

To assess the nature of the potential particle-filter interactions occurring during transient increases in filter resistance, the AN-107 filter resistance data were fit to fouling models proposed by Hermia (1982). The approach used here is similar to that applied in the FY20 AP-105 filtration testing detailed in RPT-DFTP-021 (Allred et al. 2020). The filtration laws developed by Hermia (1982) are for constant pressure DEF but can be readily recast into constant flux formulas as documented by Hlavacek and Bouchet (1993). For the present analysis, Hermia's laws are recast into scaled resistance form, such that:

$$R^n = R_o^n \, (1 + \text{sign}(n) \, \sigma v) \tag{4.4}$$

Here, the exponent n defines the blocking regime, R = scaled resistance, $v = V/A$ is the specific volume filtered, and σ is the regime dependent blocking parameter. In the present analysis, R_o is a reference resistance corresponding to the start of a given filtration period (either after startup or backflushing), and v is the specific volume filtered relative to that same reference point. The fouling mechanism is characterized by the value of n. Hermia (1982) defined four blocking regimes:

- Cake filtration blocking ($n = 1$)
- Intermediate blocking ($n = 0$)

- Standard blocking ($n = -0.5$)
- Pore / complete blocking ($n = -1$)

For the current data, a best-fit value of n is assessed for specific filtration periods using Microsoft Excel's built-in solver to minimize the root mean square error (RMSE) defined by:

$$\text{RMSE} = \sqrt{\sum_i \left(R_i^{(\text{p})} - R_i^{(\text{m})}\right)^2} \tag{4.5}$$

where $R_i^{(\text{p})}$ and $R_i^{(\text{m})}$ are the predicted and measured resistances for an individual measurement i in the filtration period. To avoid the need to regress a best fit value of σ, it is estimated as:

$$\sigma = \frac{\text{sign}(n)}{v_f}\left[\left(\frac{R_f}{R_o}\right)^n - 1\right] \tag{4.6}$$

where R_f and v_f are the final resistance and specific volume filtered of the period. An initial review of filter resistance shown in Figure 4.4 identified five "fouling" regions of interest:

- Region 1: a gradual and persistent increase in filter resistance over specific volumes of 0 to 7.5 m^3/m^2,
- Region 2: an increase in resistance with a time rate change that exponentially decays [i.e., $R \sim \left(1 - e^{-kt}\right)$, hereafter referred to as "exponential-like" behavior] over 9.0 to ~12.4 m^3/m^2,
- Region 3 & 4: secondary and tertiary, exponential-like increases in resistance over 12.5 to 12.8 m^3/m^2 and 12.8 and 13.3 m^3/m^2, respectively, and
- Region 5: a final, rapid increase in resistance over 13.6 to 13.7 m^3/m^2 immediately before the filter TMP exceeded 2.0 psid and filtration was stopped for backflush operations.

Of these five periods, only the initial and final increases (occurring over 0 to 7.5 m^3/m^2 and 13.6 to 13.7 m^3/m^2) were fit using Eq. 4.5. The fits of these two regimes are shown in Figure 4.5 and Figure 4.6. Table 4.4. Filtration regime exponent n and blocking parameter σ. tabulates the individual regime exponent and blocking parameters for two filtration periods: the initial period of filtration and the period leading up to the first and only backflush.

Table 4.4. Filtration regime exponent n and blocking parameter σ.

Period	Regime Exponent n	Blocking Parameter σ, 1/m	RMSE, 1/m
Initial Fouling (Region 1)	-0.31	0.017	1.2E+10
Backflush 1 (Region 5)	1.1	18	1.7E+09

The initial period of fouling observed from 0 to 7.5 m^3/m^2 exhibits a regime exponent that falls between standard and intermediate blocking, suggesting that the initial fouling is a mixture of surface and depth fouling. This mixture of fouling seems reasonable, as the preliminary material fed to the filter derives from the tops of the AN-107 waste feeds, which are not mixed prior to testing but which may contain difficult to colloidal waste solids that cause the observed depth fouling. The fouling observed immediately leading up to Backflush 1 has a blocking exponent that is ~1, which is consistent with cake filtration. Again, it is reasonable that "cake" fouling would be observed here, as its onset corresponds to addition of feed bottoms (which were observed to contain settled waste solids).

The three intermediate fitting periods not fit to Eq. 4.5 exhibited anomalous fouling behavior, in that the transient resistance did not show the linear or accelerating increase in filter resistance (with increasing specific volume) expected for "Hermia-like" blocking ($-1 \leq n \leq 1$). Rather, the three intermediate fouling periods a characterized by a decelerating, exponential-like increase in resistance that appears to "asymptote" to a constant fouling. Attempts to fit these intermediate fouling periods results in $n \sim O(10)$, which is well outside "Hermia-like" fouling exponent ranges and which suggests that the filter transience in these regions result from a non-fouling physical process (like a change in the viscosity of the underlying liquid phase) or represents fouling caused by a feed with a finite and/or decreasing solids content with time. The second and third resistance increases starting at 9 and 12.45 m^3/m^2 appear to coincide with the transition to feed BDEF-AN7-10 and feed heel containing BDEF-AN7-9. The filtration period following these transitions are marked by exponent-like increases in density, which can be attributed to the postulated density stratification of BDEF-AN7-9 and CST-like mixing in the BDEF feed vessel. For the period from 9 to 12.4 m^3/m^2, addition of the higher density BDEF-AN7-10 feed into the lower density "tops" from BDEF-AN7-9 leads to an increase in both the liquid density, Na content, and density of the BDEF feed vessel. The latter increase in viscosity is not accounted for in resistance calculations, which take viscosity as a constant at 4.887 mPa s (see Section 4.5.3). Thus, the increase in resistance observed in Figure 4.4 over 9 to 12.4 m^3/m^2 is likely due, in part or whole, to the unaccounted-for increase in carrier fluid viscosity in filter feed as BDEF-AN7-10 feed is added and mixed into the BDEF reservoir. The two subsequent increases in resistance (over 12.45 to 12.75 m^3/m^2 and 12.8 to 13.2 m^3/m^2) both coincide with the introduction from the feed heel containing the dense BDEF-AN7-9 bottoms, and like the increase observed over 9. to 12.4 m^3/m^2, appear to result from an increase in feed viscosity rather than fouling by waste particulates).

The increase in resistance observed in the third intermediate period (12.8 to 13.2 m^3/m^2) is similar to that observed in the previous two periods; however, its occurrence cannot be attributed to any know filtration event or feed vessel addition. The latter conclusion should be approached with some caution, as the feed bottoms are expected to be higher in solids content than the sample "tops" (as the samples are not actively mixed in the >1 week prior to filtration) and the observed increase in resistance could also result from introduction of limited quantities of solids that quickly settle in the BDEF reservoir or are depleted as a result of accumulation on the filter.

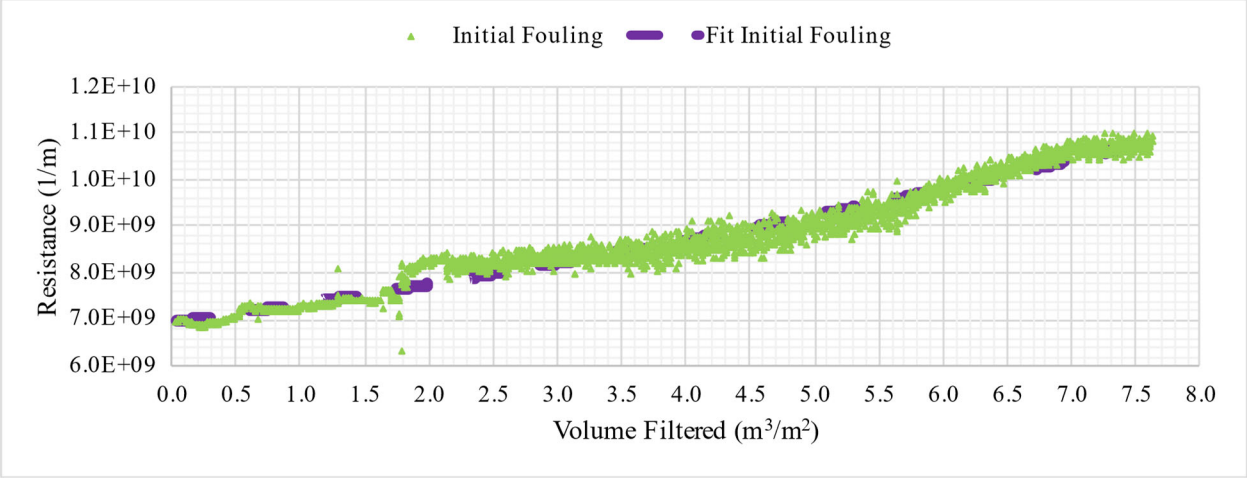

Figure 4.5. Fit to initial fouling experimental data using classical fouling mechanisms.

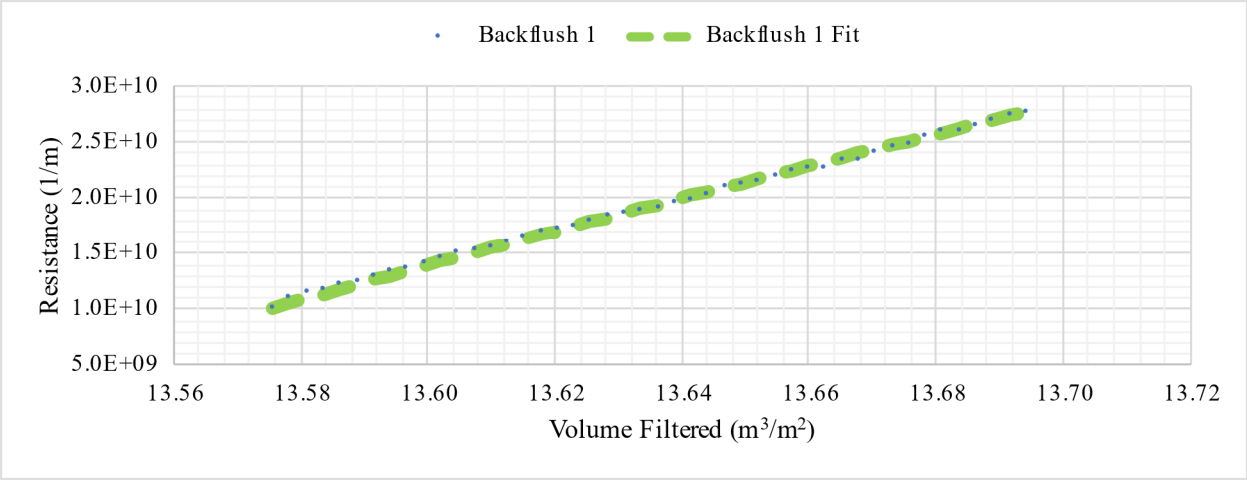

Figure 4.6. Fit to "5th" fouling section prior to Backflush 1 experimental data using classical fouling mechanisms.

4.3 Final CWF

At the conclusion of AN-107 filtration, a filter cleaning evolution was initiated to precede the final CWF. The extent of filter plugging prevented the 0.1 M NaOH solution typically used for cleaning from permeating the filter. A backpulse with the cleaning solution was performed to reestablish permeability, allowing the cleaning process to proceed. A CWF at 15.9 °C was measured following filter cleaning, producing a differential pressure averaging 0.154 psid – higher than the initial CWF TMP of 0.127 psid. The filter cleaning process was repeated using 0.5 M oxalic acid in an attempt to dissolve the deposited solids that the 0.1 M NaOH presumably failed remove. An additional and final CWF was then measured at 15.3 °C, with an average differential pressure of 0.089 psid. The significant reduction in average TMP observed in the post 0.5 M oxalic acid cleaning protocol indicates all solids deposited on the filter during the AN-107 filter test and some legacy fouling from previous tests had been removed. Figure 4.7 provides a comparison of the initial CWF, post 0.1 M NaOH filter clean CWF, and post 0.5 M oxalic acid clean CWF.

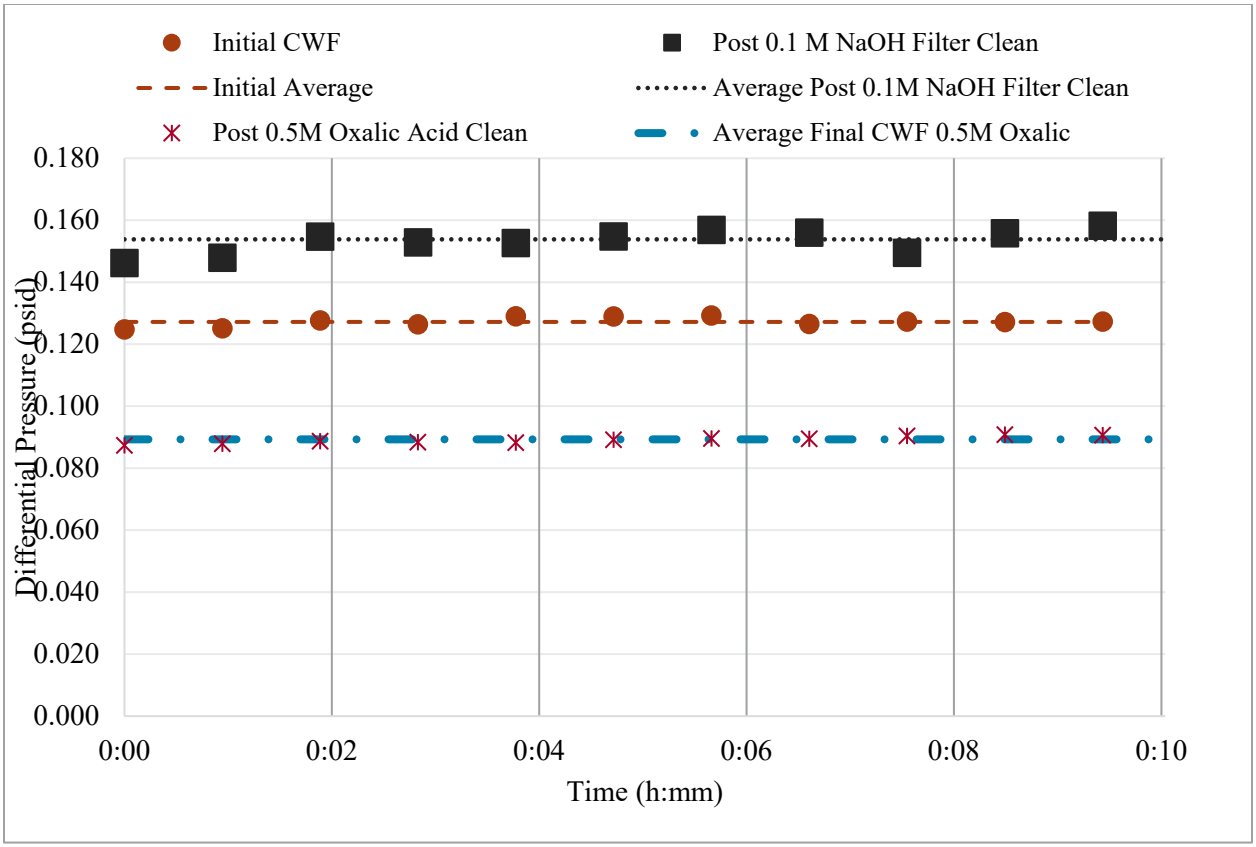

Figure 4.7. Initial, post 0.1 M NaOH filter clean, and post 0.5 M oxalic acid clean CWF.

4.4 Analytical Results

4.4.1 Diluted and Composited AN-107 Supernatant Tank Waste Analysis

ICP-OES analysis was conducted on the diluted and composited AN-107 supernatant tank waste on a mass-per-unit-mass basis (µg/g) as presented in Table 4.5. Subsequently, the molarity of the diluted and composited waste was calculated using a density of 1.254 g/mL, which was determined after sample dilution and composite completion of the AN-107 tank waste. The detailed ICP-OES report is found in Appendix D.

The molarity was calculated using the following equation:

$$M = \frac{(m * \rho)}{MW} \tag{4.7}$$

where M is the molarity, m is the mass, ρ is the density, and MW is the molecular weight of the component.

Table 4.5. ICP-OES results of diluted and composited AN-107 supernatant tank waste.

Analysis Method	Analyte	Concentration (µg/g)	Molarity (mol/L)
ICP-OES	Na	127,204	5.53

4.4.2 Total Alpha Energy Analysis

Total alpha analysis (alpha energy analysis, AEA) was conducted to determine the TRU content of the filtered permeate. The analysis results are given in Table 4.6 and show a considerable concentration of TRU soluble content as well as a breakthrough of TRU components that aren't already soluble. Additional detail is provided in Appendix C. All samples were above the 0.1 µCi/g threshold defining TRU waste per DOE M 435.1-1, *Radioactive Waste Management Manual*. The third permeate sample did show a higher alpha concentration, likely due to the consolidation of the product feed bottoms throughout filtration, as discussed in Section 4.2.

Table 4.6. AEA for permeate samples.

Analysis Method	Sample ID	IX Product Bottle Sampled From	(µCi/mL)	(µCi/g)
Total alpha analysis	TI-153-P1	IX-AN7-4	1.17	1.46
	TI-153-P2	IX-AN7-7	1.20	1.51
	TI-153-P3	IX-AN7-11	1.59	1.99

4.4.3 Rheology Analysis of Filtered and Cesium Decontaminated AN-107 Supernatant Tank Waste

The viscosity of the filtered and cesium exchanged AN-107 supernatant was measured with a Haake M5-RV20 (equipped with an M5 measuring head and RC20 controller) and an MV1 rotor and cup measuring system. Temperature was controlled using a combination of the standard measuring system temperature jacket and a NESLAB temperature-controlled circulator, Model Number RTE 111. This circulator allows heating and cooling of recirculation fluid to the rheometer over a range of -25 to 150 °C with a stability of ± 0.01 ° C. Performance checks using a Cannon-certified viscosity reference standard (Cannon Instrument Company) were carried out prior to and after measurements to verify that the system was functioning as expected. Viscosity was measured using a standard flow curve protocol comprising an up-ramp from 0 to 1000 s^{-1} for 5 minutes, a hold of 60 seconds at 1000 s^{-1}, and a finally down-ramp from 1000 to 0 s^{-1} over 5 minutes. Flow curves were measured at four temperatures: 10, 16, 25, and 35 °C. For each temperature, the Newtonian viscosity[1] of the liquid was determined by linear regression of the down-ramp data. The range of fit shear rates was generally limited to shear rates greater than 50 s^{-1} and below 600 s^{-1} to exclude data impacted by onset of secondary flows (i.e., Taylor vortices). The results of linear regression analysis and the resulting best fit Newtonian viscosities are reported in Table 4.7. In all but the 10 °C case, the measured viscosity of the AN-107 supernatant is below the recommended range of the measuring system (nominally 5.5 to 650 mPa s).

[1] While the AN-107 supernatant is expected to be Newtonian, linear regression analysis allowed for non-zero intercept to accommodate a non-zero torque offset introduced by the operator to accommodate negative torques resulting from operating the M5 viscometer outside its standard operating range (in this case, for viscosities below 5.5 mPa s).

Table 4.7. Viscosity results of filtered and Cs decontaminated sample.

Temperature (°C)	Fit Range Down-Ramp, s^{-1}	Viscosity mPa s	Viscosity Uncertainty[(a)] 3-Sigma Relative % Standard Error
10	50-1000	5.819	0.88
16	50-1000	4.887	1.03
25	50-750	3.832	2.00
35	50-600	3.243	3.80

(a) The uncertainty reported by the Haake software for the curve fit is the 3-sigma relative percent standard error.

4.5 Microscopy Solids Analysis

Material collected from the concentrated backpulse solution was submitted for examination by scanning transmission electron microscopy (STEM) imaging, x-ray energy dispersive spectroscopy (EDS), transmission electron microscopy (TEM), and selected area electron diffraction (SAED). A full report of the particle imaging and analysis can be found in Appendix E. Four samples were provided (AN-107 solids, Solution-1, Solution-3, Solution-4) and are described in Table 4.8.

Table 4.8. Microscopy Sample IDs

Sample ID	*Alternate ID*	*Content Description*
AN-107 Solids	TI-153-DEF-Solids-1	Solids scrapped off dead end filter membrane.
Solution 1	TI-153-S1	Backpulse solution of AN-107 feed.
Solution 3	TI-153-S3	Backpulse solution post 0.1 M NaOH filter cleaning.
Solution 4	TI-153-S4	Backpulse solution post 0.5 M oxalic acid filter cleaning.

The first sample (AN-107 Solids) contained semi-dried solids that were only examined with scanning electron microscopy (SEM). Three other samples contained particles in solution. These were also analyzed with SEM and two of these samples were further sub-sampled for STEM analysis. The solid sample was deposited onto a SEM carbon stub and analyzed. The solution samples were pipetted onto carbon stubs. This process did result in the precipitation of salts; however, some useful information could still be obtained. The solutions were also prepared for STEM using the holey-carbon TEM grid as a filter that prevented evaporite formation. Only two samples could be analyzed (Solution-3 and Solution-4) as the particles from Solution 1 were too large for imaging. Several TEM grids samples were prepared from each condition; however, some TEM grids possessed too high an activity to be further analyzed.

Table 4.9. Sample Analysis Summary

Samples	Techniques Applied	
	SEM	**TEM**
AN-107 Solids	SEM, EDS mapping, particle analysis	Activity too high
Solution-1	SEM, EDS mapping	Large particles – too thick for TEM
Solution-3	SEM, EDS mapping	STEM/TEM/diffraction (SAED)/EDS mapping
Solution-4	SEM	STEM/TEM/Diffraction (SAED)/EDS mapping

All four samples were analyzed during this investigation with the available tools. The 'AN-107 Solids' sample could only be examined on the SEM owing to the high activity and the size of the individual particles. The three other samples consisted of particles suspended in solution. These were prepared by drop-casting onto an SEM stub and by drop-casting onto TEM grids. Particles were visible by the naked eye in Solution-1 which also had the highest activity. Although samples of Solution-1 were prepared for TEM, there were too large particles to transfer directly to the TEM. In general, if a particle is in excess of 20-40 µm and several micrometers thick, then it is not possible to analyze in the STEM and obtain any useful data. However, with SEM, these large particles can be easily accommodated.

4.5.1 SEM Analysis of AN-107 Solids

The SEM stub prepared from the AN-107 Solids sample was dominated by Mn-Fe phases. There was little evidence of salt phases in this prepared specimen.

The material shown in Figure 4.9 was commonly found throughout the sample. The phase was found to consist mainly of Mn and Fe with Na and O. Carbon was present in the support film making it difficult to locate C-bearing phases. Figure 4.10 shows further SEM EDS maps of these Mn-Fe phases in the AN-107 solids sample. The results from this study were consistent with the results from the Savannah River National Laboratory (SRNL) study on AN-107 (Martin 2004). The SRNL study also indicated the occurrence of uranium in these particles. This was not observed during the SEM-EDS mapping investigation.

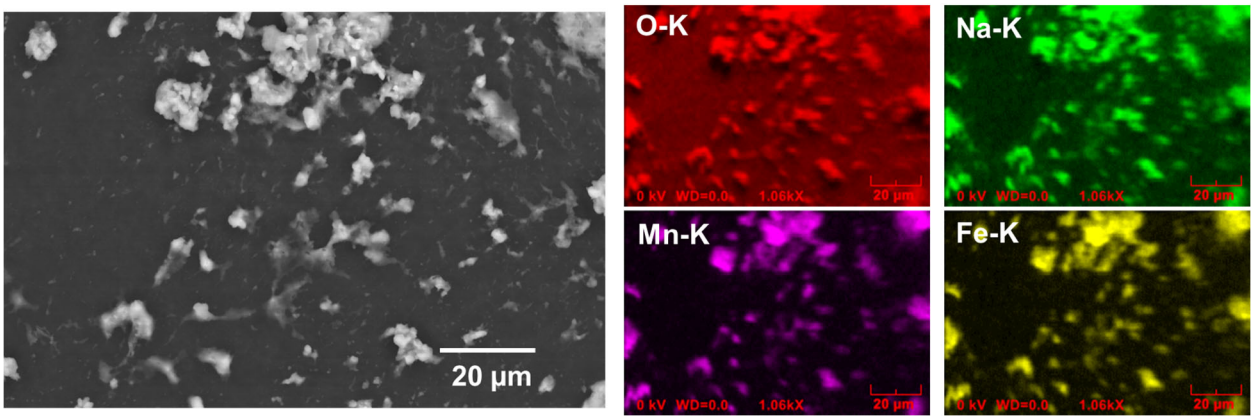

Figure 4.8 SEM image and EDS maps of Mn-Fe phases found in the AN-107 Solids sample.

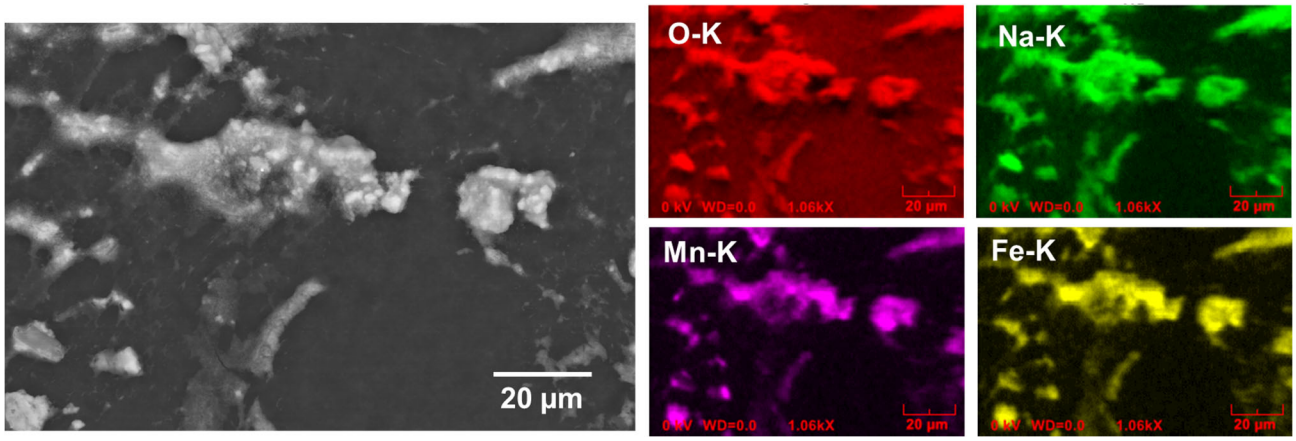

Figure 4.9 Further SEM images of Mn-Fe particles in the AN-107 Solids sample.

4.5.2 Solution 1

The major phase observed in the SEM from Solution-1 was compositionally consistent with natrophosphate ($Na_7F(PO_4)_2 \cdot 19H_2O$). In Figure 4.10, the block-like precipitate contained O, F, Na, and P as the major elements. Smaller Fe-Mn particles were attached to this phase. This phosphate phase did not precipitate out during the sample preparation operation but was observable in the solution prior to deposition onto the SEM stub. The individual particles were in some cases hundreds of micrometers across which is consistent with prior observations from tank waste characterizations (Bolling et al., 2019; Herting & Reynolds, 2016; Reynolds & Herting, 2016).

Figure 4.11 shows a higher magnification image of the natrophosphate with small particles of a Fe-Mn phase attached to the surface of the particles. EDS mapping revealed that the block-like phase consisted of O, F, Na, and P, consistent with the fluoro-natrophosphate. It is possible that these particles were deposited during the sample preparation and were suspended in the solution. However, the observation of the Fe-Mn phase is consistent with the results from the solids sample.

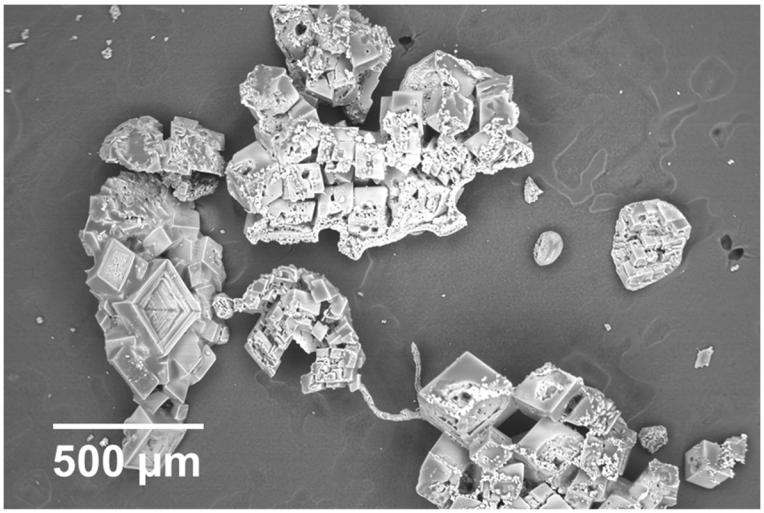

Figure 4.10 SEM image of large particles observed in AN-107 Solution-1

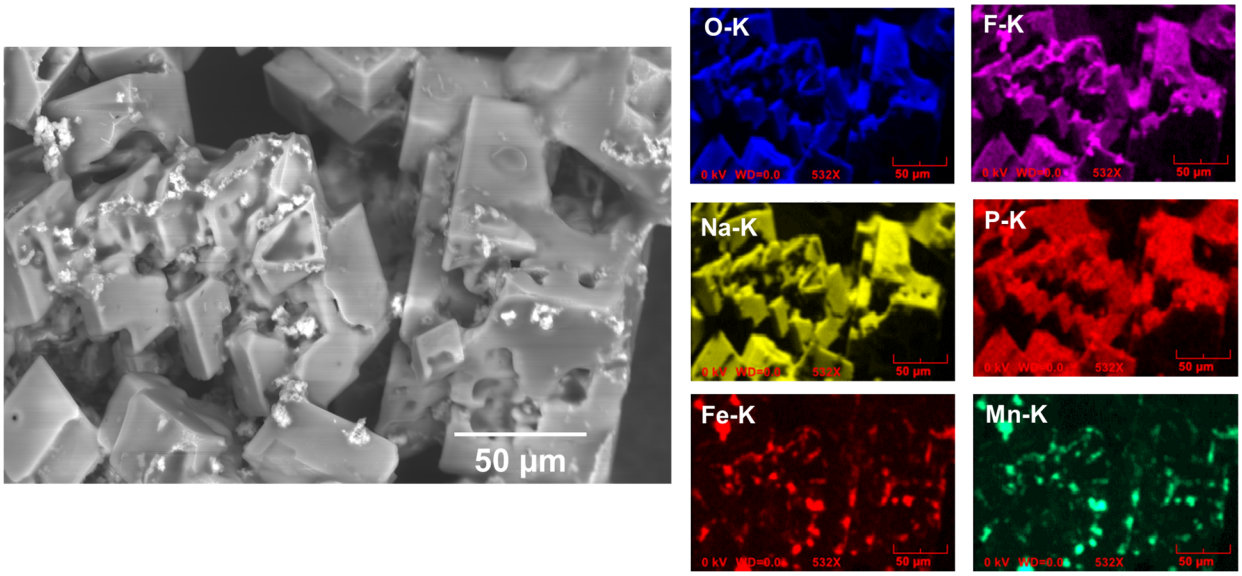

Figure 4.11 SEM and EDS analysis of a possible mixed salt sodium nitrate/fluoro-phosphate phase with particles of the Mn-Fe phase attached to the crystal surfaces in AN-107 Solution-1.

4.5.3 Solution 3

Solution-3 was examined with both SEM and TEM. Figure 4.12and Figure 4.13 show SEM images and EDS elemental maps that exhibited compositions and morphologies similar to those from the AN-107 Solids sample and Solution-1. Nitrogen was also detected in these particles which may indicate the precipitation of nitrate salts during the SEM sample preparation. The particles occurred as agglomerates ranging from a few micrometers to >20 µm in diameter.

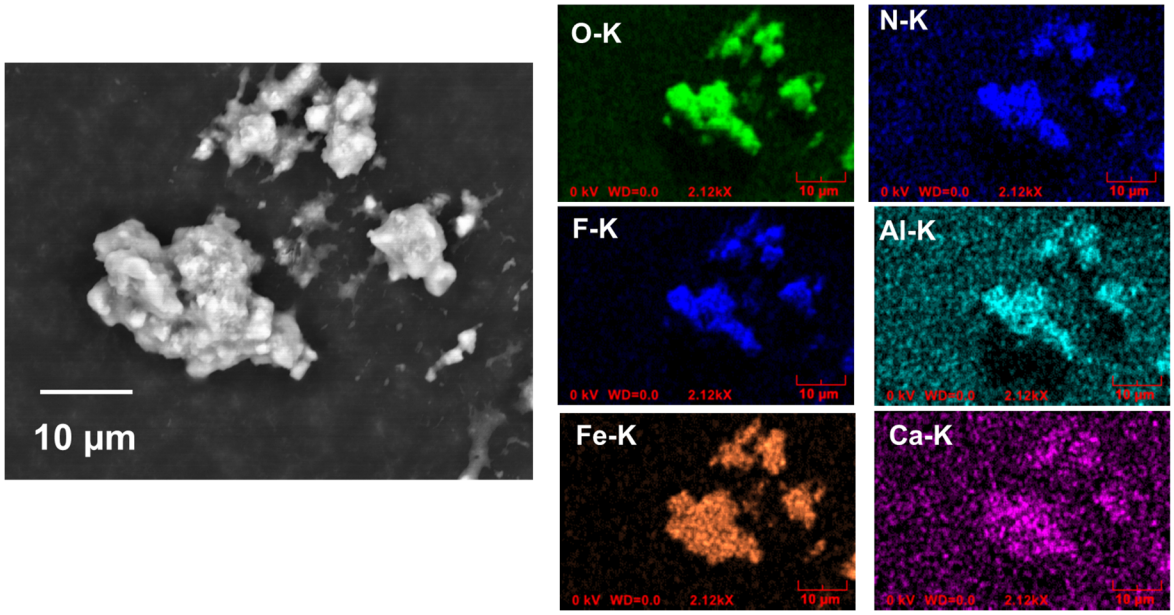

Figure 4.12 Different morphologies of a Fe-rich phase found in Solution-3.

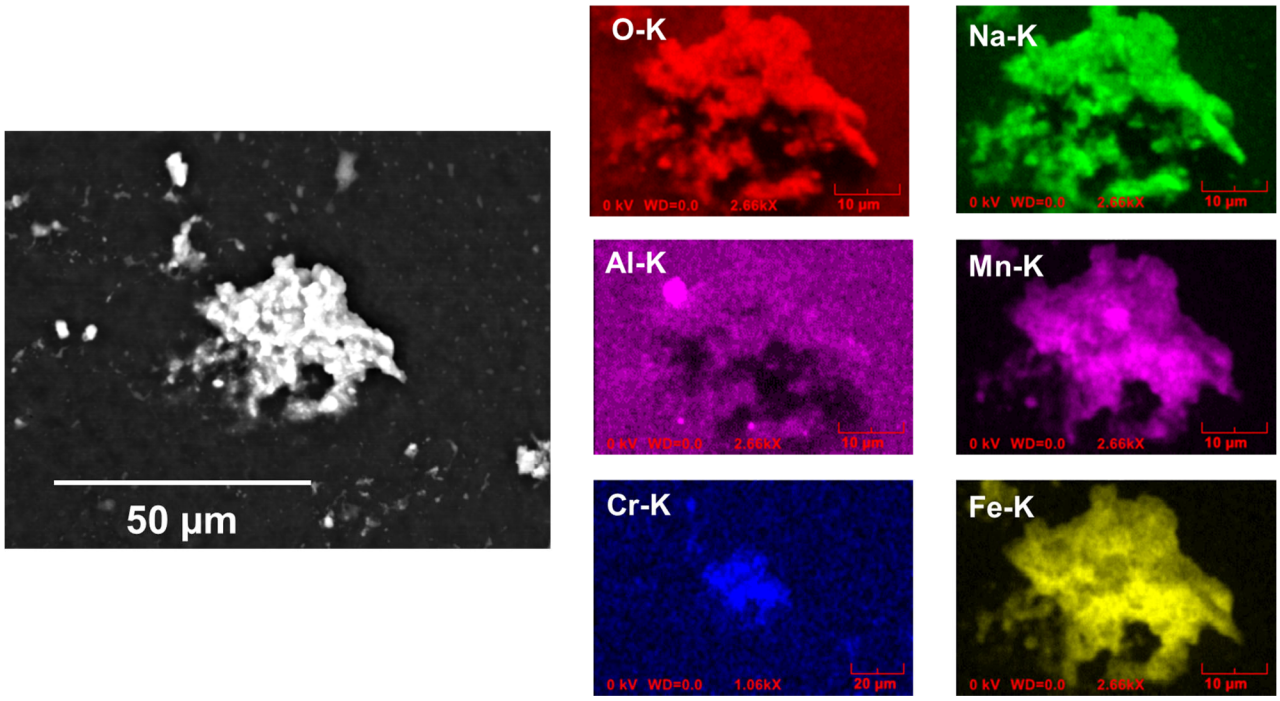

Figure 4.13 SEM image and EDS maps of Mn-Fe phase in Solution-3

4.5.4 Solution-4

Solution-4 was dominated by fibrous-like particles and was distinctly different from the solids sample and the other samples received. The SEM images of the particles and the TEM images showed similar morphologies (see Figure 4.14 and Figure 4.15). This helps to provide confidence that the particles observed in the TEM were representative of the bulk material sampled. No EDS was obtained during the SEM analysis of this specimen; however, extensive analysis was performed in the TEM of this specimen (see Appendix E).

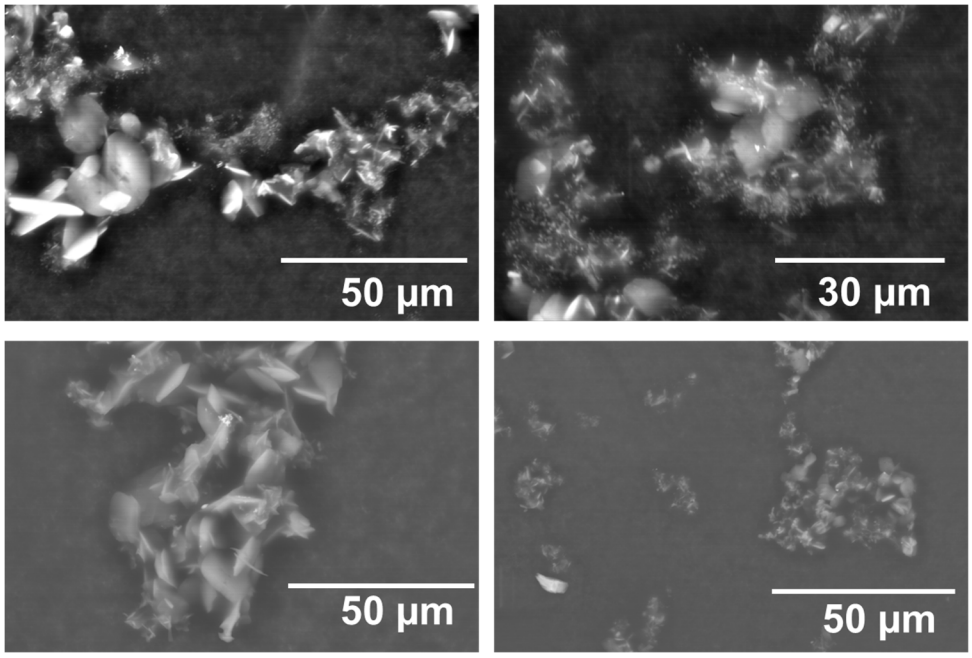

Figure 4.14 SEM image of particles observed in Solution-4.

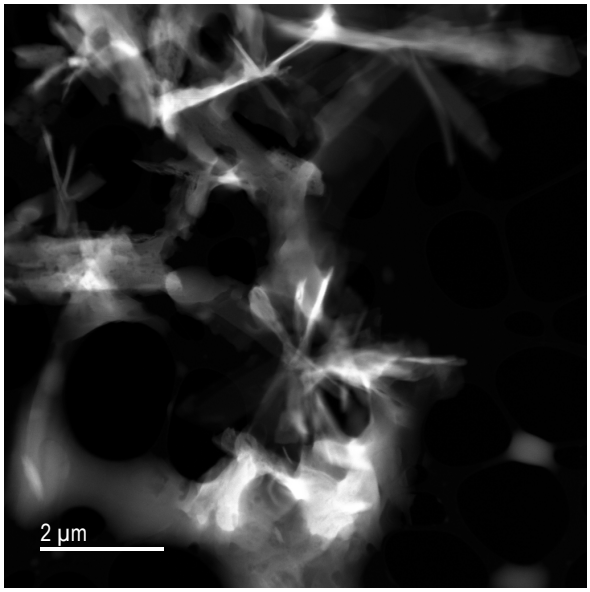

Figure 4.15 Low magnification TEM image of Solution 4 showing the same type of morphology as shown in Figure 4.14.

5.0 Conclusions

Based on the results of the filtration experiments on supernatant waste from tank 241-AN-107 at 16 °C, the following observations and conclusions were made:

- Throughout filtration, the differential pressure required to effect filtration at 0.065 gpm/ft^2 increased little over the majority of the filtration campaign, but then increased significantly once feed bottoms were filtered, exceeded the TSCR action limit of 2 psid, and the AN-107 supernatant was no longer able to permeate the filter. This indicates that the Media Grade 5 filter may be prone to quick and sudden plugging when processing AN-107 supernatant that has not been given sufficient time to settle.
- The prototypic filter cleaning process was insufficient in restoring filter performance after filtering AN-107 supernatant. Utilizing 0.5 M oxalic acid as a cleaning solution instead of 0.1 M NaOH in the filter cleaning process was effective in restoring filter performance.
- The filtered permeate samples all had total alpha content greater than the 0.1 μCi/g threshold defining TRU waste per DOE M 435.1-1, Radioactive Waste Management Manual.
- Solids concentrated from the backpulse solutions were composed of natrophosphate, Mn-Fe phases, and fluoro-natrophosphate that occurred as particle agglomerates. There was less evidence of fine salt-like particles in this sample than seen in prior tests (Allred et al. 2020, 2021, 2022, 2023a).

6.0 References

Allred JR, C Alvarez, EC Buck, CA Burns, RC Daniel, JGH Geeting, AM Westesen, and RA Peterson. 2023a. *Fiscal Year 2023 Filtration of Hanford Tank 241-SY-101 Supernatant at 16 °C*. PNNL-34509, Rev. 0 (RPT-DFTP-039, Rev. 0). Pacific Northwest National Laboratory, Richland, Washington.

Allred JR, C Alvarez, EC Buck, CA Burns, RC Daniel, JGH Geeting, AM Westesen, and RA Peterson. 2023b. *Fiscal Year 2023 Filtration of Hanford Tank 241-AP-105 Supernatant at 16 °C*. PNNL-34265, Rev. 0 (RPT-DFTP-036. Rev. 0). Pacific Northwest National Laboratory, Richland, Washington.

Allred JR, EC Buck, CC Burns, RC Daniel, JGH Geeting, ZB Webb, AM Westesen, and RA Peterson. 2022. *Fiscal Year 2022 Filtration of Hanford Tank 241-AP-101 Supernatant at 16 °C*. PNNL-32851, Rev. 0 (RPT-DFTP-032, Rev. 0). Pacific Northwest National Laboratory, Richland, Washington.

Allred JR, JGH Geeting, AM Westesen, EC Buck, and RA Peterson. 2020. *Fiscal Year 2020 Filtration of Hanford Tank Waste 241-AP-105*. PNNL-30485, Rev. 0 (RPT-DFTP-021, Rev. 0). Pacific Northwest National Laboratory, Richland, Washington.

Allred JR, JGH Geeting, AM Westesen, EC Buck, and RA Peterson. 2021. *Fiscal Year 2021 Filtration of Hanford Tank 241-AP-107 Supernatant Samples Obtained at Prototypic Tank Level and Filtered at 16 °C*. PNNL-31557, Rev. 0 (RPT-DFTP-028, Rev. 0). Pacific Northwest National Laboratory, Richland, Washington.

ASME. 2012. *Quality Assurance Requirements for Nuclear Facility Applications*. NQA-1-2012. The American Society of Mechanical Engineers, New York, New York.

Bolling, S. D., Reynolds, J. G., Ely, T. M., Lachut, J. S., Lamothe, M. E., & Cooke, G. A. (2019). *Natrophosphate and kogarkoite precipitated from alkaline nuclear waste at Hanford*. Journal of Radioanalytical and Nuclear Chemistry. https://doi.org/10.1007/s10967-019-06924-9

Geeting, JGH, Rovira, AM, Allred, JR, Shimskey, RW, Burns, CA, and Peterson, RA 2018. *Filtration of Hanford Tank AP-107 Supernatant*. PNNL- 27638, Rev. 0 (RPT-DFTP-009). Pacific Northwest National Laboratory, Richland, Washington.

Gerber M. S. 1992. *Legend and Legacy: Fifty Years of Defense Production at the Hanford Site*. WHC-MR-0293, Rev. 2. Westinghouse Hanford Company, Richland, Washington. doi:10.2172/10144167

Hermia J. 1982. "Constant Pressure Blocking Filtration Laws – Application to Power-Law Non-Newtonian Fluids." *Transactions of the Institution of Chemical Engineers* 60(3):183-187.

Herting, D. L., & Reynolds, J. G. J. E. C. L. 2016. *The composition of natrophosphate (sodium fluoride phosphate hydrate)* [journal article]. 14(3), 401-405. https://doi.org/10.1007/s10311-016-0574-2

Hlavacek, M., Bouchet, F. 1993 Constant flux rate blocking laws and an example of thief application to dead-end microfiltration of protein solutions. J. Membr. Sci, 82: 285-295. Martin, K. B. (2004). *Compositing, Homogenization, and Characterization of Samples from Hanford Tank 241-AN-107*. WSRC-TR-2003-00210 SRT-RPP-2003-00091. Savannah River Site, Aiken, SC. https://www.osti.gov/biblio/822082.

Reynolds, J. G., Cooke, G. A., Herting, D. L., & Warrant, R. W. 2012. Evidence for dawsonite in Hanford high-level nuclear waste tanks. Journal of Hazardous Materials, 209–210, 186-192. https://doi.org/http://dx.doi.org/10.1016/j.jhazmat.2012.01.018

Reynolds, J., & Herting, D. 2016. Crystallization of Sodium Phosphate Dodecahydrate and Re-crystallization to Natrophosphate in Simulated Hanford Nuclear Waste.

Siewert, J., 2019. *TSCR Filter Sizing*. RPP-CALC-62496, Rev. 3. Washington River Protection Solutions, Richland, Washington.

Urie, M. W., Wagner, JJ, Greenwood, LR, Farmer, OT, Fiskum, SK, Ratner, RT, & Soderquist, CZ. 1991. Inorganic and Radiochemical Analysis of AW-101 and AN-107 Tank Waste. PNWD-2462. Pacific Northwest National Laboratory, Richland, Washington. https://doi.org/10.2172/14537

Appendix A – BDEF Piping and Instrumentation Diagram

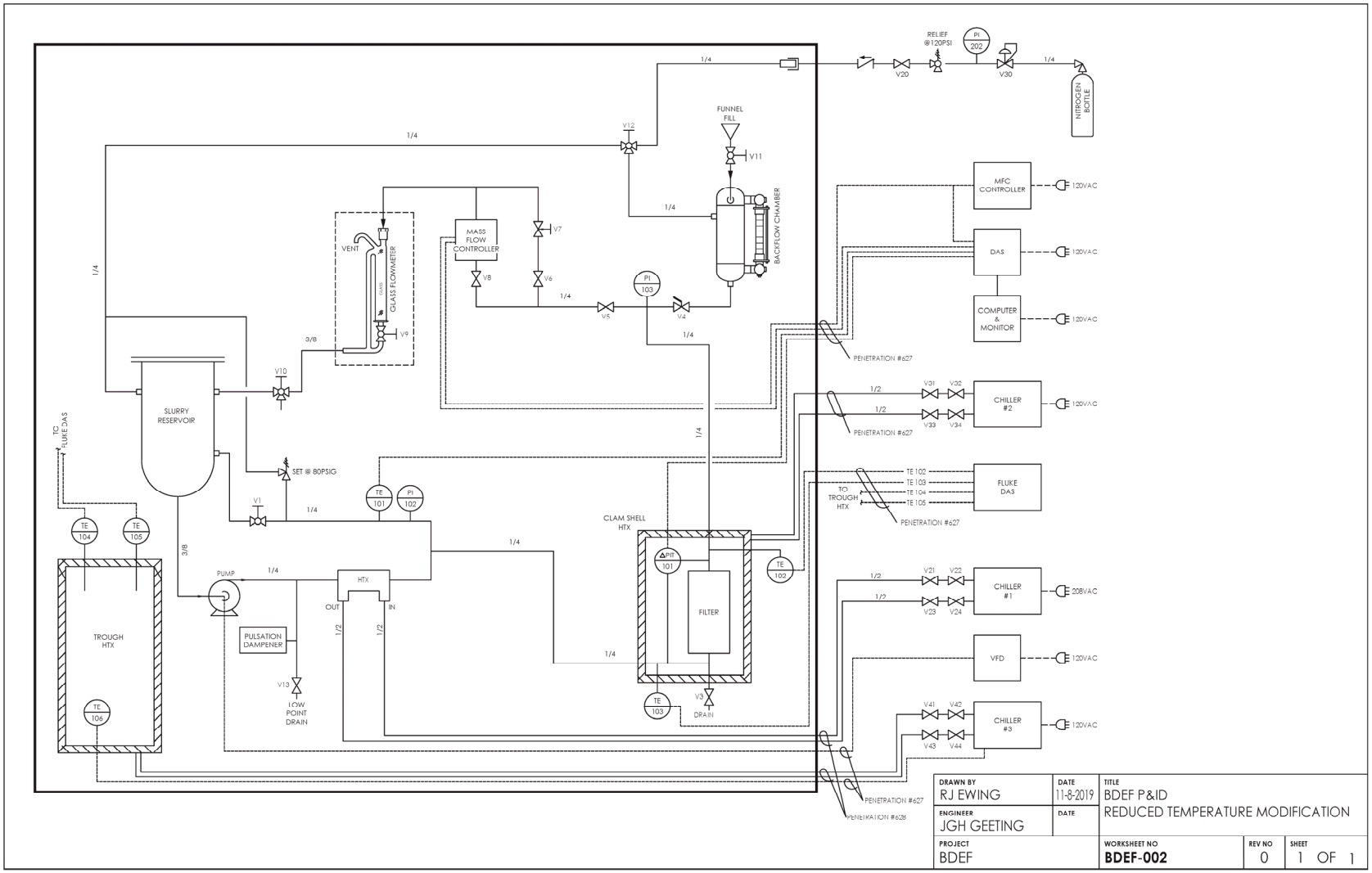

Figure A.1. BDEF piping and instrumentation diagram.

Appendix B – Feed Bottle Composite and Dilution

Composite Bottle ID	Receipt Sample Bottle ID	Sample Location (depth below liquid surface, inches)	Mass Addition to Composite Bottle (g)	Actual Mass of Water Added, g
BDEF-AN7-1	7AN-23-01	25	992.5	453.7
	7AN-23-13	123		
	7AN-23-31	270		
BDEF-AN7-2	7AN-23-07	74	1,021.5	466.4
	7AN-23-19	172		
	7AN-23-25	221		
BDEF-AN7-3	7AN-23-02	25	1,000.5	456.7
	7AN-23-14	123		
	7AN-23-32	270		
BDEF-AN7-4	7AN-23-08	74	1,030.2	470.2
	7AN-23-20	172		
	7AN-23-26	221		
BDEF-AN7-5	7AN-23-03	25	989.5	451.8
	7AN-23-15	123		
	7AN-23-33	270		
BDEF-AN7-6	7AN-23-09	74	1,008.6	463.5
	7AN-23-21	172		
	7AN-23-27	221		
BDEF-AN7-7	7AN-23-04	25	995.4	457.1
	7AN-23-16	123		
	7AN-23-34	270		
BDEF-AN7-8	7AN-23-10	74	1,000.7	457.3
	7AN-23-22	172		
	7AN-23-28	221		
BDEF-AN7-9	7AN-23-05	25	1,028.5	469.7
	7AN-23-17	123		
	7AN-23-35	270		
BDEF-AN7-10	7AN-23-11	74	1,016.3	464.0
	7AN-23-23	172		
	7AN-23-29	221		
BDEF-AN7-11	7AN-23-06	25	1,018.0	464.6
	7AN-23-18	123		
	7AN-23-36	270		
BDEF-AN7-12	7AN-23-12	74	1,015.1	463.3
	7AN-23-24	172		
	7AN-23-30	221		

Appendix C – Total Alpha Analysis for Filtration Permeate Samples

Pacific Northwest Natioanal Laboratory
Richland, WA
Radiochemical Sciences and Engineering Group

filename 24-0322 Allred
1/26/2024

Client: Allred
ASR: 1898

Project: 82508
WP: NR1595

Prepared by: Lawrence R Greenwood Digitally signed by Lawrence R Greenwood Date: 2024.01.29 09:22:28 -08'00'

Concur: Truc Trang-Le Digitally signed by Truc Trang-Le Date: 2024.01.29 09:06:22 -08'00'

Procedures: Activity #4668 Source Preparation for Gross Alpha and Gross Beta Analysis
Activity #6343 Total Alpha and Total Beta Analysis
M&TE Ludlum
Count date: 25-Jan-24

Sample	Lab ID	Measured Activity, µCi/g ± 1s Gross alpha	
TI-153-P1	24-0322	**1.20E+00**	**± 2%**
TI-153-P1	24-0322 DUP	**1.13E+00**	**± 2%**
TI-153-P2	24-0323	**1.20E+00**	**± 2%**
TI-153-P3	24-0324	**1.59E+00**	**± 2%**
	24-0322 PB	-1.64E-06	± 48%

*Blank Spike 105%
*Matrix spike 102%

Page 1 of 1

Appendix D – ICP-OES Analysis for Diluted and Composited 241-AN-107 Supernatant

PRELIMINARY

Battelle PNNL/RPG/Inorganic Analysis ... ICPOES Data Report

		Run Date >	4/3/2024	4/3/2024	4/3/2024	4/3/2024	4/3/2024	4/3/2024	4/3/2024	4/3/2024	4/3/2024	4/3/2024	4/3/2024
		Process Factor >	1.0	1.0	158.8	397.1	1914.1	159.1	406.0	2010.2	155.1	396.1	1938.0
			24-0925 PB @1x	405 Diluent	24-0924 @10x	24-0924 @25x	24-0924 @125x	24-0925 @10x	24-0925 @25x	24-0925 @125x	24-0925 Dup @10x	24-0925 Dup @25x	24-0925 Dup @125x
Instr. Det. Limit (IDL)	Est. Quant. Limit (EQL)	Client ID >			TI155-Feed-Comp	TI155-Feed-Comp	TI155-Feed-Comp	TI155-EFF-Comp	TI155-EFF-Comp	TI155-EFF-Comp	TI155-EFF-Comp	TI155-EFF-Comp	TI155-EFF-Comp
µg/g	µg/g	(Analyte)	µg/g	µg/g	µg/g	µg/g	µg/g	µg/g	µg/g	µg/g	µg/g	µg/g	µg/g
0.0101	0.101	Al	0.530	--	1,100	1,100	1,080	2,160	2,160	2,200	1,320	1,350	1,340
0.0619	0.619	As	[0.091]	--	--	[47]	[130]	--	--	[220]	--	[27.0]	--
0.0001	0.001	Ba	0.0019	--	1.88	1.87	[1.8]	2.63	2.71	2.80	2.68	2.71	2.32
0.0056	0.056	Ca	0.0999	--	279	273	241	272	277	240	273	273	234
0.0014	0.014	Cd	[0.0030]	[0.0016]	33.3	32.3	29.5	31.8	33.6	30.7	32.2	34.6	37.1
0.0020	0.020	Cr	[0.0025]	--	50.9	50.9	51.6	65.7	67.7	70.7	65.8	67.4	70.7
0.0014	0.014	Fe	0.0586	--	384	384	378	612	631	635	620	637	636
0.0312	0.312	K	0.652	--	936	853	750	895	851	744	890	843	780
0.0073	0.073	Na	3.46	--	98,100	102,000	102,000	98,900	99,400	102,000	96,600	102,000	104,000
0.0022	0.022	Ni	[0.0027]	--	264	264	265	256	268	276	258	265	259
0.0269	0.269	Pb	[0.045]	[0.029]	129	133	[180]	143	153	[200]	145	143	[180]
0.0001	0.001	Sr	[0.0009]	[0.0002]	1.31	1.27	[1.5]	1.28	1.31	[1.3]	1.19	1.19	[1.3]
0.0410	0.410	U	--	--	[22.0]	[21.0]	--	[12.0]	[24.0]	--	[12.0]	[30.0]	--
0.0027	0.027	Zn	0.0383	--	12.3	18.3	68.0	14.5	22.3	69.8	14.2	23.6	71.6
Other Analytes													
0.0019	0.019	Ag	--	--	[0.49]	--	--	[0.35]	--	--	[0.50]	[0.82]	--
0.0060	0.060	B	0.455	[0.018]	72.0	75.3	[100]	46.2	50.3	[68.0]	41.5	44.6	[56.0]
0.0001	0.001	Be	--	--	--	--	--	--	--	--	--	--	--
0.0245	0.245	Bi	--	--	[6.0]	[12]	--	[4.8]	[17.0]	--	[4.5]	[13.0]	--
0.0103	0.103	Ce	--	--	[11.0]	[13.0]	--	[14]	[13]	--	[15.0]	[15]	--
0.0043	0.043	Co	--	--	[1.8]	[2.9]	--	[2.2]	[1.8]	--	[2.9]	[3.3]	--
0.0023	0.023	Cu	[0.0032]	--	17.9	17.6	[16.0]	17.4	17.9	[17.0]	17.3	17.6	[16.0]
0.0023	0.023	Dy	--	--	--	--	--	--	--	--	--	--	--
0.0006	0.006	Eu	--	--	[0.66]	[0.48]	--	[0.32]	[0.68]	--	[0.34]	[0.46]	--
0.0019	0.019	La	--	--	9.30	9.31	[9.9]	10.8	11.3	[12.0]	11.0	11.0	[11.0]
0.0007	0.007	Li	[0.0031]	--	[0.74]	[0.39]	--	[0.38]	[0.86]	--	[0.40]	[0.60]	--
0.0018	0.018	Mg	0.0185	--	3.26	[2.6]	[3.6]	[2.4]	[3.9]	--	[2.3]	[3.1]	--
0.0002	0.002	Mn	[0.0006]	--	82.2	82.1	80.7	126	130	130	125	128	128
0.0044	0.044	Mo	--	--	18.2	[17]	[20.0]	16.2	19.5	[15.0]	16.6	19.1	[19.0]
0.0088	0.088	Nd	--	--	22.6	[25]	[19]	29.2	[32.0]	[18.0]	29.3	[33]	[34.0]
0.0905	0.905	P	--	--	324	[310]	[220]	308	[300]	[370]	309	[330]	[320]
0.0054	0.054	Pd	--	--	[2.5]	[3.0]	--	[1.1]	--	--	--	--	--
0.0211	0.211	Rh	--	--	--	--	--	--	--	--	--	--	--
0.0063	0.063	Ru	--	--	15.3	[14.0]	[18.0]	14.3	[17.0]	--	13.8	[14.0]	[14.0]
0.1262	1.262	S	--	--	1,450	1,430	[1,500]	1,390	1,410	[1,900]	1,390	1,500	[1,400]
0.0598	0.598	Sb	--	--	--	--	--	--	--	--	--	--	--
0.1656	1.656	Se	--	[0.17]	--	--	--	--	--	--	--	--	--
0.0086	0.086	Si	[0.066]	[0.010]	42.1	40.3	[72]	23.6	[32.0]	[35.0]	30.5	37.1	[35.0]
0.0291	0.291	Sn	--	--	[11.0]	--	[56]	--	--	--	--	--	--
0.0246	0.246	Ta	--	--	--	--	--	--	--	--	--	--	--
0.0197	0.197	Te	[0.030]	--	[5.5]	--	--	[4.7]	--	--	--	--	--
0.0071	0.071	Th	--	[0.0084]	[9.0]	[10.0]	[19.0]	[7.4]	[11]	--	[6.8]	[10.0]	[19.0]
0.0006	0.006	Ti	[0.0031]	--	[0.39]	[0.29]	--	1.83	[2.0]	[1.4]	1.71	[1.7]	[2.2]
0.0814	0.814	Tl	--	--	--	--	--	--	--	--	--	--	--
0.0013	0.013	V	[0.0031]	--	[0.68]	[0.63]	--	[0.60]	[0.96]	--	[0.53]	[1.1]	--
0.0161	0.161	W	[0.055]	--	71.3	76.1	[110]	70.4	70.2	[96]	70.8	79.4	[110]
0.0006	0.006	Y	--	--	2.79	2.87	[3.0]	3.07	3.27	[3.4]	3.13	3.22	[3.0]
0.0014	0.014	Zr	[0.0030]	--	11.4	11.2	[12.0]	12.2	12.3	[13.0]	12.3	12.7	[15.0]

1) "--" indicates the value is < MDL. The method detection limit (MDL) = IDL times the "multiplier" near the top of each column. The estimated sample quantitation limit = EQL (in Column 2) times the "multiplier". Overall error for values ≥ EQL is estimated to be within ±15%.

2) Values in brackets [ ] are ≥ MDL but < EQL, with errors likely to exceed 15%.

na = not applicable; KOH flux and Ni crucible or Na_2O_2 flux and Zr crucible for fusion preparations, or Si for HF assisted digests.

ASR Staging Final from ASR-1965 Data Work-up 24-0924 & 24-0925 Non-HF

PRELIMINARY

PRELIMINARY

Battelle PNNL/RPG/Inorganic Analysis ... ICPOES Data Report

QC Performance 4/3/2024

Criteria >	≤ 20%	80%-120%	80%-120%	75%-125%	80%-120%	80%-120%	≤ 10%
QC ID >	24-0925 @10x Dup	Instrument LCS/BS	BS-24-0925 @10x LCS/BS	24-0925 @10x MS	24-0924 @25x + PS-A	24-0925 @25x + AS-B	24-0924 @125x 5-fold Serial Dil
Analytes	RPD (%)	%Rec	%Rec	%Rec	%Rec	%Rec	%Diff
Al	46.0	102	114	51	102		1.1
As		95	115	101	96		
Ba	4.3	104	111	88	97		
Ca	3.0	102	112	92	100		8.6
Cd	3.9	99	111	97	101		5.3
Cr	2.8	96	108	94	97		5.1
Fe	3.7	99	111	nr	98		2.2
K	2.0	99	109	99	100		8.8
Na	0.2	98	130	144	103		4.2
Ni	3.4	99	109	98	98		3.9
Pb	3.9	96	109	92	96		
Sr	4.5	100	114	89	101		
U		96	105	84		96	
Zn	0.1	96	120	90	102		285.8
Other Analytes							
Ag		99	17	57	96		
B	8.0	103			101		
Be		94	106	83	92		
Bi		138	167	123	141		
Ce		93	102	86		93	
Co		98			97		
Cu	2.0	105	113	98	103		
Dy		92				90	
Eu		91				90	
La	4.7	91	98	83		90	
Li		106	115	98	104		
Mg		100	111	88	98		
Mn	1.5	105	115	88	102		1.9
Mo	4.7	101			100		
Nd	2.8	90	97	81		89	
P	3.0	99			99		
Pd		88				88	
Rh		94				92	
Ru	1.2	89				91	
S	2.4	99				99	
Sb		92			94		
Se		119			124		
Si	28.3	93			95		
Sn		91			91		
Ta		99			99		
Te		93				94	
Th		91	99	84		89	
Ti	4.4	101			99		
Tl		94			93		
V		94	105	87	93		
W	3.2	94			94		
Y	4.2	95			93		
Zr	3.6	102			101		

Shaded results are outside the acceptance criteria.

nr = spike concentration less than 25% of sample concentration. Matrix effects can be assessed from the serial dilution.

na = not applicable; KOH flux and Ni crucible or Na_2O_2 flux and Zr crucible for fusion preparations, or Si for HF assisted digests.

PRELIMINARY

ASR Staging Final from ASR-1965 Data Work-up 24-0924 & 24-0925 Non-HF

David L Jr Blanchard Digitally signed by David L Jr Blanchard
Date: 2024.04.11 16:29:47 -07'00'

Appendix E – Backpulsed Solids from AN-107 Characterization with Scanning Transmission Electron Microscopy

Materials from a concentrate from Hanford tank waste material representing double-shell tank 241-AN-107 (herein AN-107) were run through the backpulse dead-end filter system at 16 °C. These concentrates were examined with scanning electron microscopy (SEM), scanning transmission electron microscopy (STEM) with X-ray energy dispersive spectroscopy (EDS), and transmission electron microscopy (TEM) with selected area electron diffraction (SAED) in the Radiochemical Processing Laboratory at Pacific Northwest National Laboratory.

The waste involved in this study was from AN-107. Previous, studies of AN-107 have described the occurrence of natron ($Na_2CO_3•H_2O$), sodium oxalate ($Na_2C_2O_4$), and natrophosphate ($Na_7F(PO_4)_2•19H_2O$) (Reynolds et al. 2012) [see Figure E.1 for an x-ray diffraction (XRD) scan a sub-sample of AN-107]. Felmy modeled the effect of carbonate as a function of added CO_2 in AN-107 (Felmy, 2005). He showed that with the introduction of atmospheric CO_2, net neutralization of the excess NaOH occurred with the formation of aqueous Na_2CO_3:

$$CO_{2(g)} + 2NaOH = Na_2CO_{3(aq)} + H_2O$$

As the aqueous carbonate concentration was increased, equilibrium with natron ($Na_2CO_3•H_2O$) occurred. Dawsonite ($NaAlCO_3(OH)_2$) was predicted to form with the presence of aluminum, but with the continued introduction of CO_2, trona ($Na_3(CO_3)(HCO_3)·2H_2O$) precipitated:

$$CO_{2(g)} + NaOH + Na_2CO_3 + 2H_2O = Na_3(CO_3)(HCO_3)·2H_2O \text{ (Trona)}$$

The final predicted solid phases in equilibrium with the waste exposed to the atmosphere included both trona and dawsonite. Dawsonite has been observed in several waste tanks by Reynolds and co-workers (Reynolds et al., 2012) and trona has been reported by Cooke (LAB-RPT-10-00001, Rev. 0, pg. B-4).

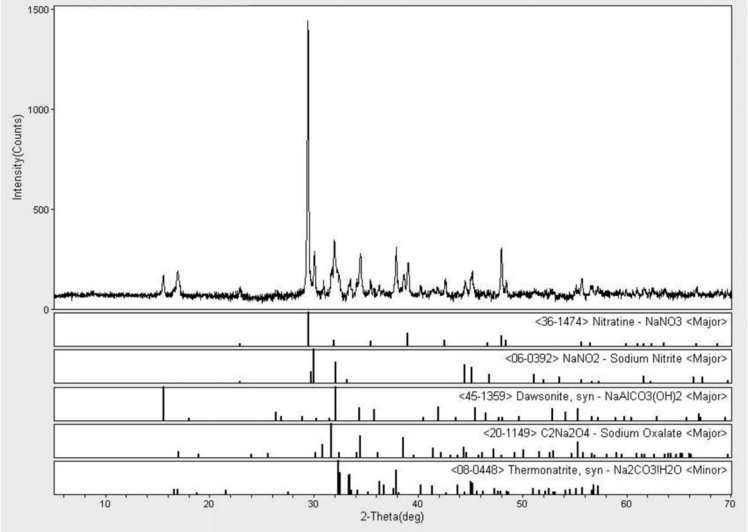

Figure E.1 XRD Results from Reynolds and co-workers on AN-107 (Reynolds et al., 2012) reporting the occurrence of nitratine ($NaNO_3$), sodium nitrite ($NaNO_2$), dawsonite, sodium oxalate ($C_2Na_2O_4$), and thermonatrite; however, no indication of phosphfluorite minerals or trona was in these XRD results.

Savannah River National Laboratory (SRNL) also performed SEM combined with EDS analysis of AN-107 particles and described some of the morphologies observed. Their observations may be useful for interpreting the data obtained in this study. They were unable to provide any particle size measurements because the dose rates were too high for the quantity of sample that was required. Qualitative analysis of the AN-107 solids revealed the occurrence of Na, S, Cl, K, Ca, Cr, Mn, Fe, Ni, Al, and U (Martin 2004). The presence of uranium-bearing particles is interesting and was found consistently. Figure E.2 shows an example SEM analysis from this study revealing the U-phase.

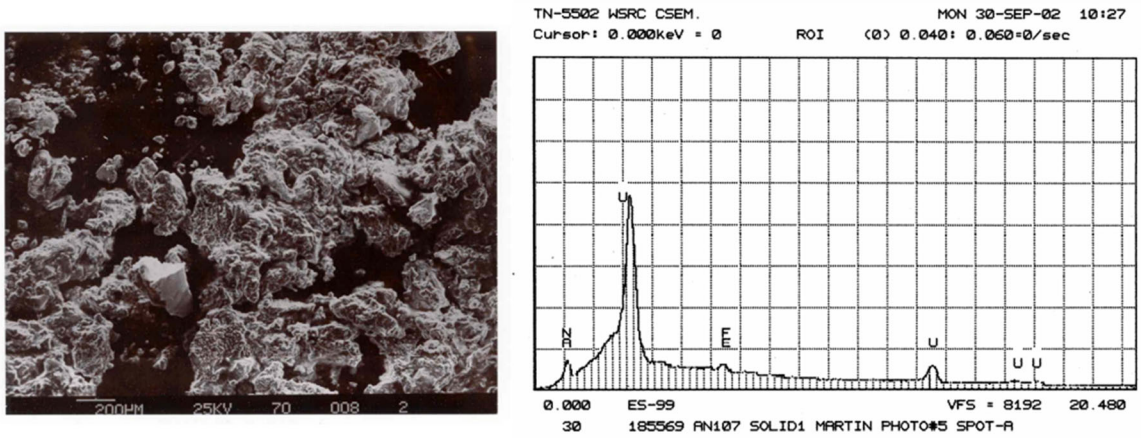

Figure E.2 Results from the solids characterization of AN-107 reported by Martin and co-workers (Martin, 2004).

The presence of solids has been observed in previous filtration experiments. It is postulated that addition of process water contributes to precipitate formation in diluted wastes; such “dilution-induced” precipitation has been demonstrated and characterized using a non-radioactive AP-105 tank waste simulant (Daniel et al., 2020). The latter study attributes the cause of precipitation to the interaction of solutes in the process water with those in the waste supernatant.

In this investigation, an effort was made to look for these previously observed and predicted phases in the various samples received with a combination of SEM and TEM with SAED. SAED is not as reliable as XRD in direct phase identification because multiple scattering and the random orientation of individual crystals in the TEM can eliminate or change the intensities of various Bragg reflections required for phase identification. However, with the combination of EDS and electron diffraction, it is possible to narrow down possible phases together with referring to prior analyses and predictions (Wells et al. 2011).

In this study, SEM and EDS mapping and STEM combined EDS mapping, as well as TEM/SAED was used to identify the solids from the received AN-107 samples. STEM/TEM is an inherently statistically poor tool for determining the relative amounts of particle types. However, the technique is much better at clearly identifying phases and compositions. The report contains several STEM/TEM analyses and SEM analyses.

E.1 Experimental Procedure

Materials representing AN-107 were sub-sampled for microscopy. Four samples were provided (AN-107 Solids, Solution-1, Solution-3, Solution-4). The first sample (AN-107 Solids) contained semi-dried solids that were only examined with SEM. Three other samples contained particles in solution. These were also analyzed with SEM and two of these samples were further sub-sampled for STEM analysis. The solid sample was deposited onto a SEM carbon stub and analyzed. The solution samples were pipetted onto carbon stubs. This process did result in the precipitation of salts however some useful information could still be obtained. The solutions were also prepared for STEM using the holey-carbon TEM grid as a filter that prevented evaporite formation. Only two samples could be analyzed (Solution-3 and Solution-4) as the particles from Solution 1 were too large for imaging. Several TEM grid samples were prepared from each condition; however, some TEM grids possessed too high an activity to be further analyzed.

Table E.1. Sample Analysis Summary

Samples	Techniques Applied	
	SEM	**TEM**
AN-107 Solids	SEM, EDS mapping, particle analysis	Activity too high
Solution-1	SEM, EDS mapping	Large particles – too thick for TEM
Solution-3	SEM, EDS mapping	STEM/TEM/diffraction (SAED)/EDS mapping
Solution-4	SEM	STEM/TEM/diffraction (SAED)/EDS mapping

SEM was performed using the Quattro S (Thermo-Fisher, Inc., Hillsboro, OR) equipped with an iXRF Systems (Austin, TX) EDS system. STEM analysis used a JEOL (JEOL Inc., Japan) ARM300F (GrandARM) microscope. STEM images were collected using a high angle annular dark field (HAADF) detector and compositional analysis was obtained with EDS. SAED patterns were analyzed with DigitalMicrograph 3.0 software and utilizing scripts developed by Mitchell (Mitchell, 2008) and CrysTBox (Crystallographic Tool Box) software (Klinger, 2017). Crystallographic files for the phases of interest were obtained from the American Mineralogist Crystallographic Database (https://rruff.geo.arizona.edu/AMS/amcsd.php).

E.2 Microscopy Solids Analysis Results

All four samples were analyzed during this investigation with the available tools. The 'AN-107 Solids' sample could only be examined on the SEM owing to the high activity and the size of the individual particles. The three other samples consisted of particles suspended in solution. These were prepared by drop-casting onto an SEM stub and by drop-casting onto TEM grids. Particles were visible by the naked eye in Solution-1 which also had the highest activity. Although samples of Solution-1 were prepared for TEM, there were particles that were too large to transfer directly to the TEM. A particle in excess of 20-40 µm and several micrometers thick is not possible to analyze in the STEM and obtain any useful data. However, with SEM, these large particles can be easily accommodated.

E.2.1 SEM Analysis of AN-107 Solids

The SEM stub prepared from the AN-107 Solids sample was dominated by Mn-Fe phases. There was little evidence of salt phases in this prepared specimen.

The material shown in Figure E.3 was commonly found throughout the sample. The phase was found to consist mainly of Mn and Fe with Na and O. Carbon was present in the support film making it difficult to locate C-bearing phases. Figure E.4 shows further SEM EDS maps of these Mn-Fe phases in the AN-107 solids sample. The results from this study were consistent with the results from the SRNL study on AN-107 (Martin, 2004).

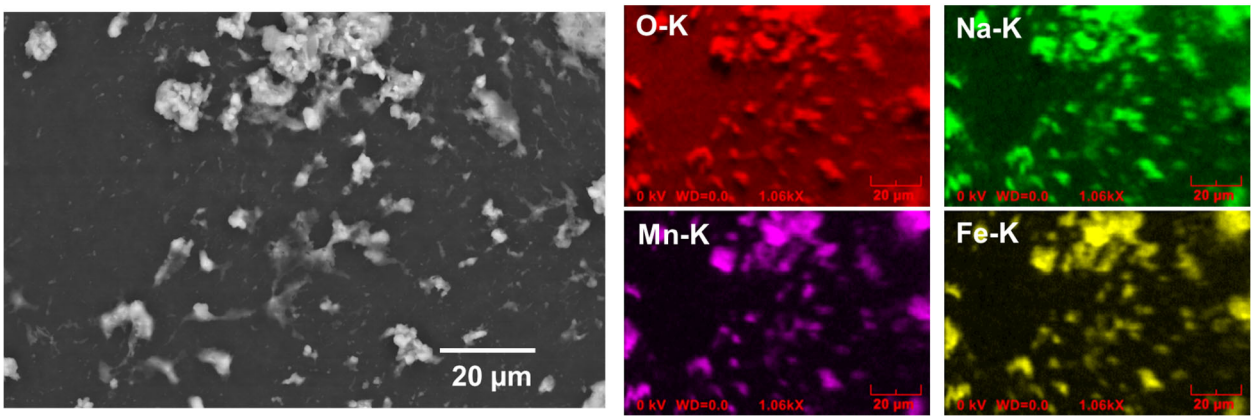

Figure E.3 SEM Image and EDS maps of Mn-Fe phases found in the AN-107 Solids sample.

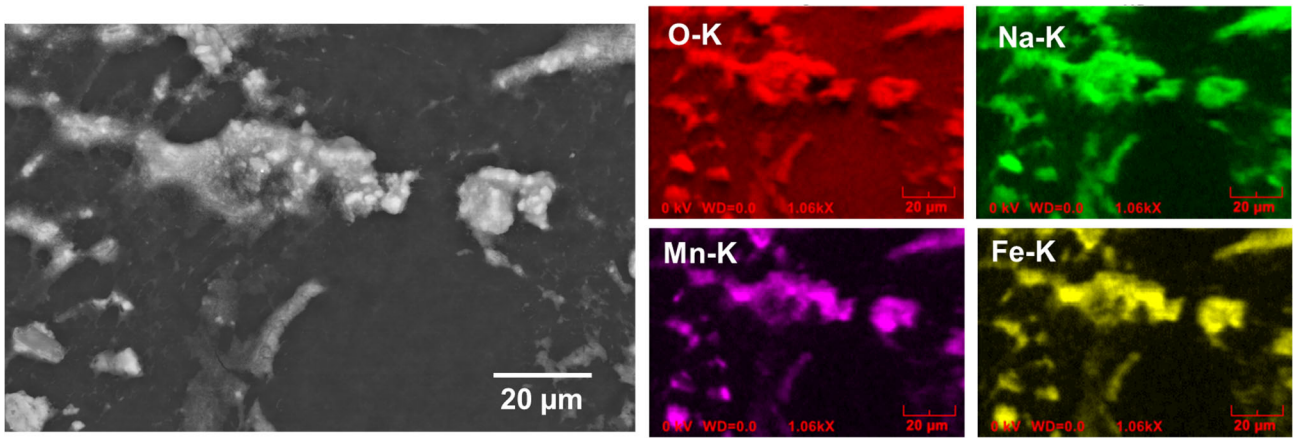

Figure E.4 Further SEM images of Mn-Fe particles in the AN-107 Solids sample.

The SRNL study also indicated the occurrence of uranium in these particles. This was not observed during the SEM-EDS mapping investigation.

E.2.2 Solution-1

The major phase observed in the SEM from Solution-1 was compositionally consistent with natrophosphate ($Na_7F(PO_4)_2 \cdot 19H_2O$). In Figure 4.11, the block-like precipitate contains O, F, Na, and P as the major elements. Smaller Fe-Mn particles were attached to this phase. This phosphate phase did not precipitate out during the sample preparation operation but was observable in the solution prior to deposition onto the SEM stub. The individual particles were in some cases hundreds of micrometers across which is consistent with prior observations from tank waste characterizations (Bolling et al., 2019; Herting & Reynolds, 2016; Reynolds & Herting, 2016).

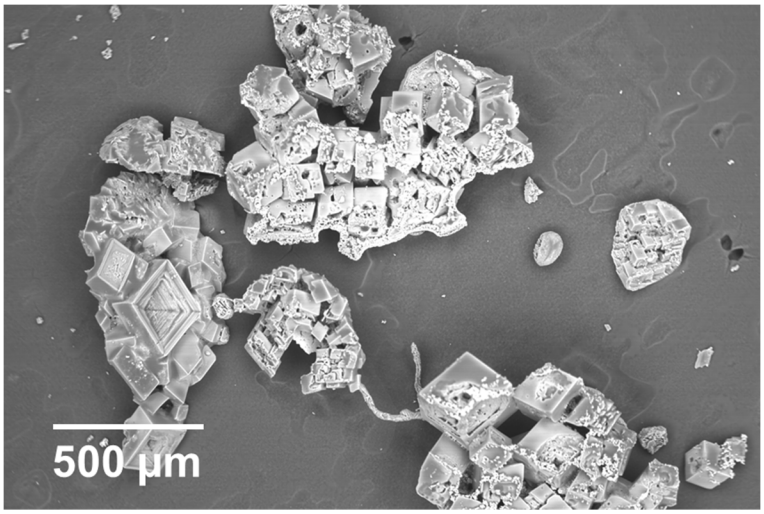

Figure E.5 SEM image of large particles observed in AN-107 Solution-1

Figure 4.11 shows a higher magnification image of the natrophosphate with small particles of a Fe-Mn phase attached to the surface of the particles. EDS mapping revealed that the block-like phase consisted of O, F, Na, and P consistent with the fluoro-natrophosphate. It is possible that these particles were deposited during the sample preparation and were suspended in the solution. However, the observation of the Fe-Mn phase is consistent with the results from the solids sample.

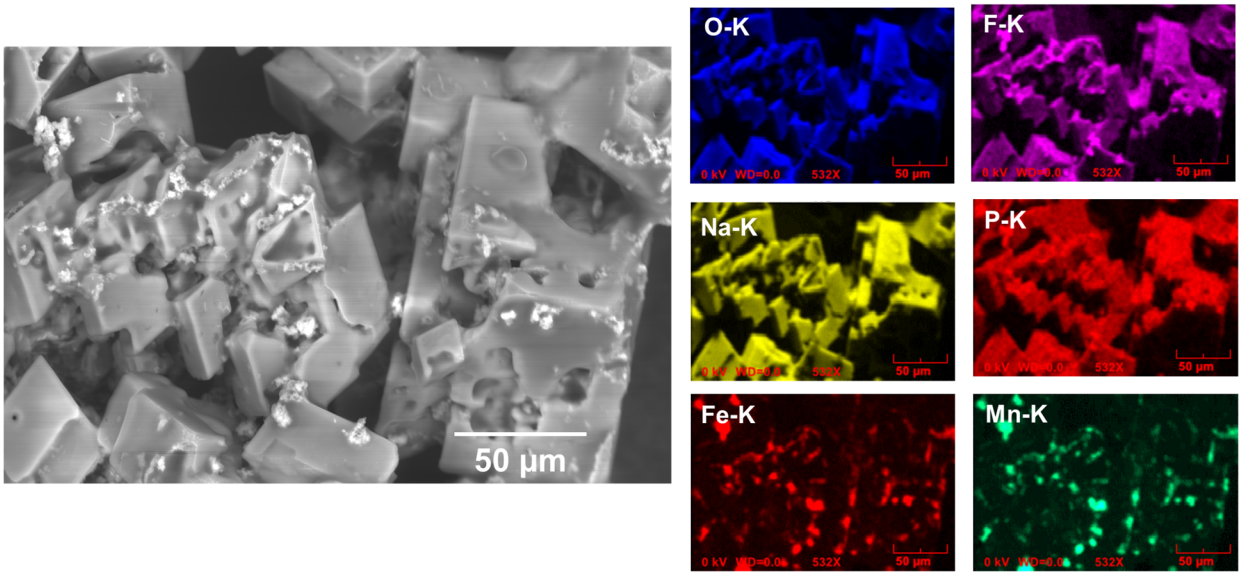

Figure E.6 SEM and EDS analysis of a possible mixed salt sodium nitrate/fluoro-phosphate phase with particles of the Mn-Fe phase attached to the crystal surfaces in AN-107 Solution-1.

E.2.3 Solution-3

Solution-3 was examined with both SEM and TEM. Figure E.7 and Figure 4.13 show SEM images and EDS elemental maps that exhibited compositions and morphologies similar to those from the AN-107 Solids sample and Solution-1. Nitrogen was also detected in these particles, which may indicate the precipitation of nitrate salts during the SEM sample preparation. The particles occurred as agglomerates ranging from a few micrometers to >20 µm in diameter.

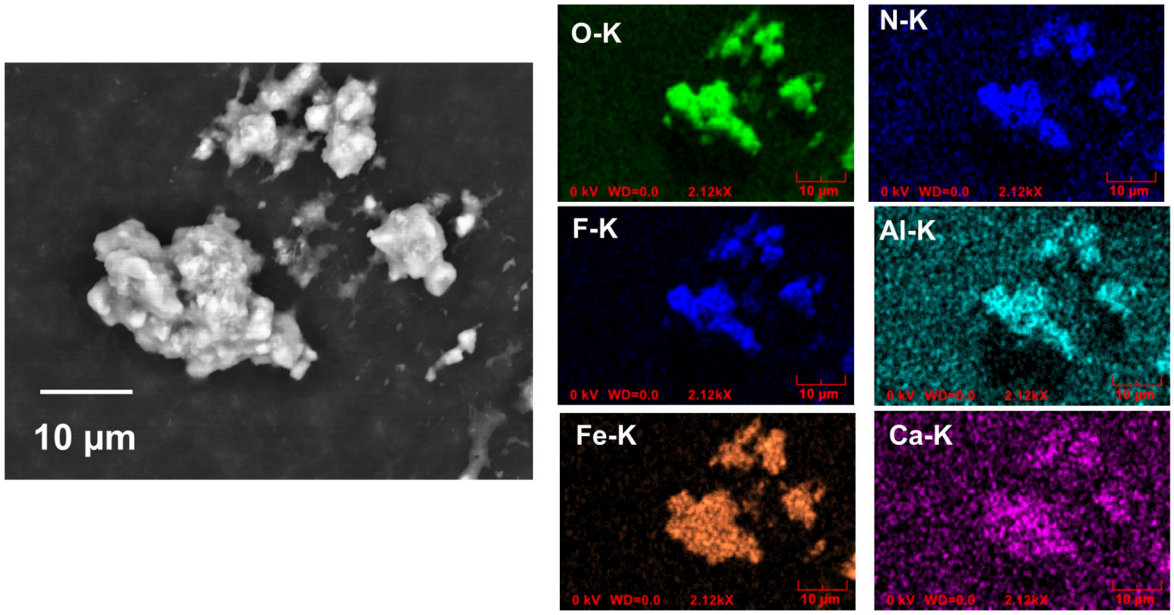

Figure E.7 Different morphologies of a Fe-rich phase found in Solution-3.

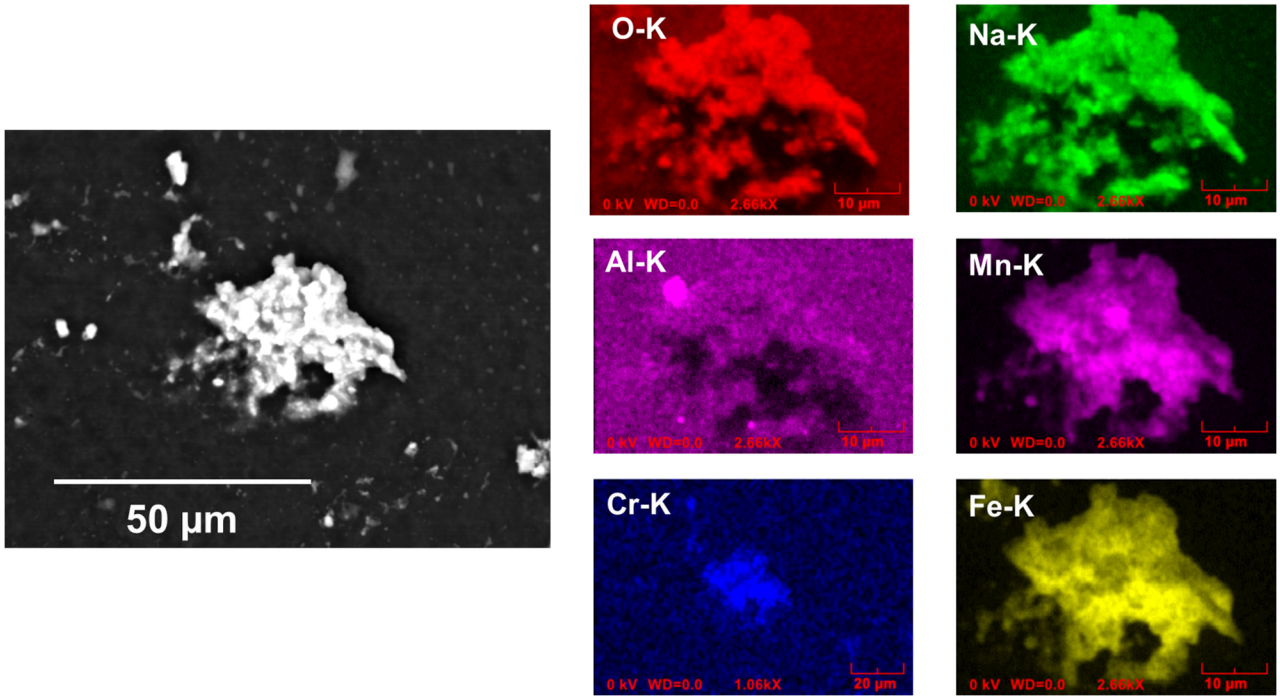

Figure E.8 SEM image and EDS maps of Mn-Fe phase in Solution-3

E.2.4 Solution 4

Solution-4 was dominated by fibrous-like particles and was distinctly different from the solids sample and the other samples received. The SEM images of the particles and the TEM images showed similar morphologies (see Figure 4.14 and Figure 4.15). This helps to provide confidence that the particles

observed in the TEM were representative of the bulk material sampled. No EDS was obtained during the SEM analysis of this specimen; however, extensive analysis was performed in the TEM of this specimen.

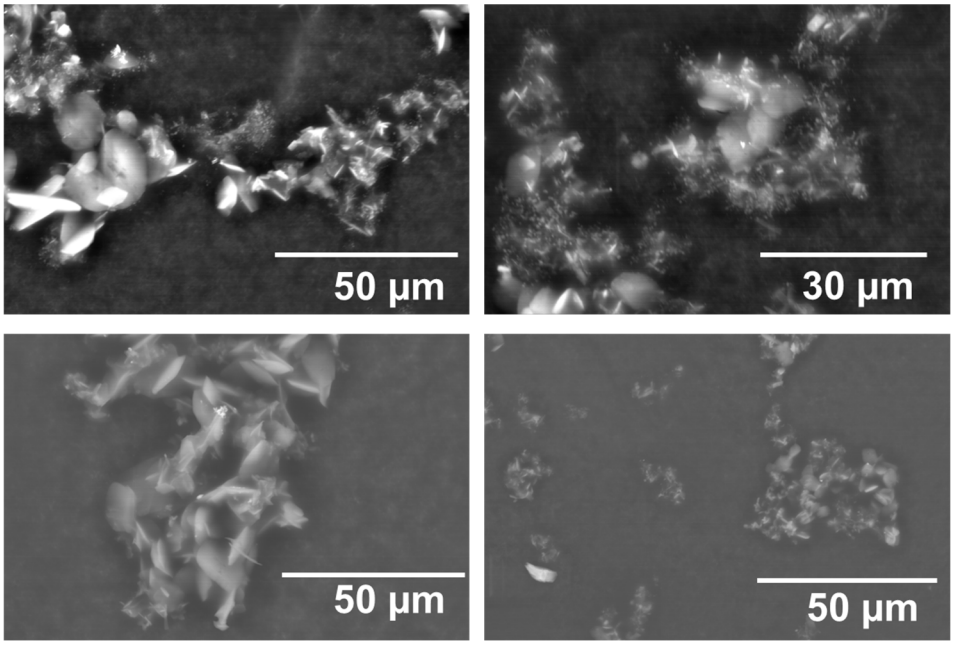

Figure E.9 SEM image of particles observed in Solution-4.

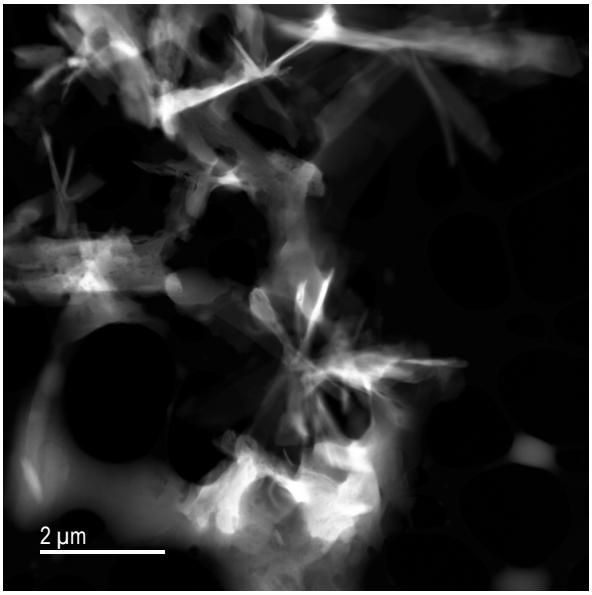

Figure E.10 Low-magnification TEM image of Solution-4 showing the same type of morphology as shown in Figure 4.14.

E.3 AN-107 TEM Analysis

All three of the solutions samples were prepared for TEM. However, the particles present in Solution-1 were too large to image on the TEM. Other techniques such as ultramicrotomy were not applied in this instance.

E.3.1 Solution-3

Figure E.11 shows STEM-HAADF images and STEM-EDS elemental maps of a collection of different particles found in the Solution-3 sample.

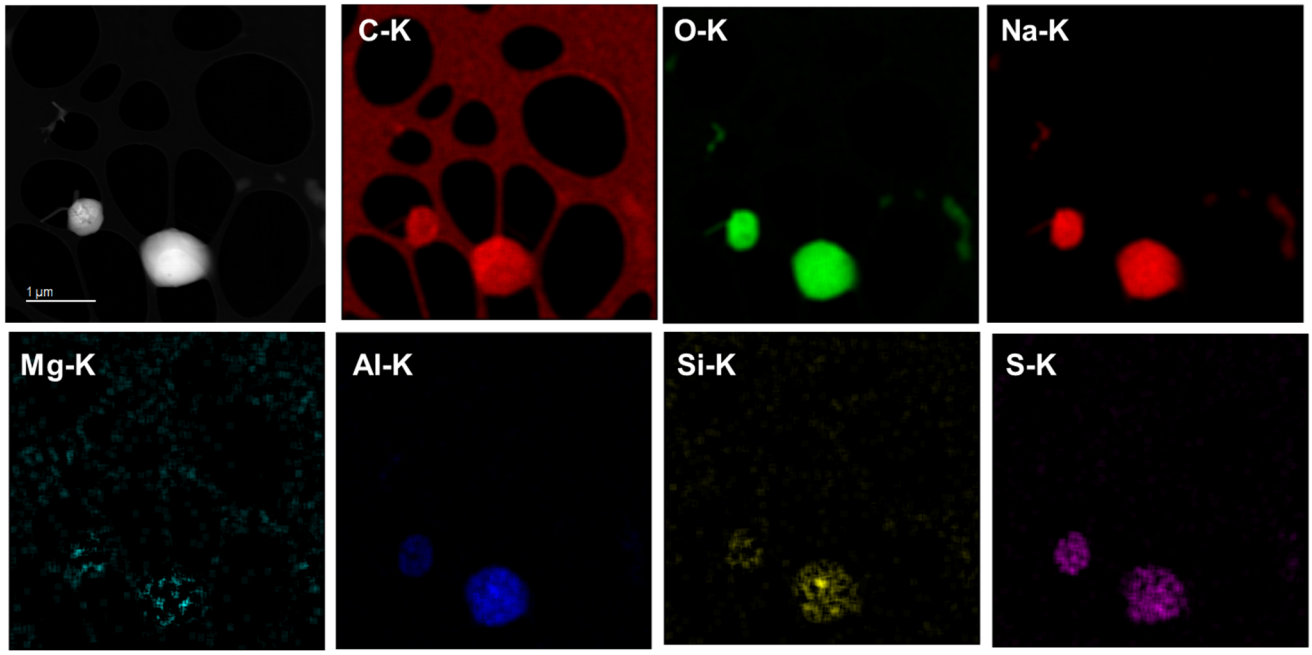

Figure E.11 HAADF image and STEM-EDS maps of sodium-rich particles, possibly sodium oxalate in Solution-3.

Other unusual compositions were found. Most of the particles proved to be amorphous or could have been damaged by the electron beam prior to analysis. In Figure E.12, STEM-HAADF and STEM-EDS maps of a silicate particle that also contained uranium are shown. Uranium was observed in the study of AN-107 by Martin and co-workers (Martin, 2004). The uranium-bearing particles were confined to two regions on the silicate particle.

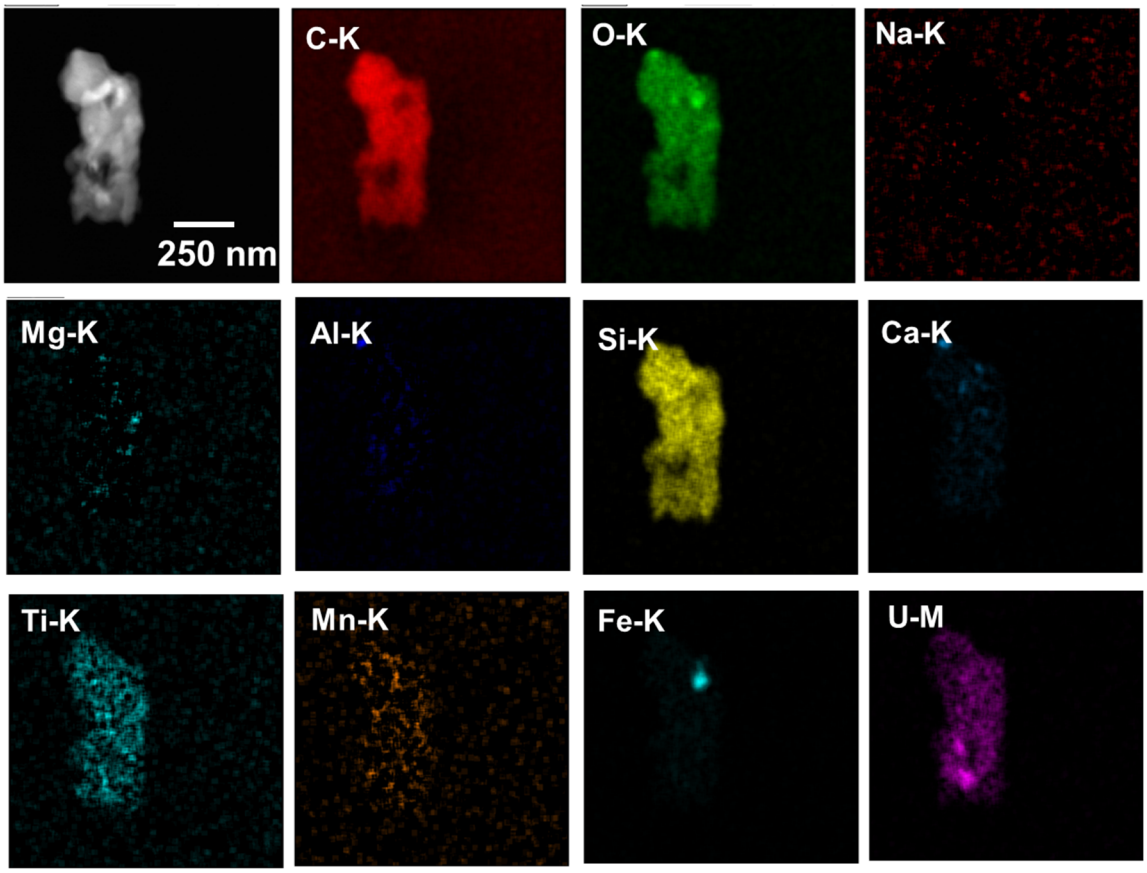

Figure E.12 HAADF image and STEM-EDS analysis of a particle agglomerate consisting of possibly silicon but had a noticeable quantity of uranium.

Figure E.14 shows a series of particles with SAED patterns. The compositional analysis of these particles is shown in Figure E.18. The SAED did not reveal any reflections. The composition was mainly Si and O, and possibly C in the phase. A smaller region was also uranium-rich. Figure E.14 shows low-magnification TEM images of particles attached to the holey carbon film used to capture particles. The large holes in the carbon film prevent salts depositing yet are able to capture many of the suspended particles and colloids that may have been present in the solution.

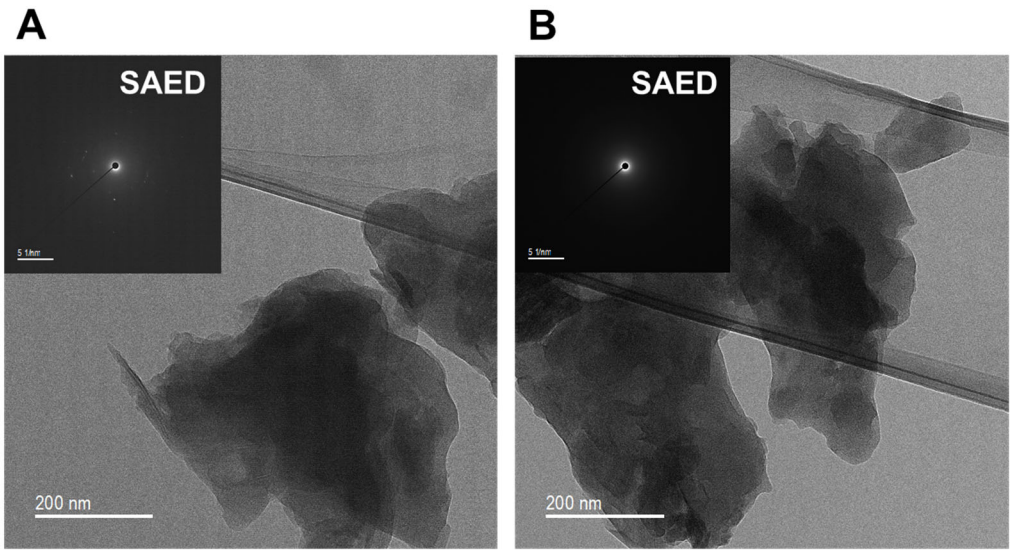

Figure E.13 TEM images and electron diffraction patterns of a particle agglomerate in Solution-3.

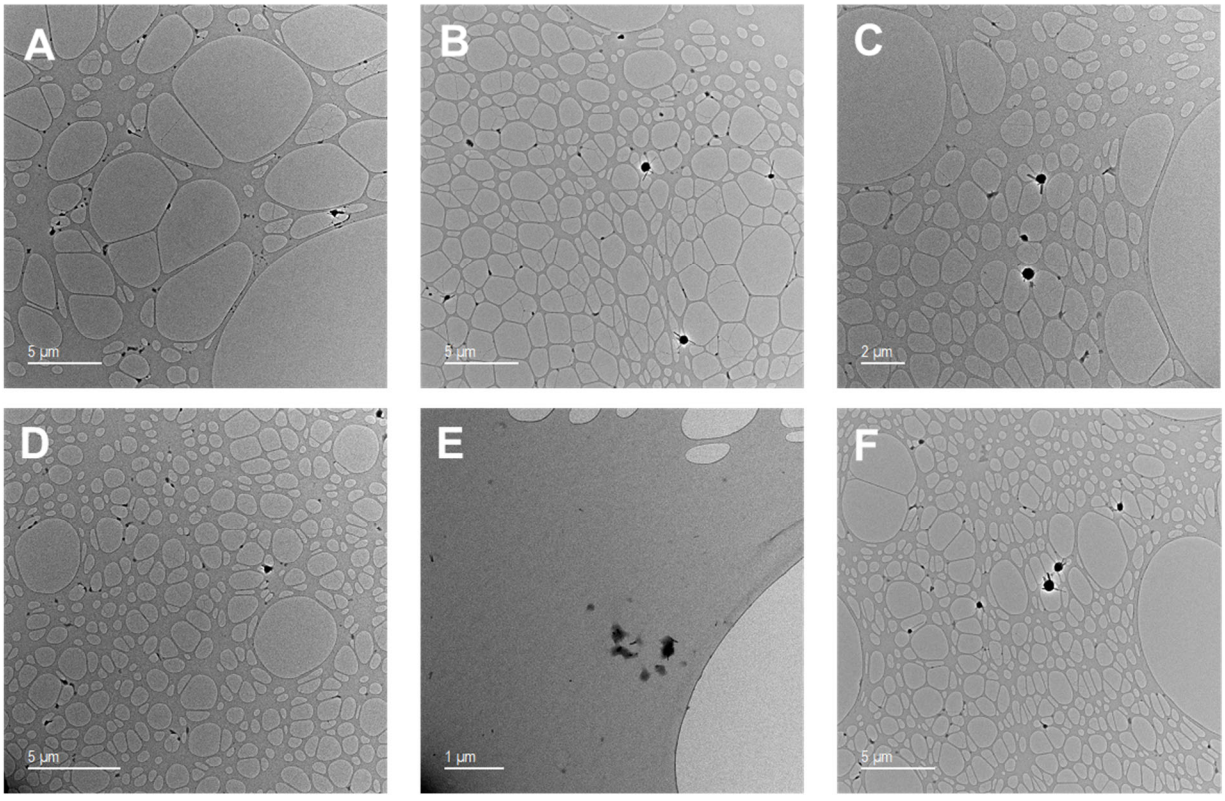

Figure E.14 TEM images of particles observed in the AN-107 Solution-3 sample.

Higher magnification images of particles from Solution-3 are shown in Figure E.15 and Figure E.16. There are a few particles that were crystalline, but the SAED patterns were poor. In Table E.1, these d-spacings are listed but no attempt was made here to identify the phase.

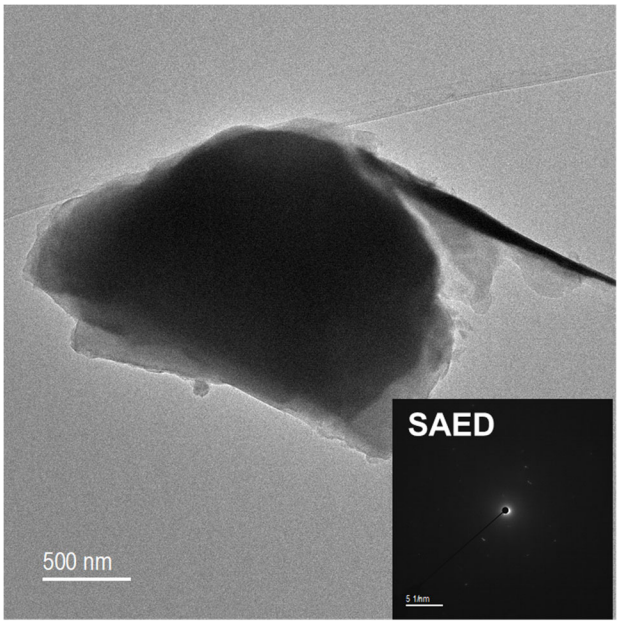

Figure E.15 TEM analysis and insert SAED of a particle observed in the Solution-3 sample.

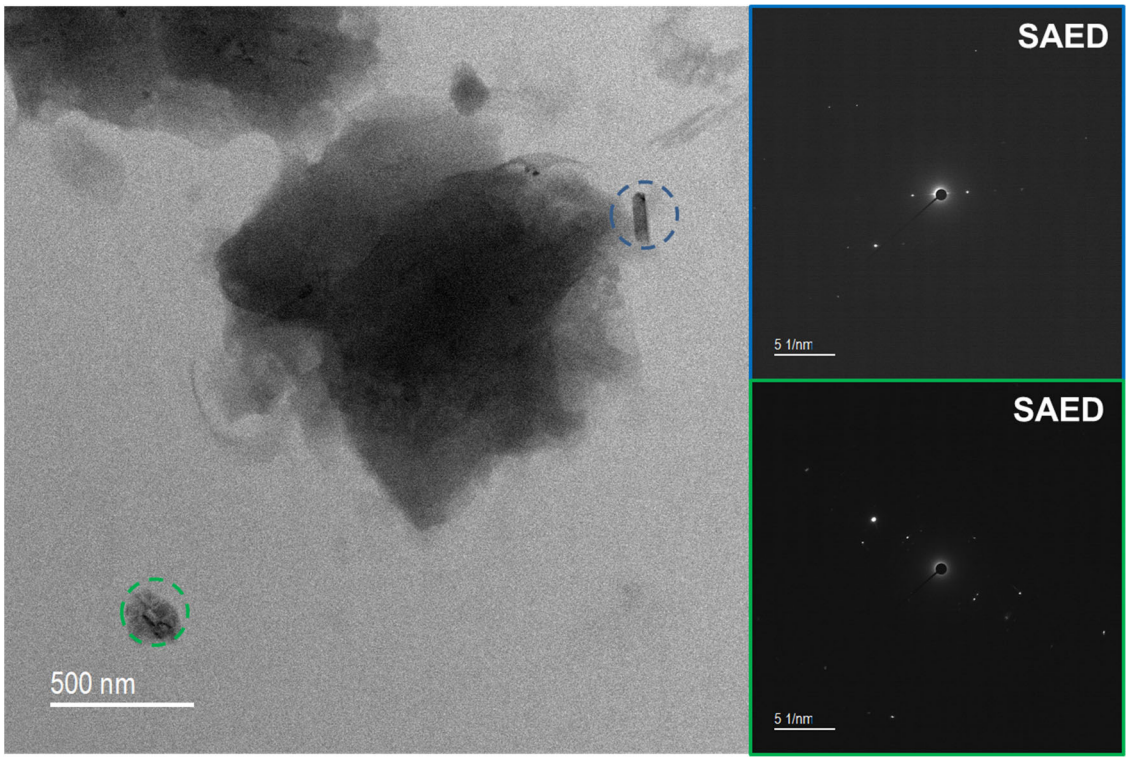

Figure E.16 TEM image and electron diffraction patterns obtained from a particle in Solution-3.
Ref: Diff004_80cm AN-107 0278.dm4 and Diff006_80cm AN-107 0278.dm4

Table E.1 Electron diffraction from Figure E.18

Measured (Diff004)	Measured (Diff006)
0.454	0.272
0.354	0.150
0.288	0.137
0.246	0.091
0.228	0.079
0.201	0.074
0.150	0.071
0.102	0.067
0.067	

Other silicate particles were observed in the specimen, Solution-3. In Figure E.17, TEM, STEM, and EDS analysis of a phase showed a silicate particle and TiO_2 particles.

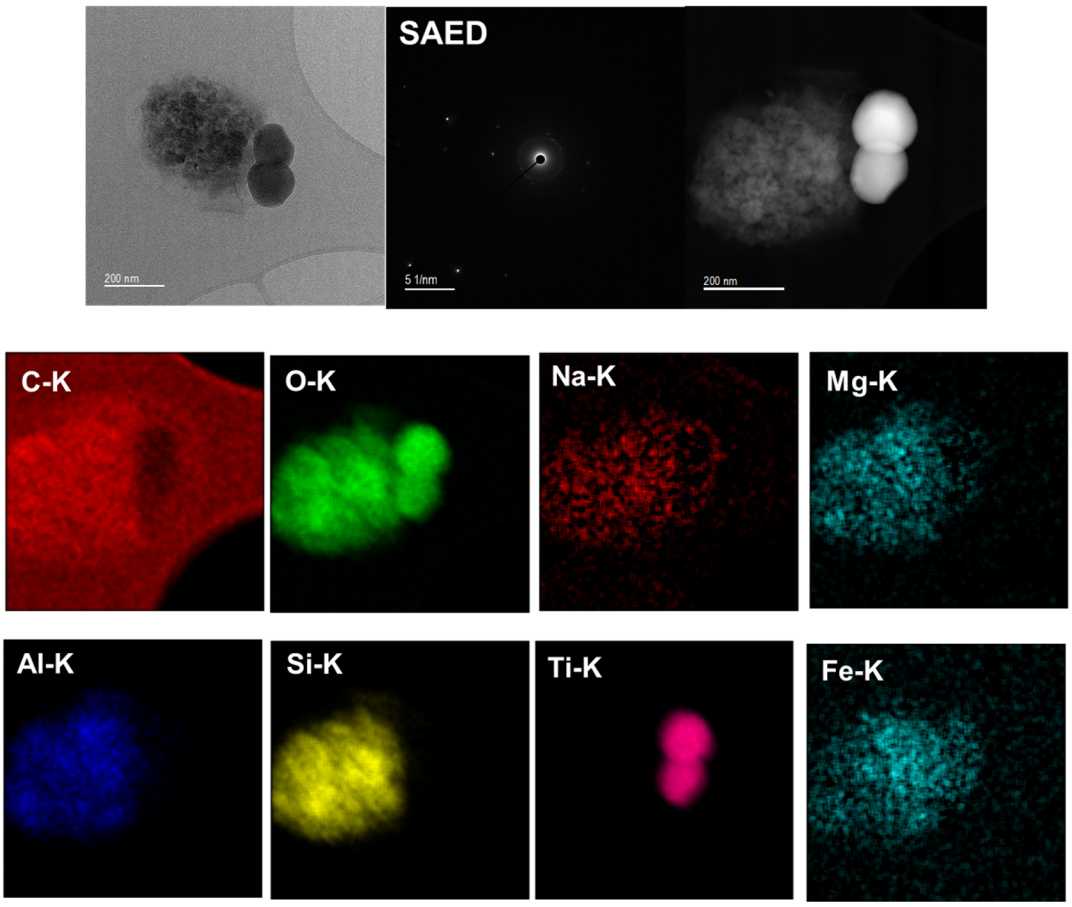

Figure E.17 TEM image and STEM-HAADF image together with an electron diffraction pattern and a series of STEM-EDS elemental maps of a particle consisting of an aluminosilicate and a titanium oxide phase.

Ref: Diff007_80cm AN-107 0278.dm4

STEM-EDS maps from sample Solution-3 are shown in Figure E.18 and Figure E.19. These represent much of the data that was collected on the sample.

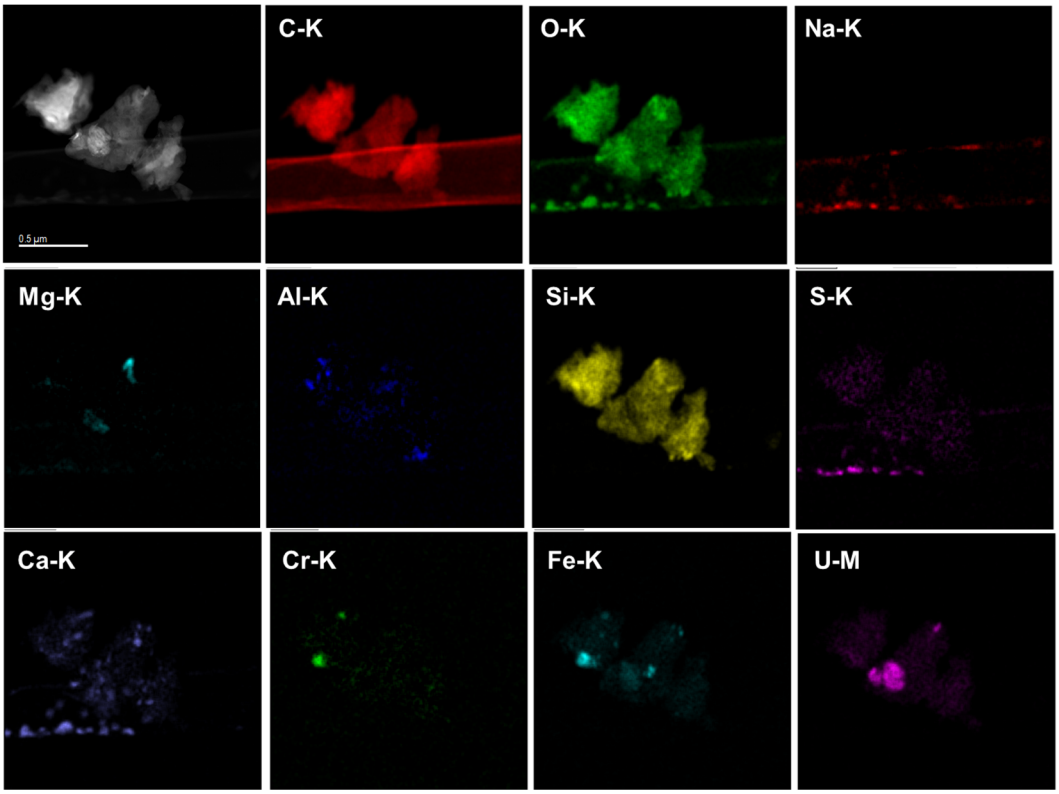

Figure E.18 STEM-EDS of particles from AN-107 Solution-3 and shown in Figure E.13.

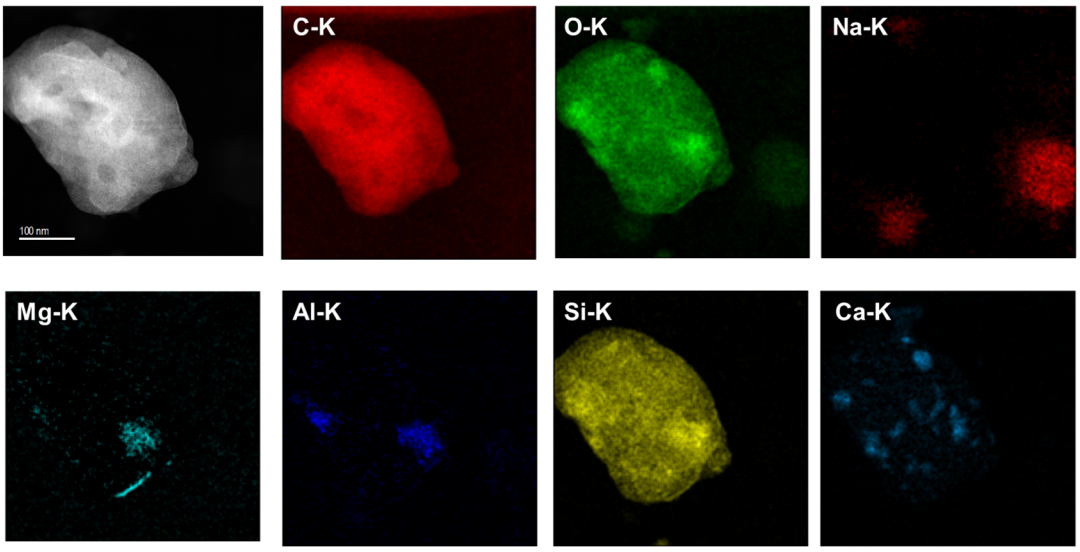

Figure E.19 STEM EDS analysis of possible oxalate phase. The Mg, Al, Si, and Ca were minor components. The Ca appeared to be on the surface of the particle.

Figure E.20 shows a potassium aluminosilicate phase, possibly a feldspar which has been observed previously in these analyses and tends to be derived from dust from the environment rather than actual wastes. Attached to the potassium aluminosilicate phase were Mg- and Fe-rich phases.

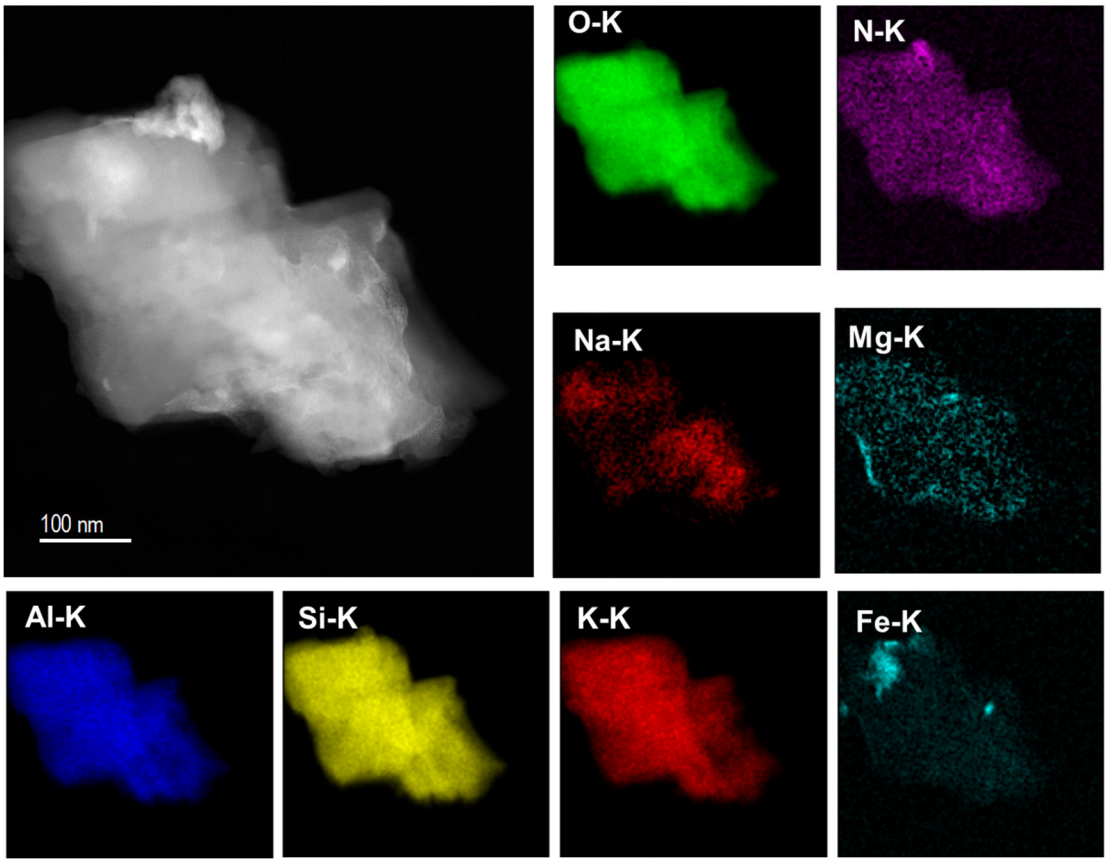

Figure E.20 STEM HAADF image and STEM-EDS maps of an aluminosilicate particle observed in Solution-3.

Electron diffraction from this phase did not reveal any noticeable reflections and hence is not reported here. Figure E.21 and Figure E.22 show further STEM-EDS maps of particles in the specimen that appeared to be some type of C-N-O-Na phase which might mean a combination of nitrate and oxalate phases. The Fe-Mn phases and phosphates phases were not observed in Solution-3. This may have been due to sample preparation errors. It demonstrates the need to examine more samples and perform additional SEM analyses. Particle analysis software was not available in this study as there were technical problems in operating this system which otherwise would have provided more statistically relevant information.

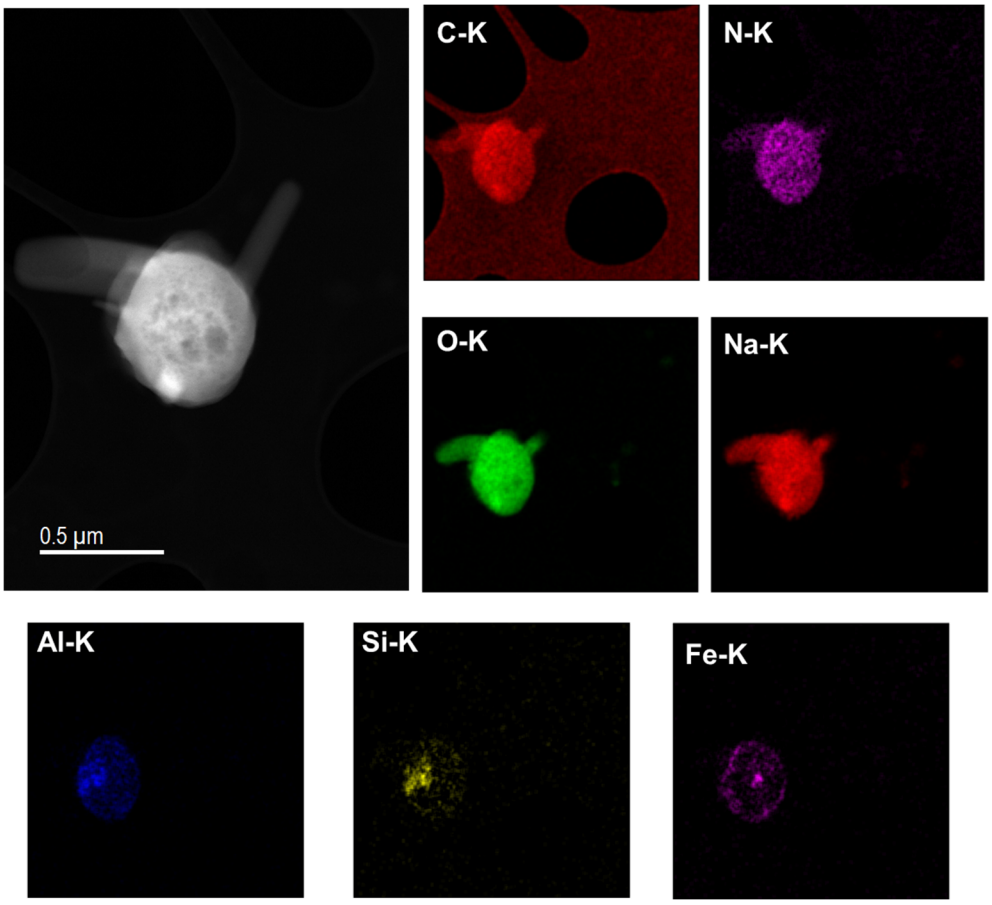

Figure E.21 STEM image and STEM-EDS maps of possible sodium carbonate (Na_2CO_3) particle.

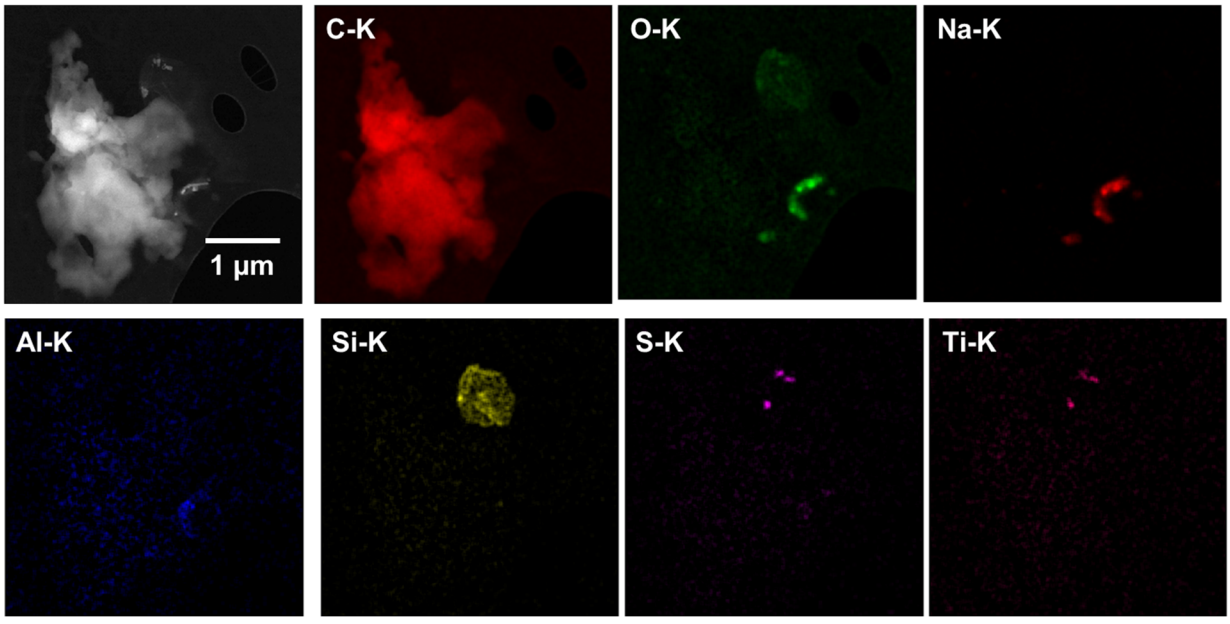

Figure E.22 STEM-HAADF image and STEM-EDS maps of a carbon-based particle that was carrying other minor phases.

E.3.2 Solution 4 STEM Analysis

Solution-4 was found to contain many of the phases both expected and supported by the earlier findings from the SEM. Figure E.23 shows a Mg-phosphate phase in the waste that has been observed in other Hanford tank waste samples.

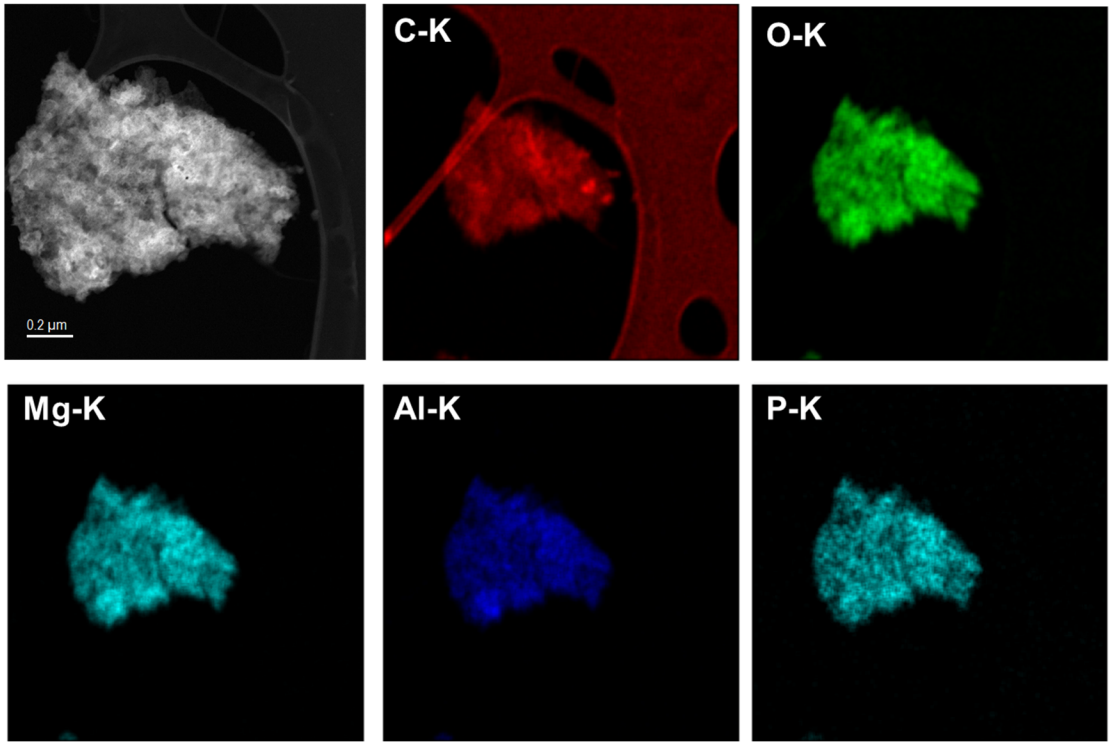

Figure E.23 STEM-HAADF image and STEM EDS analysis of possible Mg-phosphate phase.

The carbonate phases trona and dawsonite were predicted for the AN-107 wastes and there was evidence from STEM-EDS mapping and also electron diffraction for the occurrence of these phases (Felmy 2005). Figure E.24 and Figure E.25 show the STEM-EDS and TEM-diffraction of a carbonate phase in the Solution-4 sample. The presence of carbon can be confirmed because of the much stronger signal from carbon from the particle than from the carbon film (which is a few nanometers thick). Similar results are also shown for STEM-EDS and electron diffraction in Figure E.26 and Figure E.27. The electron diffraction results are displayed in Table E.2 and Table E.3 with matches to dawsonite and trona.

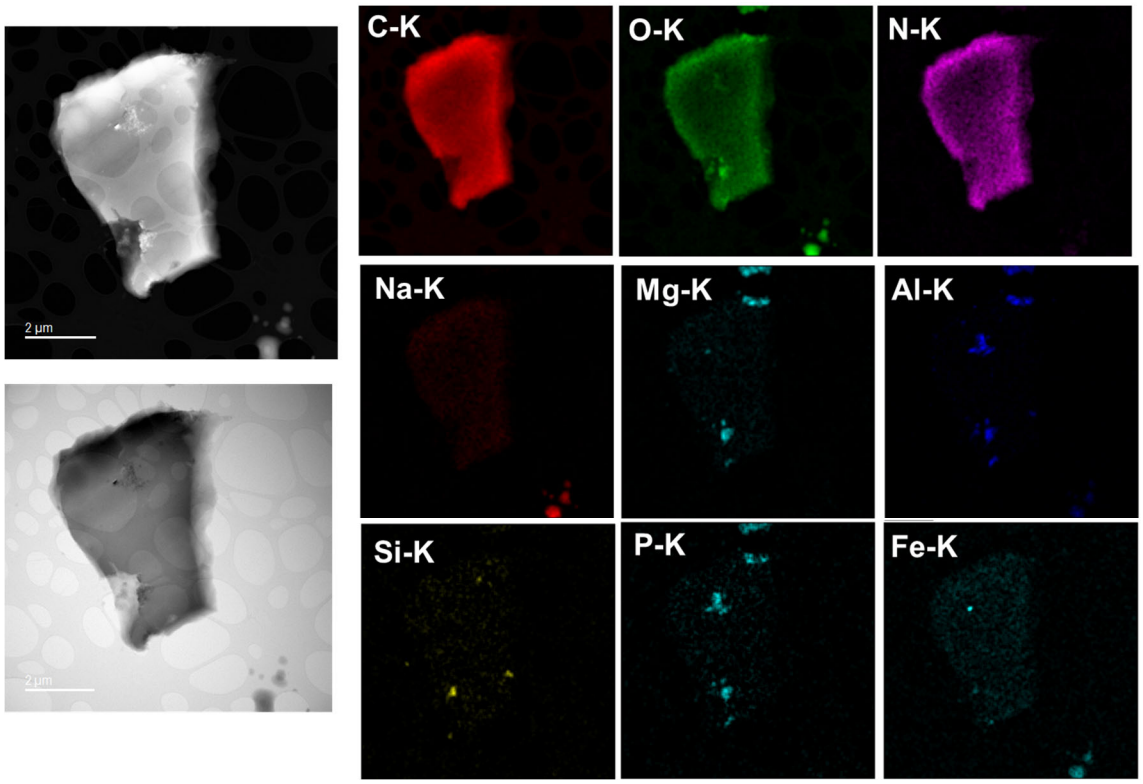

Figure E.24 STEM-HAADF and STEM-BF image together with STEM-EDS maps of a Na-C-N phase. Minor particles containing P, Al, and Mg were also present and attached to this larger particle.

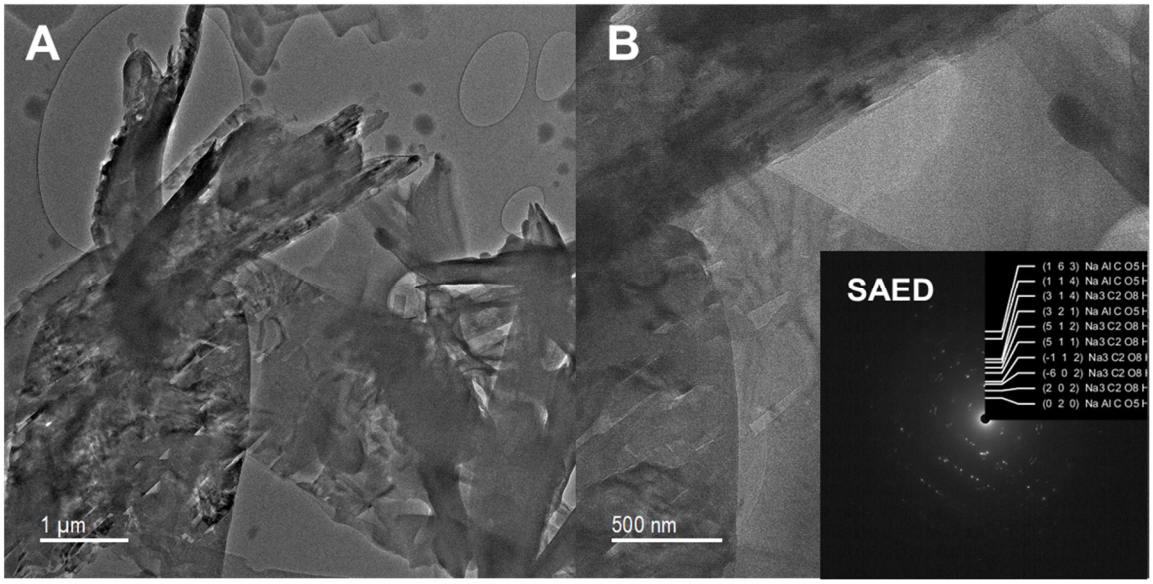

Figure E.25 TEM image and a diffraction pattern of particles from the Solution-4 sample that has been matched to reflections from trona and dawsonite.
Ref: Diff001 OneView 80cm AN-107 0305.dm4

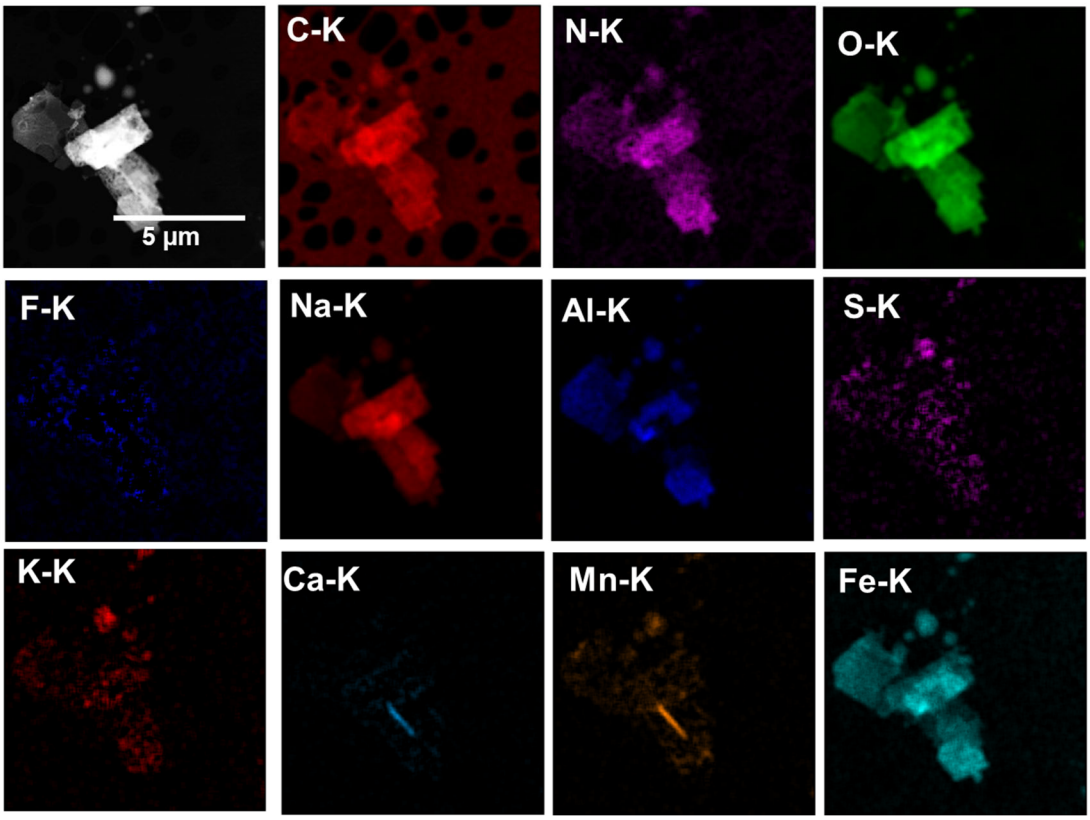

Figure E.26 STEM-EDS elemental maps of the large particle agglomerates containing C, Na, and O as major elements, as well as minor Al and Fe.

Table E.2 Electron diffraction from Figure 4.13D with possible matches to trona ($Na_3C_2O_8H_5$) and dawsonite ($NaAlCO_5H_2$)

Plane/ Phase	Radius [1/nm]		d-spacing [nm]	
	theor.	measured	theor.	measured
(0 2 0) $NaAl(OH)_2CO_3$	1.921	1.940	0.521	0.515
(2 0 2) $Na_3(CO_3)(HCO_3)\cdot 2H_2O$	2.517	2.617	0.397	0.382
(-6 0 2) $Na_3(CO_3)(HCO_3)\cdot 2H_2O$	3.165	3.205	0.316	0.312
(-1 1 2) $Na_3(CO_3)(HCO_3)\cdot 2H_2O$	3.470	3.440	0.288	0.291
(5 1 1) $Na_3(CO_3)(HCO_3)\cdot 2H_2O$	4.161	4.234	0.240	0.236
(5 1 2) $Na_3(CO_3)(HCO_3)\cdot 2H_2O$	4.676	4.704	0.214	0.213
(3 2 1) $Na_3(CO_3)(HCO_3)\cdot 2H_2O$	5.186	5.204	0.193	0.192
(3 1 4) $Na_3(CO_3)(HCO_3)\cdot 2H_2O$	5.530	5.498	0.181	0.182
(1 1 4) $NaAl(OH)_2CO_3$	7.384	7.350	0.135	0.136
(1 6 3) $NaAl(OH)_2CO_3$	8.021	8.026	0.125	0.125

Ref: Diff001 OneView 80cm AN-107 0305.dm4

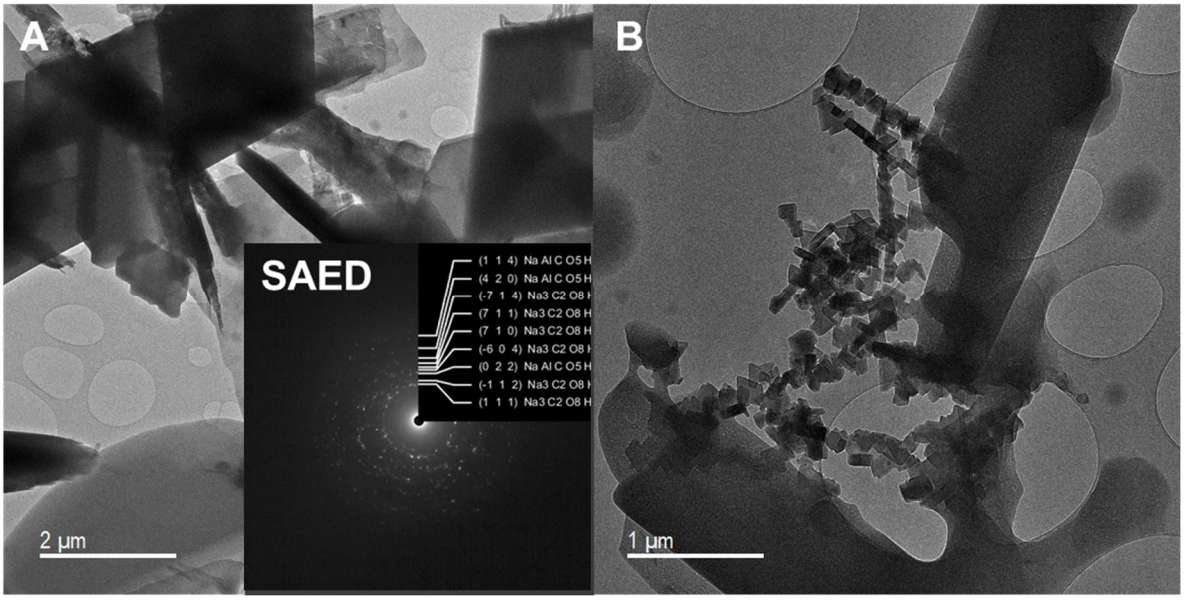

Figure E.27 TEM images and ring diffraction pattern from particles found in the Solution-4 sample.

Table E.3 Electron diffraction from Figure 4.13D with possible match to trona and dawsonite

Plane/Phase	Radius [1/nm]		d-spacing [nm]	
	theor.	measured	theor.	measured
(1 1 1) $Na_3(CO_3)(HCO_3)\cdot 2H_2O$	3.137	3.146	0.319	0.318
(-1 1 2) $Na_3(CO_3)(HCO_3)\cdot 2H_2O$	3.470	3.440	0.288	0.291
(0 2 2) $Na_3(CO_3)(HCO_3)\cdot 2H_2O$	4.067	4.087	0.246	0.245
(-6 0 4) $Na_3(CO_3)(HCO_3)\cdot 2H_2O$	4.337	4.381	0.231	0.228
(7 1 0) $Na_3(CO_3)(HCO_3)\cdot 2H_2O$	4.595	4.616	0.218	0.217
(7 1 1) $Na_3(CO_3)(HCO_3)\cdot 2H_2O$	4.919	4.969	0.203	0.201
(-7 1 4) $Na_3(CO_3)(HCO_3)\cdot 2H_2O$	5.413	5.410	0.185	0.185
(4 2 0) $Na_3(CO_3)(HCO_3)\cdot 2H_2O$	6.263	6.262	0.160	0.160
(1 1 4) $NaAl(OH)_2CO_3$	7.384	7.350	0.135	0.136

Ref: Diff003 OneView 80cm AN-107 0310.dm4

Compositionally, the phases observed in the wastes are seldom perfect matches for a specific phase. The particles tend to be aggregates of several phases, all of which may be interfering with the diffraction results. Figure E.28 shows an example of this where we have a composition that is consistent with a carbonate phase but there is also Al, Fe, and a small amount of Mn present. It appears that the Fe-Mn phase is also attached to this particle. This phase could not be observed isolated, and it was not possible to extract a well-defined diffraction pattern (see Figure E.29) from it which may also indicate that it is only partially crystalline.

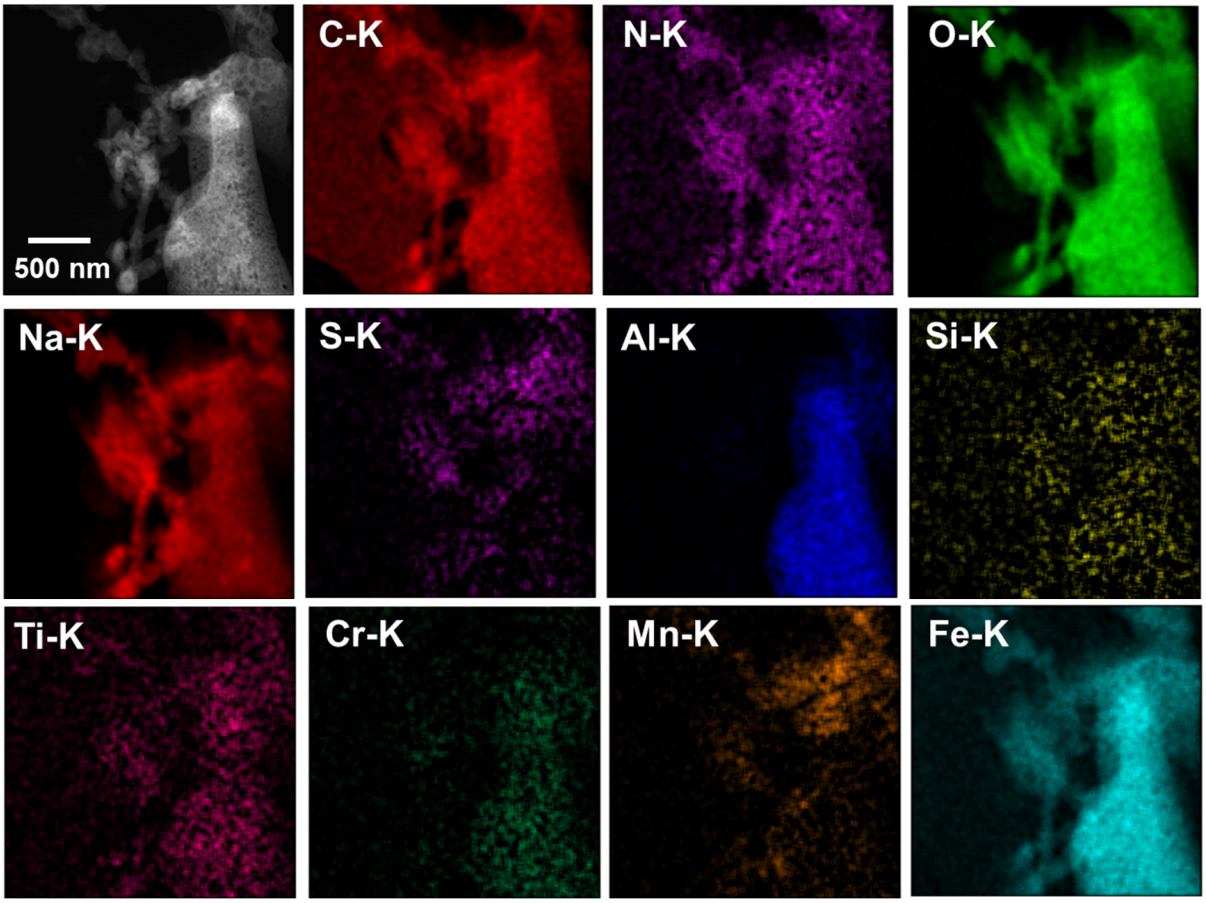

Figure E.28 STEM-EDS elemental maps of particles found in the Solution-4 sample dominated by C, O, and Na with Al and Fe also.

The composition of the phase shown in Figure E.29 is shown in Figure E.30. The small Fe-Mn phase was visible in part of the particle.

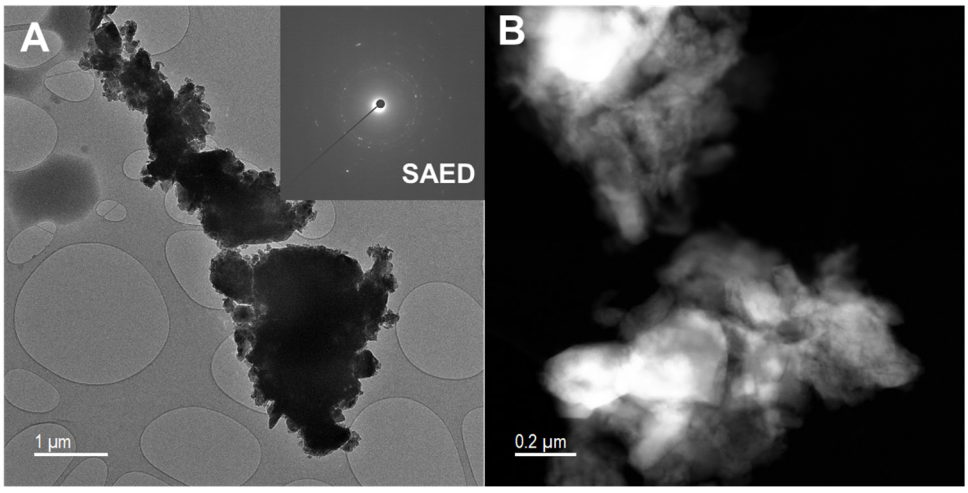

Figure E.29 TEM image, insert SAED pattern, and STEM-HAADF image of particle agglomerates found in Solution-4.

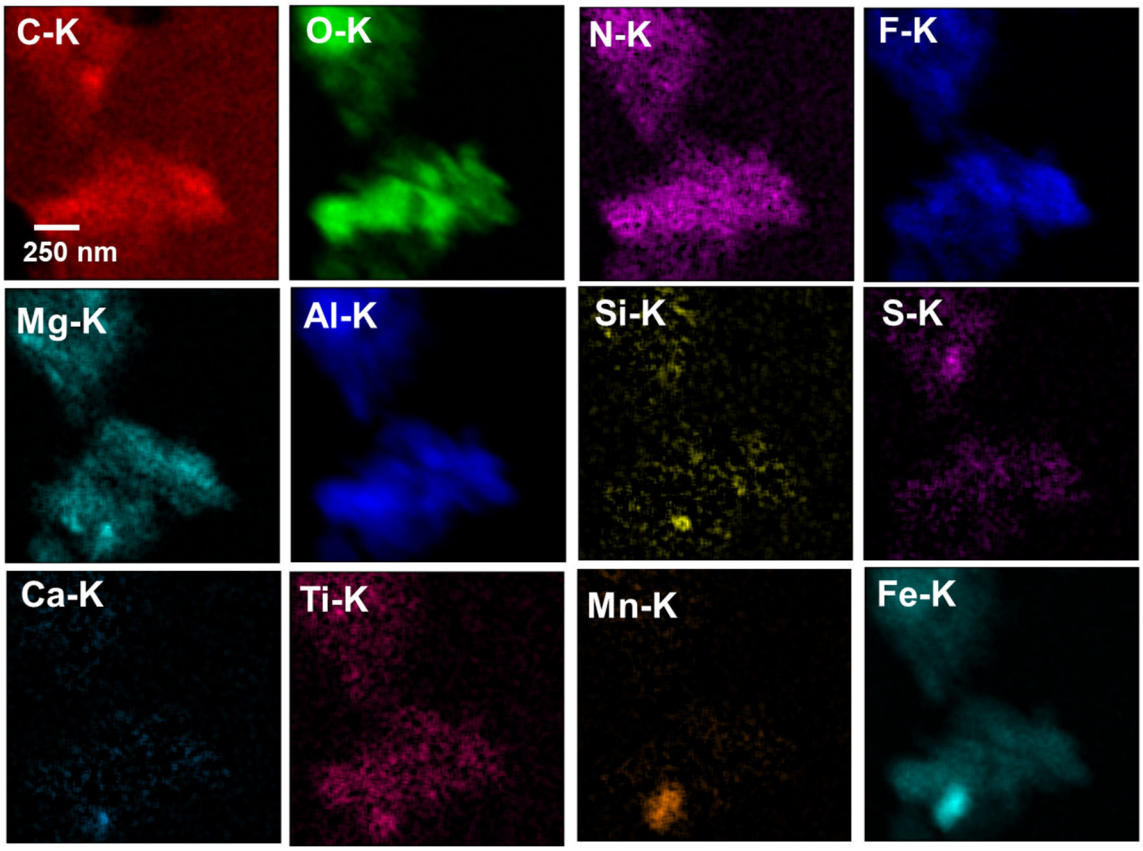

Figure E.30 STEM-EDS elemental maps of particle agglomerate found in Solution-4.

E.4 Conclusions

The four samples from AN-107 were examined with SEM and STEM. The ability to examine the sample with specific techniques did depend on the activity and the size of the observed particles. The most common feature were the fluorophosphates that were visible to the naked eye and the Fe-Mn phases. The sampling with STEM is relatively haphazard and did not provide clear view of the entirety of the specimen; however, it is the only technique where we will be able to extract structural information and reach a possible conclusion on the phase. There is evidence of trona in the sample along with a Fe-Mn phase. These results are consistent with previous analyses of these samples. The observation of U-bearing phases is also interesting, but these phases were only observed in the STEM analysis and not in the SEM analyses.

E.5 References

Bolling, S. D., Reynolds, J. G., Ely, T. M., Lachut, J. S., Lamothe, M. E., & Cooke, G. A. (2019). Natrophosphate and kogarkoite precipitated from alkaline nuclear waste at Hanford. *Journal of Radioanalytical and Nuclear Chemistry*. https://doi.org/10.1007/s10967-019-06924-9

Daniel, R. C., Burns, C. A. M., Peterson, R. A., Saldana, V. L., & Canfield, N. L. (2020). *Testing of an AP-105 Precipitation Simulant*. PNNL-29690-Rev.0 (RPT-DFTP-016-Rev.0). Pacific Northwest National Laboratory, Richland, WA. https://www.osti.gov/biblio/1609062

Felmy, A. R. (2005). *Thermodynamic Modeling of Hanford Waste Tank 241-AN-107*. PNNL-15351. Pacific Northwest National Laboratory, Richland, WA. https://www.osti.gov/biblio/939053

Gephart, R. E. (2003). *Hanford: A Conversation about Nuclear Waste and Cleanup*. Battelle Press. https://books.google.com/books?id=syFSAAAAMAAJ

Herting, D. L., & Reynolds, J. G. (2016). The composition of natrophosphate (sodium fluoride phosphate hydrate). Environmental Chemistry Letters, *14*(3), 401-405. https://doi.org/10.1007/s10311-016-0574-2

Klinger, M. (2017). More features, more tools, more CrysTBox. *Journal of Applied Crystallography*, *50*(4), 1226-1234. https://doi.org/doi:10.1107/S1600576717006793

Martin, K. B. (2004). *Compositing, Homogenization, and Characterization of Samples from Hanford Tank 241-AN-107*. WSRC-TR-2003-00210 (SRT-RPP-2003-00091). Savannah River Site, Aiken, SC. https://www.osti.gov/biblio/822082

Mitchell, D. R. G. (2008). DiffTools: Electron diffraction software tools for DigitalMicrograph™. *Microscopy research and technique*, *71*(8), 588-593. https://doi.org/10.1002/jemt.20591

Reynolds, J. G., Cooke, G. A., Herting, D. L., & Warrant, R. W. (2012). Evidence for dawsonite in Hanford high-level nuclear waste tanks. *Journal of Hazardous Materials*, *209–210*, 186-192. https://doi.org/http://dx.doi.org/10.1016/j.jhazmat.2012.01.018

Reynolds, J., & Herting, D. (2016). *Crystallization of Sodium Phosphate Dodecahydrate and Re-crystallization to Natrophosphate in Simulated Hanford Nuclear Waste – 16188*. Waste Management Symposia 2016. Phoenix, AZ. https://www.osti.gov/biblio/22838063

Wells, B. E., Kurath, D. E., Mahoney, L. A., Onishi, Y., Huckaby, J. L., Cooley, S. K., Burns, C. A., Buck, E. C., Tingey, J. M., & Daniel, R. C. (2011). *Hanford Waste Physical and Rheological Properties: Data and Gaps*. PNNL-20646 (EMSP-RPT-006). Pacific Northwest National Laboratory, Richland, WA. https://www.osti.gov/biblio/1025093

Pacific Northwest National Laboratory

902 Battelle Boulevard
P.O. Box 999
Richland, WA 99354
1-888-375-PNNL (7665)

www.pnnl.gov